Dynamic regulation of yeast glycolysis through trehalose cycling

a probabilistic view of metabolic transitions

Johan H. van Heerden

Members of the Doctoral Examination Committee:

prof. dr. Hans V. Westerhoff
VU University, Amsterdam

prof. dr. Stefan Hohmann
University of Gothenburg

prof. dr. Barbara M. Bakker
University of Groningen

prof. dr. Frank J. Bruggeman
VU University, Amsterdam

dr. S. Aljoscha Wahl
Delft University of Technology

“The task is...not so much to see what no one has yet seen; but to think what nobody has yet thought, about that which everybody sees.”

- Erwin Schrödinger

List of abbreviations

2PGA	2-Phosphoglycerate
3PGA	3-Phosphoglycerate
6PG	6-Phosphogluconate
6Pgdh	6-Phosphogluconate dehydrogenase
Adh	Alcohol dehydrogenase
ADP	Adenosine diphosphate
Ald	Aldolase
AMP	Adenosine monophosphate
ATP	Adenosine triphosphate
BPG	1,3-Bisphosphoglycerate
DHAP	Dihydroxyacetone phosphate
Eno	Enolase
EtOH	Ethanol
F6P	Fructose-6-phosphate
FA	Formic Acid
FBP	Fructose-1,6-bisphosphate
G3P	Glycerol-3-phosphate
G3pdh	Glycogen-3-phosphate dehydrogenase
G6P	Glucose-6-phosphate
G6pdh	Glucose-6-phosphate dehydrogenase
GAL	Galactose
Gal1	Galactokinase
Gal10	UDP-glucose 4-epimerase
Gal2	Galacotose permease
Gal5	Phosphoglucomutase
Gal7	Galactose-1-phosphate uridyl transferase
Gapdh	Glyceraldehyde-3-phosphate dehydrogenase
GLU	Glucose
Glk	Glucokinase
Gys	Glycogen synthase
Hxk	Hexokinase
Hxt	Hexose transporter
NADH	Nicotinamide adenine dinucleotide
Nth1/2	Neutral trehalase 1 or 2
Pdc	Pyruvate decarboxylase
PEP	Phosphoenolpyruvate

Pfk	Phosphofrutcokinase
Pgi	Phosphoglucose isomerase
Pgm	Phosphogluco mutase
pHi	Intracellular pH
Phosex	Phosphate exhange
P_i	Inorganic phosphate
PPP	Pentose phosphate pathway
Pyg	Glycogen phosphorylase
Pyk	Pyruvate Kinase
Pyr	Pyruvate
T6P	Trehalose-6-phosphate
Tps1	Trehalose 6-phosphate synthase
Tps2	Trehalose 6-phosphate phosphatase
Tps3	Trehalose phosphate synthase
Tsl1	Trehalose synthase long chain
UDP	Uridine disphosphate
UDP-GLU	UDP-glucose
Ugp	UDP-glucose pyrophosphorylase

1 Preface

Understanding how cells coordinate and dynamically regulate central metabolic activities is not only of fundamental interest, but is of importance for our continued efforts to manipulate metabolism in both biotechnological and medical settings. However, even for glycolysis, arguably one of the best studied metabolic pathways, untangling the regulatory mechanisms that underlie metabolic robustness still remains a major challenge.

This thesis attempts to advance this understanding, by explaining how the model eukaryote *Saccharomyces cerevisiae* maintains robustness in glycolysis in response to sudden changes in glucose supply. Specifically, focus is on the regulatory role of trehalose metabolism during such transitions. We show how this pathway functions to significantly increase, but not guarantee, a cell's chances of transitioning to a viable high glycolytic flux state. Our findings reveal that metabolic regulation can be highly dynamic, involving transient mechanisms that function to steer cells from one metabolic state to another, and that cell-to-cell metabolic heterogeneity can have a significant impact on such transitions.

Introduction

In most living organisms the activity of glycolysis lies at the heart of metabolism. This central metabolic pathway consists of a core series of enzymes that transform sugar to pyruvate; often glucose is used, but other sugars converge at different glycolytic intermediates (Fig. 1.1). The biochemical transformations and their associated thermodynamic properties are conserved amongst species [1] – with a reaction sequence possibly dating back to the pre-biotic world [2]. The breakdown of sugar by glycolysis yields free-energy equivalents (ATP and NADH), and biosynthetic precursors (e.g. for amino acids). In addition, precursors for metabolic stress protectants (e.g. glycerol, and trehalose in yeast) and hormones (or other secondary products) are also directly derived from the intermediates of this pathway (Fig. 1.1).

Insight into the function and regulation of glycolysis is not only of academic interest, but is of significant importance to biotechnology and health. In the biotechnological setting, the fermentation of sugars to ethanol or lactate represents one of the first human exploits of a biological pathway. Today, the glycolytic process has become an indispensable tool of the food-industry (e.g. alcoholic beverages, dairy and baking) and substantial research efforts are being directed towards ways of utilizing this process for the production of biofuels [3–5]. In health, glycolytic (dys)function has been established as a core feature of major diseases such as cancer [6, 7] and diabetes [8], and recently also in many other disease areas, such as immunology [9, 10]. This has led to a renaissance in research on metabolism that aims to unravel the mechanisms that underlie such disease states. For both applications in biotechnology and health, the goal is to intervene and manipulate the behaviour of the glycolytic pathway. This requires an understanding of how the activities of constituent components are coordinated and regulated to provide robustness and ensure metabolic homeostasis.

The autocatalytic design of glycolysis and its danger

Glycolysis generates four molecules of ATP per glucose molecule, but requires an initial investment of two ATP molecules to activate this substrate when it enters the pathway. With ATP being both a product and a substrate of the pathway, glycolysis displays what is termed an autocatalytic design (Fig 1.2). Thermodynamic and theoretical considerations indicate that the organization of glycolysis into an initial ATP-consuming part (‘upper glycolysis’), followed by ATP-producing steps (‘lower glycolysis’) (Fig. 1.2) facilitates a high flux ([11] and references therein) at low enzyme costs [12].

However, this autocatalytic stoichiometry causes a trade-off between 'robustness' (the ability to maintain a specific state or function in response to perturbations) and efficiency (obtaining maximal performance with minimal enzyme cost and regulatory complexity) [13]. Under dynamic conditions, this trade-off comes with major risk if sudden increases in flux are not managed properly [14].

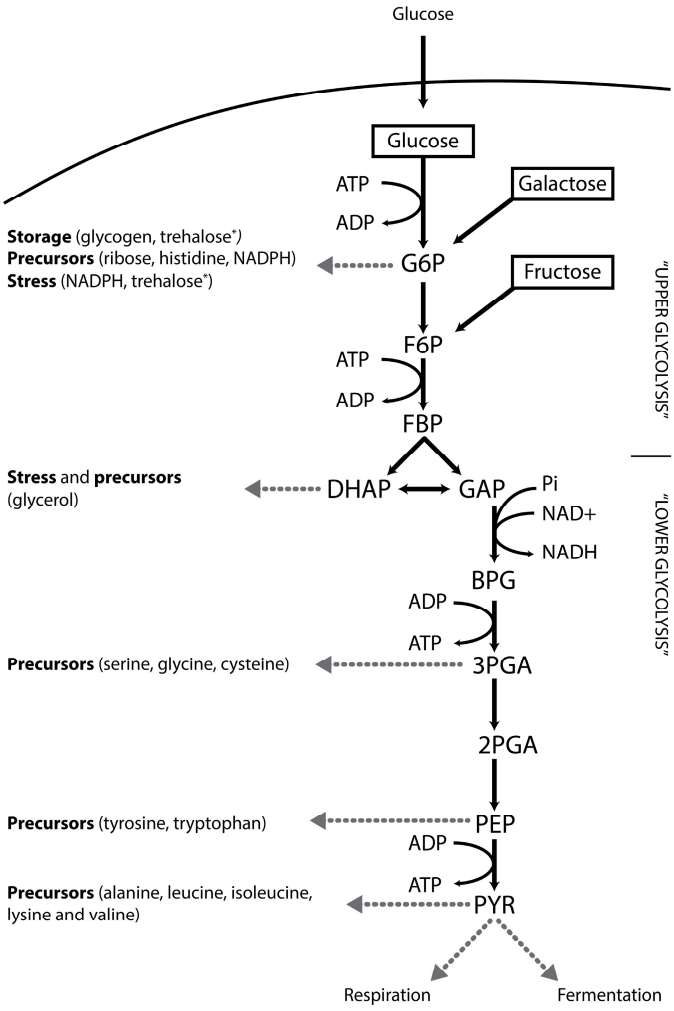

Figure 1.1: The glycolytic pathway. Shown is a schematic representation of the core structure of the glycolytic pathway, consisting of a series of enzymatic steps that convert sugar (glucose, fructose, galactose etc.) to pyruvate. Besides yielding energy equivalents, many important biosynthetic precursors and stress molecules are derived from intermediates of this pathway (indicated by the grey dotted arrows). *Trehalose biosynthesis is absent from vertebrates [15].

When excess glucose becomes available, its rapid phosphorylation results in the decrease of ATP and inorganic phosphate (P_i) as glycolysis is initiated. As a consequence of the autocatalytic architecture, regulatory mechanisms are required to ensure that ATP consumption by upper glycolysis does not outpace production by the lower part [14]; failure to do so results in the rapid depletion of ATP and P_i, and the accumulation of upper-glycolytic sugar phosphates [16, 17]; a state that is incompatible with growth. The consequences of this failure have been extensively studied in S. *cerevisiae*, where the trehalose pathway has been implicated as a key component of the regulatory machinery that ensures robustness in response to a sudden increase in glucose supply.

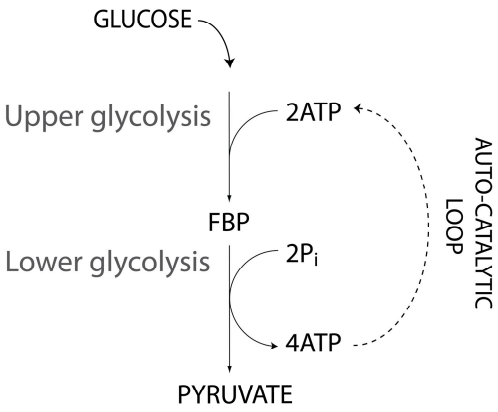

Figure 1.2: Autocatalytic design of glycolysis. Shown is a simplified schematic that illustrates the autocatalytic organization of glycolysis, with initial ATP-dependent activation steps (upper glycolysis), followed by ATP-producing reactions (lower glycolysis).

Glycolysis and the regulatory function of trehalose metabolism

In *S. cerevisiae,* trehalose is synthesized by an enzyme complex (Fig. 1.3), consisting of two catalytic subunits, trehalose-6-phosphate synthase (Tps1) and trehalose-6-phosphate phosphatase (Tps2), and two regulatory subunits, trehalose synthase long chain (Tsl1) and trehalose phosphate synthase (Tps3). Tps1 catalyses the first reaction in this pathway, generating trehalose 6-phosphate (T6P) from glucose 6-phosphate (G6P) and uridine diphosphate glucose (UDP-GLU). Subsequently, T6P is dephosphorylated by Tps2 to yield trehalose. The two regulatory subunits stabilise the complex [18]

and have been shown to contain allosteric binding [19] and phosphorylation sites [20, 21] that allow the activities of the two catalytic subunits to be modified. Finally, intracellular trehalose can be hydrolysed by the cytosolic neutral trehalases, Nth1 and Nth2, to yield two molecules of glucose [22].

It has been known for a long time that a working trehalose pathway is indispensable for the proper functioning of glycolysis in *S. cerevisiae* (see [17] for an early account). Cells lacking Tps1, the first enzyme in the trehalose pathway, are unable to grow on glucose or any other rapidly fermentable sugars [17]. A sudden shift from glucose limiting conditions to excess glucose leads to the hyper-accumulation of FBP concomitant with low ATP and P_i levels; a metabolic profile that suggests an imbalance in glycolytic fluxes where lower glycolysis is unable to keep up with upper glycolysis. The appearance of this state has been linked to the autocatalytic design of the pathway (see above) [14] and has been interpreted to result either from (i) unregulated influx of glucose, and therefore unregulated consumption of ATP as glucose is phosphorylated, or (ii) insufficient phosphate availability, which limits the reaction rate of Gapdh and consequently restricts flux through the lower (ATP-generating) part of the pathway.

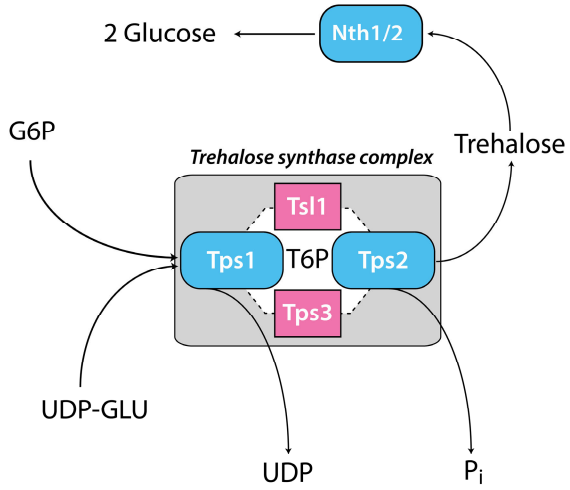

Fig 1.3: Trehalose metabolism in *S. cerevisiae*. Trehalose is synthesized by a trehalose synthase enzyme complex (grey square), which consists of two catalytic (Tps1 and Tps2, shown in blue) and two regulatory subunits (Tsl1 and Tps3, shown in pink). A third reaction, catalysed by trehalase (Nth1/ Nth2), hydrolyses trehalose to yield two molecules of glucose, completing the pathway.

The trehalose pathway appears to be required to balance ATP-consumption and production with phosphate homeostasis, when the upper-glycolytic flux suddenly increases. However, how the trehalose pathway participates in this regulation has been challenging to determine and has been the subject of active investigation for more than 30 years.

The regulatory mechanisms that have been ascribed to the trehalose pathway involve the regulation of glycolytic flux, either by inhibition of the upper-part or by stimulation of the lower-part [17]. To date, two mechanisms have dominated (Fig. 1.4): (1) regulation of glucose entry into the pathway through the direct inhibition of Hexokinase (Hxk) -the first ATP consuming step- by the intermediate trehalose 6-phosphate (T6P), or (2) enhancement of Glyceraldehyde 3-phosphate dehydrogenase (Gapdh) activity -the first reaction in lower glycolysis- through supply of P_i. However, many paradoxical observations have indicated that neither of these mechanisms can fully explain the metabolic deficits of *tps1Δ* mutants. A third mechanism, involving physical interactions between the Tps1 protein and the hexokinases and/or glucose transporters [17, 23–26] has also been proposed, but there has been no direct experimental evidence in support of this hypothesis. However, a very recent study by Petitjean *et al.* [27] provides evidence that suggests that the Tps1 protein could fulfil general functions not related to its catalytic activity.

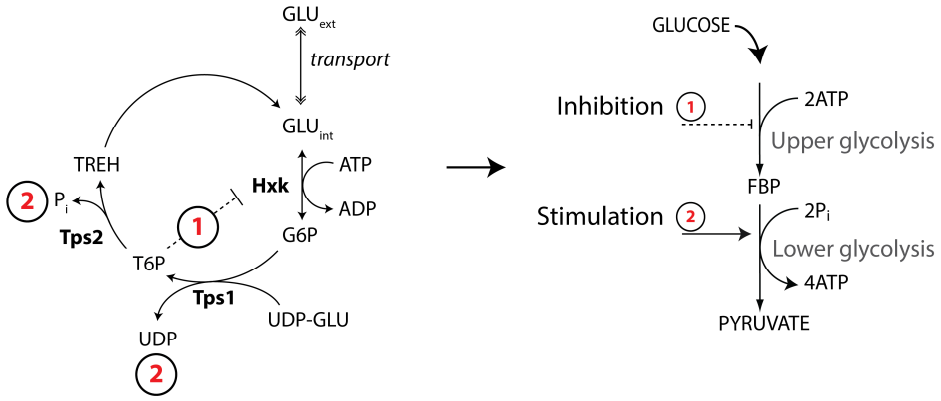

Figure 1.4: Regulatory functions proposed for the trehalose pathway. The trehalose pathway is thought to regulate glycolytic flux either by (1) the inhibition of Hxk, and hence upper glycolysis, by T6P, or by (2) the stimulation of lower glycolysis through the liberation of phosphate.

For insight into the dynamic regulation of glycolysis, the *tps1Δ* mutant provides an interesting case study. While the exact regulatory mechanism of the trehalose pathway is uncertain, there is

substantial evidence for the origin of the metabolic imbalance. An overcapacity in upper glycolysis has been shown to produce similar outcomes in pancreatic β-cells [28], where it was termed acute glucose intolerance. The next section provides a brief summary of attempts to assign a metabolic regulatory function to the trehalose cycle and highlights many of the interpretive difficulties historically encountered and which we resolve in this thesis.

T6P as a competitive inhibitor of the hexokinase

Early experimental evidence linked the metabolic defects of *tps1Δ* mutants to a deficiency in trehalose 6-phosphate (T6P) synthesis. T6P was shown to function *in vitro* as a competitive inhibitor of the hexokinases (Hxk1 and Hxk2), with respect to glucose [24]. The demonstration that a reduction in hexokinase activity, by deletion of Hxk2, restores growth on glucose appears to corroborate this interpretation [24]. The behaviour of trehalose 6-phosphate phosphatase (Tps2) mutants [24] was also suggested to provide support for this mechanism. These cells (tps2Δ) are unable to convert T6P to trehalose and consequently accumulate high levels of T6P. Furthermore, deletion of the *tps2* gene restores growth on glucose in cells expressing a mutant Tps1 allele (*byp1-3*) with low and normally suboptimal T6P synthase activity levels.

These insights appear to paint a coherent picture of a “brake at the gate of glycolysis" [17]. However, the *in vivo* relevance of T6P-mediated inhibition as sole regulatory mechanism has been questioned. *In vitro* experiments demonstrated that 1 mM of glucose was sufficient to completely outcompete the inhibitory effect of 0.4 mM T6P [24], implying that the efficiency of inhibition will quickly diminish following a glucose pulse. Hohmann and colleagues [24] re-measured the inhibition constants (K_i) of T6P for both Hxk1 and Hxk2 and while they found higher values than initially reported, 1 mM vs. 0.2 mM and 0.1 mM vs. 0.04 mM, respectively, it is clear that the potential for T6P inhibition as an efficacious inhibitor of glucose influx will be limited to a narrow metabolic range. Based on dynamic metabolite profiles [25, 26, 29] and the calculated T6P inhibition constants (K_i) of the two hexokinases [24, 30], the T6P-mediated inhibition of glucose phosphorylation is, if anything, transient and only relevant immediately following a glucose pulse.

Although there is ample evidence that T6P-inhibits Hxk activity, two other studies [25, 31] provide evidence that suggest that this inhibition cannot be the sole mechanism by which Tps1 regulates glycolysis.

First, wild-type cells expressing only a T6P-insensitive form of Hxk2 from *Saccharomyces pombe*, were shown to be capable of utilizing glucose without exhibiting the population-level metabolic defects typically associated with the *tps1Δ* phenotype [25]. A second and complementary study [31] similarly addressed the necessity and sufficiency of T6P-mediated inhibition of Hxk2, by evaluating the consequences of native Hxk2 overexpression in the WT background. While no major growth defects were reported (data not shown in [31]), metabolite measurements display a clear Hxk2 dose-dependent effect for both FBP and ATP pools. Overexpression resulted in FBP and ATP profiles that initially resembled the pattern seen for *tps1Δ*, and eventually recovered to levels which were intermediate between WT and *tps1Δ*, i.e. FBP was higher than in WT, but lower than in *tps1Δ* and vice versa for ATP.

These findings are difficult to interpret. On the one hand there is clear evidence for T6P-mediated inhibition of Hxk as an important regulatory interaction, while on the other, direct manipulations of Hxk activity levels suggests that this mechanism might be of less importance than originally thought.

Trehalose metabolism functions as a phosphate recovery mechanism

An alternative mechanism focuses on the phosphate depletion phenotype exhibited by *tps1Δ* mutants. The rapid and sustained depletion of phosphate is thought to result in a flux bottleneck at the level of the glyceraldehyde 3-phosphate dehydrogenase (Gapdh) reaction, as evidenced by metabolite profiles; consequently manipulations that improve phosphate recovery should alleviate this bottleneck [17]. Support for this hypothesis is provided by the observation that enhanced glycerol production can restore growth of *tps1Δ* mutants on glucose (see [32] for overview). Within this framework, an increase in the glycerol flux serves to facilitate recovery of NAD^+ and P_i, both substrates of the Gapdh reaction. From this it was inferred that trehalose synthesis provides a means for cells to recover phosphate when needed. Looking at the stoichiometry of the trehalose cycle, this suggestion is appealing, with 3 phosphate equivalents (2 during synthesis of UDP-GLU and 1 during dephosphorylation of T6P) liberated per trehalose molecule synthesized. Furthermore, the differential phosphate-dependent regulation of catalytic and regulatory proteins within the trehalose cycle [19, 18] suggests a capacity to integrate and respond to the phosphate status of the cell.

However, the plausibility of a phosphate recovery role was critically questioned and has generally been dismissed by most commentators as unlikely [17, 29, 33, 34]. The two most cited arguments are: (1) The trehalose flux is expected to have a low flux capacity compared to glycolysis, such that this capacity is insufficient to recover the necessary phosphate and (2) *Tps2Δ* mutants show an improved viability while these mutants cannot recover phosphate from T6P.

Consolidating the regulatory function of trehalose metabolism

It is intriguing that more than thirty years of active research on this phenomenon has failed to provide a satisfactory explanation for the regulatory role of trehalose metabolism [16, 23–26, 29, 35]. While previous efforts have generated lots of descriptive evidence, very few attempts have been made to explore the consequences of trehalose metabolism deficiency at a systemic level, using approaches involving theory and modelling.

The historical overview in the previous section serves to provide a contextualization of the current work, by highlighting the most important, to date, experimental observations and attempts at ascribing a metabolic regulatory role for the trehalose cycle. While there appears to be compelling evidence for each of the proposed mechanisms, it is clear that none are able to fully explain the deficits associated with *tps1Δ*. In the chapters that follow, we will show how a more integrated and dynamic view of regulation by this system facilitates a re-interpretation of existing data and hypotheses and, importantly, provides a single consolidated model that integrates previously proposed functions into a coherent systemic mechanism.

This dissertation specifically set out to understand the regulatory role of trehalose metabolism during glycolytic transitions as a case study for need to regulate metabolism under dynamic conditions. We chose to study transitions from galactose to glucose in *S. cerevisiae*, as this afforded us a large degree of historical reference and comparability. As such, one of the aims of this thesis was to extend previous observations and explanations with modelling and theory, to derive more informative experiments and ultimately provide a systemic account of the regulatory deficits underlying the *tps1Δ* mutant phenotype. In our efforts we made several other interesting observations that have general implications for studies of metabolic regulation. We show that noise in metabolism can lead to phenotypic heterogeneity and that regulatory interactions can be transient and only relevant immediately following perturbations. This latter point has significant implications for efforts that aim to assign regulatory functions to metabolic components in response

to dynamic conditions. The observation of phenotypic heterogeneity highlighted important pitfalls in population level measurements. In line with other recently published studies [36, 37], we show that lag phases can be explained by growing and non-growing subpopulations, with obvious implications for the interpretation of population level metabolite measurements.

Structure and scope of this thesis

Rather than a series of related topics or studies, a single coherent summary is presented in Chapter 2, with Chapters 3 to 7 serving as appendices containing supporting materials, methodological details and additional discussions.

In **Chapter 2** we solve the long standing puzzle of a regulatory role for trehalose metabolism during glycolytic transitions. We employ both modelling and experiments to demonstrate how yeast glycolysis can operate in two modes, functional or detrimental to growth. We show how metabolic regulation affects the probability to end up in either of these states and implicate cell-to-cell metabolic variation as an important component of these probabilistic outcomes. Finally we describe how the transient activation of the trehalose cycle is an essential part of *S. cerevisiae's* regulatory machinery that ensures robust startup of glycolysis. Additionally, an appendix details a reduced model of glycolysis that is not presented as part of the body of this dissertation; it is included to provide information that will assist the reader in interpreting a subset of results included in this chapter.

Chapter 3 provides details on a kinetic model of glycolysis that was used to explore glycolytic dynamics in response to activation by high glucose. Changes to and extensions of an existing model of glycolysis are described and the updated model is compared to the original. We also describe initial-condition dependent bistable behaviour for the updated model.

Chapter 4 describes the experimental identification and characterization of two subpopulations (viable and non-viable) in a population of otherwise genetically identical cells. We identify two distinct phenotypic states and show that after sugar transitions these states appear spontaneously and reproducibly in any population of sufficient size. In addition, we show that these states arise as a consequence of phenotypic plasticity and that their relative sizes can be manipulated by changes in extracellular conditions. Using *in vivo* readouts of intracellular pH, we provide evidence that the growth phenotypes correspond to distinct metabolic subpopulations.

Chapter 5 demonstrates how small continuously distributed variations in metabolic variables can explain the appearance of two glycolytic subpopulations. Using a random sampling approach we find that the successful initiation of glycolysis is determined by an interplay between components that tend to reduce the flux through the upper (ATP consuming) part of glycolysis and those that enhance the flux through lower (ATP producing) part. Importantly, these results show that while specific regulatory mechanisms are required to ensure the proper startup of glycolysis, cell-to-cell variations at a purely metabolic level can produce unexpected phenotypic outcomes.

Chapter 6 details the experimentally determined dynamic flux behaviour of the trehalose pathway, following a glucose pulse. We use a ^{13}C tracer enrichment approach, and show that sudden perturbation with excess glucose leads to the transient activation of this pathway, with a significant percentage of the glucose uptake flux channelled towards trehalose. We argue that this observed behaviour is consistent with our model's prediction that transient hydrolysis of ATP through futile (trehalose) cycling would facilitate the proper initiation of glycolysis.

Finally, **Chapter 7** provides concluding remarks and reflections. In addition, we return to previous interpretation of the trehalose cycle's regulatory role and show how insights from the current work can account for many previously perplexing observations.

2 Lost in Transition: startup of glycolysis yields subpopulations of non-growing cells

Authors: Johan H. van Heerden, Meike T. Wortel, Frank J. Bruggeman, Joseph J. Heijnen, Yves J.M. Bollen, Robert Planqué, Josephus Hulshof, Tom G. O'Toole, S. Aljoscha Wahl and Bas Teusink

Abstract:

Cells need to adapt to dynamic environments. Yeast that fail to cope with dynamic changes in the abundance of glucose can undergo growth arrest. We show that this failure is caused by imbalanced reactions in glycolysis, the essential pathway in energy metabolism in most organisms. The imbalance arises largely from the fundamental design of glycolysis, making this state of glycolysis a generic risk. Cells with unbalanced glycolysis co-existed with vital cells. Spontaneous, non-genetic metabolic variability among individual cells determines which state is reached and consequently which cells survive. Transient ATP hydrolysis through futile cycling reduces the probability of reaching the imbalanced state. Our results reveal dynamic behavior of glycolysis and indicate that cell fate can be determined by heterogeneity purely at the metabolic level.

This chapter was published as: van Heerden *et al*. LOST IN TRANSITION: startup of glycolysis yields subpopulations of non-growing cells. Science, 343: (2014).

Introduction

Key properties of biological systems are adaptability and robustness - the ability to maintain the physiological state in response to perturbations or dynamic conditions [38]. Cells use multilayered regulation to respond adequately to changing environments or sudden perturbations. Failures in regulation underlie cellular malfunctioning, loss of fitness, or disease. In recent years, there has been a revived interest in metabolic processes as many diseases are associated with metabolic aberrations, such as diabetes and cancer [39]. Glycolysis is the central pathway in energy metabolism, which converts glucose to pyruvate with a net production of two adenosine 5'-triphosphate (ATP) molecules per glucose molecule. However, this net formation of ATP in "lower glycolysis" is preceded by an initial ATP investment at the first steps in the pathway ("upper glycolysis", Fig. 2.1). This sequence of enzymatic steps in glycolysis, which is adopted by many organisms [12], implies a serious risk. If upper glycolysis outpaces lower glycolysis, a massive accumulation of glycolytic intermediates can occur with much reduced ATP production [14]. This phenotype is observed in pancreatic beta-cells overexpressing glucokinase (coined acute glucose intolerance) [28], the enzyme that catalyzes the first step of glycolysis. Similarly, *Saccharomyces cerevisiae* mutants defective in the biosynthesis of the disaccharide trehalose, that branches off from glycolysis at the level of glucose-6-phosphate (Fig. 2.1), show accumulation of the glycolytic intermediate fructose 1,6-bisphosphate (FBP) at low concentrations of ATP [40]. We call this detrimental state of glycolysis an *imbalanced state*. We find that this imbalanced state is a risk also for normal cells. Through detailed system-level analysis of yeast glycolysis, we explain how phosphate dynamics is at the origin of the imbalance, and reveal how specific regulatory mechanisms affect the probability for cells to get trapped in it.

S. cerevisiae mutants with a defect in trehalose 6-phosphate synthase (Tps1), the first committed step in trehalose biosynthesis (Fig. 2.1), exhibit the imbalanced-state phenotype and are unable to grow on glucose [17]. The molecular mechanism underlying this imbalanced phenotype has proven challenging to elucidate (see Chapter 1 for a summary). Trehalose 6-phoshate (T6P), the product of Tps1, acts *in vitro* as a competitive inhibitor of the hexokinases (Hxk1 and Hxk2), with respect to glucose [24]. This negative feedback loop was hypothesized to slow down the upper part of glycolysis and restore the balance in wild-type cells [14], but T6P-insensitive hexokinase mutants do grow on glucose [25]. An alternative hypothesis assumes a reduced activity of glyceraldehyde 3-phosphate dehydrogenase (Gapdh) because of the low amounts of its substrate, cytosolic phosphate (P_i), in *tps1Δ* mutants. Accordingly, P_i release should enhance Gapdh activity and restore balance. In line with this hypothesis, enhanced glycerol production, which releases P_i, restores growth of *tps1Δ*

mutants on glucose [23]. Trehalose production from glucose 6-phosphate (G6P) also releases P_i (Fig. 2.1); however, the capacity of trehalose synthesis was believed to be too low to provide enough P_i for the high flux of glycolysis [34].

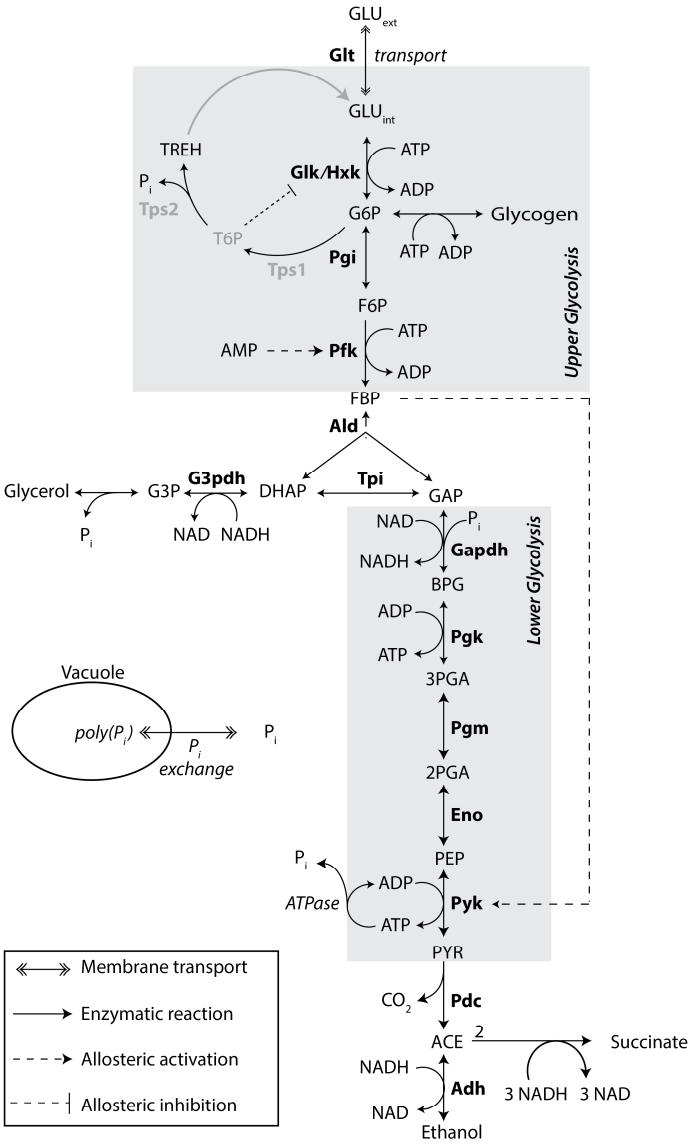

Figure 2.1. Schematic illustration of glycolysis and the trehalose cycle.

We used a computational approach to better understand the complex phenotype of *tps1Δ* mutants. We adapted an existing kinetic model of glycolysis [41] by (i) introducing P_i as an explicit variable in the model (rather than as a fixed "commodity" metabolite); and (ii) allowing for the mobilization of P_i from vacuolar stores, based on *in vivo* NMR data that describe this behavior [40]. The latter was necessary, as the net accumulation of phosphate-containing glycolytic intermediates that is observed experimentally in the imbalanced state (Fig. 2.2B), is not possible without the import of P_i (see Chapter 3 for details).

Two glycolytic states co-exist

Simulations representing the *tps1Δ*-mutant resulted in dynamic metabolite profiles that were qualitatively similar to experimentally observed profiles (Fig. 2.2), *i.e.* all metabolites were balanced, except for the intermediates between the upper and lower parts of glycolysis (Fig. 2.2 and Chapter 3, Fig. 3.2). Known experimental rescue mechanisms for the *tps1Δ*-mutant, such as reduced activity of hexokinase [24] or enhanced glycerol production [23] could be reproduced *in silico* (Chapter 5, Fig. 5.1 and Appendix A, Fig. A.3).

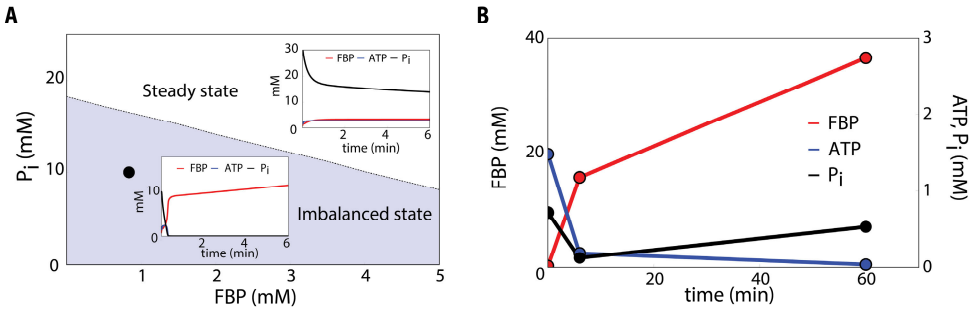

Figure 2.2. Glycolysis exhibits initial condition-dependent bistable behaviour. Depending on initial conditions, the *tps1Δ*-like model can reach one of two stable states (A): A normal steady state (white area), or an imbalanced state (grey area). The black circle indicates the initial values for P_i and FBP used (Chapter 3, Table 3.2). (B) Simulations of the imbalanced state are qualitatively similar to experimentally-observed profiles (data reproduced from [21]).

Our *tps1Δ*-mutant model could reach another state, which resembled the wild-type steady state with proper flux, high ATP and P_i levels, and normal FBP levels. Whether this state was reached

depended on the initial concentrations of the metabolites, as shown for FBP and P_i (Fig. 2.2A). Hence two stable outcomes (states) co-existed in the model, a global steady state and the imbalanced state: the latter is a non-typical stable state as some variables are not constant in time but rather accumulate. Other systems with more than one stable state, as found in sporulation [42] or differentiation [43], often result in phenotypically different subpopulations in an isogenic population. We assessed experimentally whether we could find evidence for such subpopulations as well, by asserting that only the functional glycolytic state would support growth. Based on serial-dilution plating of wild-type and *tps1Δ* cultures on galactose and glucose (Chapter 4), we estimated that approximately 1 in 10^3 - 10^4 *tps1Δ* cells grew on excess glucose (Fig. 2.3A). This small subpopulation size is consistent with the very long lag phase we observed in glucose liquid cultures (Fig. 2.3B). In the past, glucose-positive *tps1Δ* colonies were usually discarded as revertants or rescue mutants [44]. However, when *tps1Δ* colonies were directly picked from glucose plates and subjected to another transition via galactose to glucose, the original subpopulation structure with less than 1 in 10^3 glucose-tolerant colonies was restored (Fig. 2.3C and Chapter 4, Fig. 4.2). This argues against a genetic basis. We therefore conclude that there is a small subpopulation of glucose-positive *tps1Δ* cells that arises from spontaneous phenotypic –as opposed to genetic- variability.

We re-examined the reported inhibitory effect of low concentrations of glucose on *tps1Δ* mutant growth in the presence of excess galactose [35]. Plating experiments again showed that the growth inhibition observed at the population level is in fact caused by a glucose-dependent increase in the size of a subpopulation that was unable to grow (Chapter 4, Fig. 4.4A). A simple mathematical model of population growth dynamics with different growing and non-growing subpopulation sizes (Chapter 4) reproduced the experimental data [35] very well (Chapter 4, Fig. 4.4B).

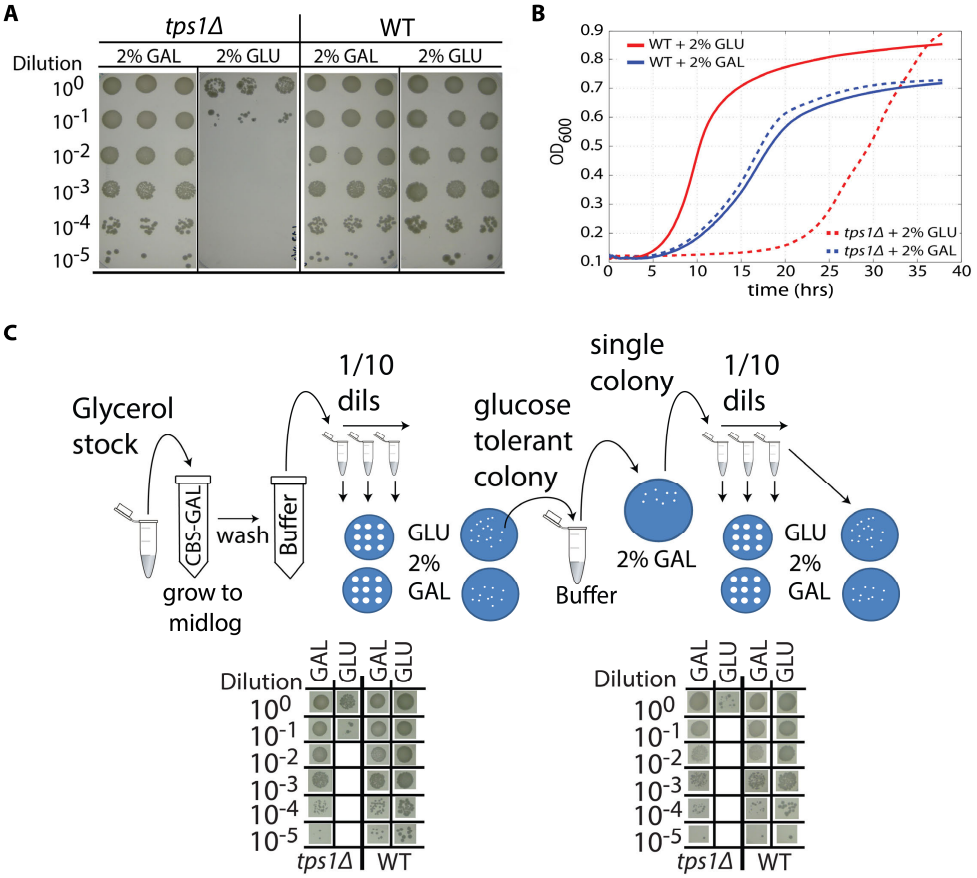

Figure 2.3. Small non-genetic glucose tolerant subpopulations appear in *tps1Δ* cultures. (A) Serial dilution plating reproducibly shows glucose-tolerant subpopulations of between 1 in 10^3-10^4 *tps1Δ* cells (n=3). (B) Growth curves for wild-type and *tps1Δ* on glucose (GLU) and galactose (GAL): on GLU *tps1Δ* cells show extended lag phase as a consequence of a large non-growing background. (C) Summary of the propagation scheme and a representative result (see Chapter4, Fig. 4.2 for full scheme) show that glucose tolerance can be reset, as populations derived from a glucose tolerant colony exhibit subpopulation structures similar to initial populations derived from glycerol stocks.

Intracellular pH reveals two metabolic subpopulations

To visualize the two subpopulations, we made use of the observation that *tps1Δ* mutants, when exposed to glucose, are unable to maintain pH homeostasis because they produce too little ATP

[40]. Hence, after glucose addition, the intracellular pH (pH_i) of *tps1Δ* populations decreased by more than 1 pH unit compared to that of wild-type cells (Fig. 2.4A).

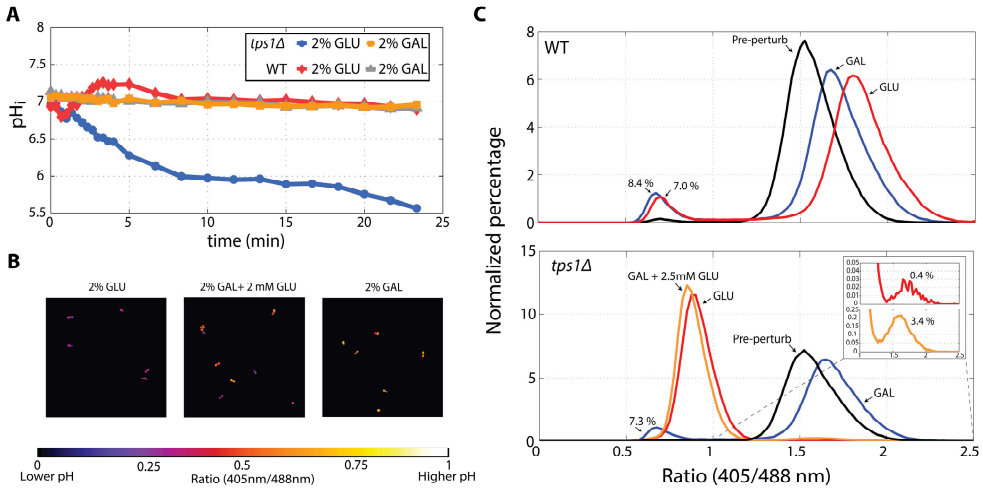

Figure 2.4. Intracellular pH reveals distinct metabolic subpopulations. (A) Population-level pH_i responses show the disruption of pH homeostasis of *tps1Δ* cells in response to 2 % glucose. Following a 2 % glucose or galactose pulse, the pH_i of WT and *tps1Δ* populations are shown in time. (B) Fluorescent microscopy shows that distinct metabolic states can be visualized using pH_i readouts. (C) Flow cytometery measurements based on pHluorin signals, reveal the presence of distinct subpopulations in both WT (top graph) and *tps1Δ* populations (bottom graph) following perturbations with glucose and galactose (black, pre-perturbation sample in wash buffer; blue, 2 % GAL; red, 2 % GLU; orange, 2 % GAL + 2.5mM GLU).

After confirming that different subpopulations could be distinguished on the basis of pH_i signals (Fig. 2.4B) we used flow cytometry as a high-throughput approach to study the structure of both *tps1Δ* and wild-type populations exposed to galactose and glucose. We found two subpopulations of *tps1Δ* cells of sizes that agreed with the plating assays and growth lag phases (Fig. 2.4C). We also tested wild-type cells, because analysis of the wild-type version of the model also showed two stable states (Chapter 3, Fig. 3.4). Indeed, a subpopulation of wild-type cells with low pH appeared in cultures exposed to glucose, but a similar response was observed for galactose (Fig. 2.4C). The size of the subpopulation, about 7 %, was larger than the model suggested (Chapter 3, Fig. 3.4). These results

indicate that the imbalanced state is a general property of glycolysis that cannot be fully prevented by regulatory mechanisms operative in wild-type cells.

Metabolic variability determines state of glycolysis

We tested *in silico* whether the observed phenotypic variability in the response to sugar addition could be reproduced by introducing spontaneous variation in enzyme and initial metabolite concentrations (see Chapter 5 for details). We sampled these concentrations from Gaussian distributions with realistic coefficients of variation [45]. The mean of the initial metabolite concentrations was based on metabolite data for wild-type cells grown on galactose [46], the sugar on which we grew *tps1Δ* before glucose addition. We generated 10^6 *tps1Δ*-like models each with unique initial conditions and simulated a galactose-to-glucose transition. Less than one in a thousand models actually reached a functional steady state. Thus, heterogeneity in the amounts of glycolytic enzymes and metabolites appears to cause some cells to survive glucose dynamics whereas others do not. This is striking, as metabolism is often considered to operate in a deterministic regime due to rather high concentrations of enzymes and intermediates. Phenotypic variation by non-genetic variability is usually studied in genetic circuits that naturally operate at a stochastic regime with low copy numbers for key components [47].

It is relevant to compare the above observations with frameworks such as fluctuation-induced bistable switching [48, 49] which has previously been linked to the emergence of phenotypic heterogeneity. In contrast to such stochastic-switching phenomena, the emergence of the two distinct phenotypes (viable and non-viable) described here does not depend on the co-existence of two qualitatively different physiological states prior to a glucose perturbation. Our interpretation of the above data is that spontaneous, non-genetic variation between cells creates a continuous probability distribution for metabolite concentrations and metabolic fluxes. Within the space of these initial physiological states, a subspace exists that characterizes the cells that survive a sudden glucose excess exposure (see Chapter 7, Fig. 7.7).

To assess which parameters and initial conditions most affect the probability to reach an imbalanced or functional steady state, we performed a linear discriminant analysis over all our model simulations (Chapter 5). A single discriminant accounted for 99 % of the differences in initial conditions that lead to either the balanced or imbalanced states (Fig. 5.1A). This discriminant identified parameters and initial metabolite concentrations that either tend to reduce the flux

through the upper part of glycolysis or enhance the flux through lower glycolysis (Fig. 2.5A). The parameters related to the primary mechanisms known to rescue the *tps1Δ* mutant phenotype [33] were all represented.

Size of subpopulations can be manipulated

We looked for ways to experimentally influence the size of the two subpopulations. Respiratory inhibitors, in particular Antimycin A [32], have been shown to improve growth in the presence of glucose. However, ethanol, the solvent of Antimycin A, produced pronounced decreases in the lag phase (Fig. 2.5B), completely dominating the Antimycin A effect (Chapter 4, Fig. 4.3A). These results were confirmed by plating assays (Chapter 4 Fig. 4.5A), and flow cytometry measurements of pH_i (Chapter 4, Fig. 4.6). We repeated the *in silico* random-sampling approach at different ethanol concentrations and reproduced the positive effect of ethanol (Fig. 2.5C). The model showed that the increase in ethanol concentration increased P_i release through glycerol formation (Chapter 5, Fig. 5.1B) driven by an increased NADH/NAD ratio [50].

This model prediction was experimentally tested in *tps1Δ* mutant cultures by addition of formate. Although formate cannot be used as a carbon source by yeast, its conversion to CO_2 by formate dehydrogenase [51] enhances NADH formation. Indeed, formate additions similarly decreased the lag phase, implying a NADH-driven increase in glycerol production that subsequently increases the proportion of *tps1Δ* cells in the population that could grow on glucose (Chapter 4, Fig. 4.3B).

Core model explains and generalizes dynamics

To generalize our findings and to provide a deeper understanding of the observed co-existence of two stable states, we captured the essential features of the large model in a reduced model (see Appendix A). This generalized core model only considers the concentrations of FBP, ATP and P_i and four reactions: a lumped upper glycolysis reaction (v_{upper}), a lumped lower part of glycolysis (v_{lower}), an ATP-demand reaction (v_{ATP}), and a P_i import or export reaction (v_P) (Fig. 2.6). Detailed mathematical analysis showed that such a generalized glycolytic pathway has two stable states representing a functional steady state and an imbalanced state.

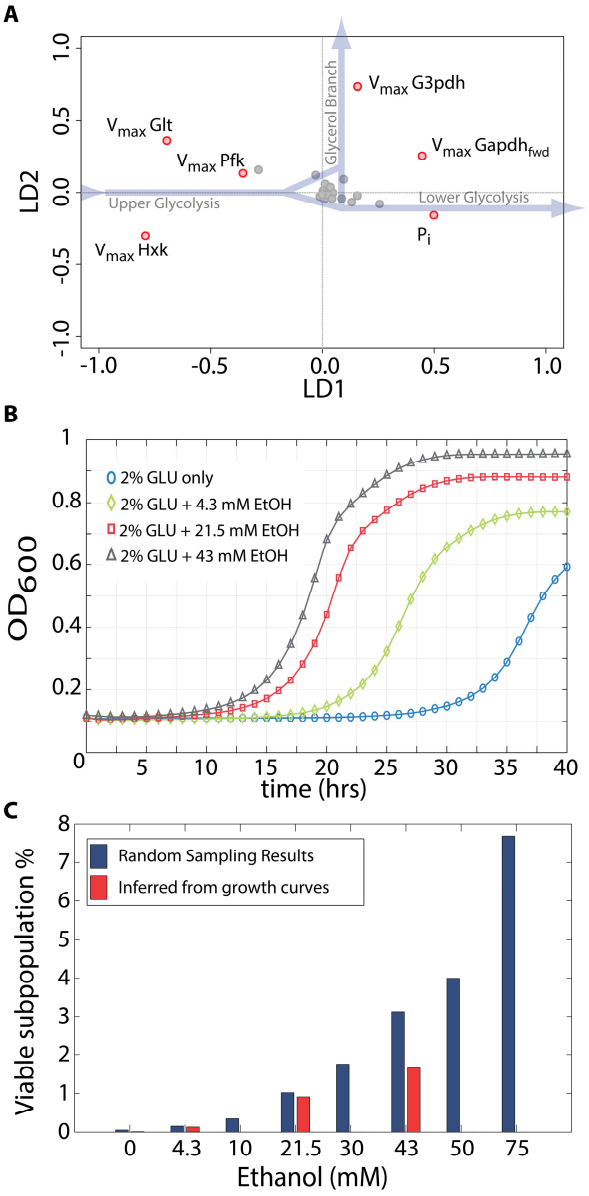

Figure 2.5. **Metabolic subpopulations are caused by small variation in metabolic variables, and their sizes can be manipulated.** (A) Linear discriminant analysis of randomly sampled initial conditions (metabolites and Vmaxes) highlights the variables which most significantly affect the probability of reaching either the normal steady state or the imbalanced state. (B) In liquid cultures, lag phases of *tps1Δ* cultures decreased with increasing concentrations of ethanol (EtOH) in the medium. (C) The positive effect of ethanol as percentage of viable cells (experimental data: red bars; Chapter 4, Fig. 4.5B) can be reproduced by a population of models with initial conditions sampled from a Gaussian distribution as described in Chapter 5.

Figure 2.6 shows the system dynamics that lead to these two states: the difference between the left and right panel is only the initial P_i level (10.4 and 9.4 mM, respectively). How can the different outcomes in these simulations be explained? At the start of the simulation (when glucose is added), $v_{upper} > v_{lower}$, and this difference causes the concentration of the intermediate FBP to increase (as $dFBP/dt = v_{upper} – v_{lower}$). For a balanced steady state, v_{lower} needs to accelerate to equal the rate of v_{upper} (note that this challenge becomes bigger if the activity of v_{upper} is higher). P_i is the phosphate source for FBP and therefore FBP accumulation results in a drop in P_i (Fig. 2.6). As both FBP and P_i are substrates of v_{lower} the accumulation of FBP stimulates v_{lower}, while the drop in P_i tends to slow it down: Which effect is dominant may determine the fate of the system. If P_i is high initially, a drop in P_i will not affect v_{lower} and the FBP increase will dominate, resulting in the functional steady state being reached (Fig. 2.6, left panel). Similarly, if P_i is liberated quickly enough directly by storage/uptake (v_P) or indirectly by ATP hydrolysis (v_{ATP}), P_i will drop less quickly and the balanced steady state can also be reached. If, however, P_i is low at the onset of glucose addition, or P_i mobilization is too slow, or both, the decrease in P_i will quickly become a limiting factor for v_{lower} and will dominate the stimulating effect of accumulating FBP. In this case, v_{lower} will not accelerate quickly enough to reach the rate of v_{upper}, and the system will collapse to the imbalanced state (right panel Fig. 2.6).

Once in this imbalanced state, continuous P_i mobilization from uptake or storage paradoxically *maintains* the imbalance. In this low P_i, low ATP state, imported P_i enhances the rate of v_{lower}, but the concomitant production of ATP will increase v_{upper} two times more (due to the stoichiometric coupling of ATP in glycolysis, Fig. 2.6B). Hence, the imbalance and thus FBP accumulation will only get bigger with faster P_i import as observed in the core model and the detailed model (Chapter 3, Fig. 3.3).

Trehalose metabolism constitutes transient futile cycling

The core model predicted that enhanced P_i mobilization through ATP hydrolysis by v_{ATP} could enlarge the set of initial conditions that leads to a functional steady state, or could even result in the disappearance of the imbalanced state altogether (Fig. A.3). This was confirmed in the detailed model. We realized that, in yeast, the full trehalose cycle (Fig. 2.1) could act as a mechanism for ATP hydrolysis through futile cycling. This cycling of trehalose should be able to remove the existence of the imbalanced state or at least reduce the probability to reach it, providing a rationale why trehalose metabolism affects glycolytic function.

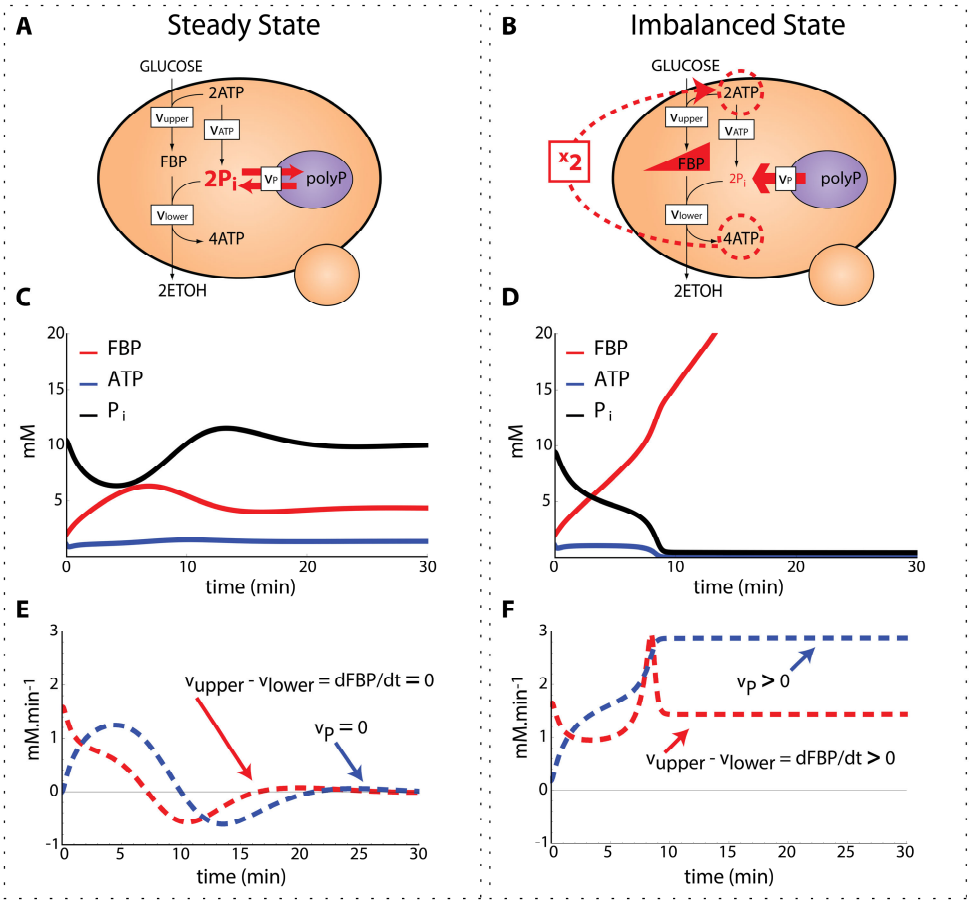

Figure 2.6. **Generalized core model of glycolysis can reach two stable, co-existing, states.** The left panel shows the global steady state, the right panel the imbalanced state. The difference between panels is the initial P_i level (10.4 and 9.4, respectively). (A and B) Stoichiometry of the core model, with red arrows emphasizing the vacuolar flow of P_i from polyphosphates (polyP). The coupling between the upper and lower part of glycolysis through ATP is emphasized by the red dashed line (B). (C and D) Metabolite levels for a simulation of the core model, resulting in steady state (metabolite levels constant in time, C) or imbalance (FBP accumulation at very low P_i and ATP levels, D). (E and F) Characteristic rates that specify the states: the red dashed lines indicate the difference in rate between upper and lower glycolysis ($v_{upper} - v_{lower}$), which is zero at steady state (E) and is positive at the imbalanced state (F). The dashed blue lines represent the vacuolar import rate of P_i (v_P), which should be zero at steady state. In Fig. 2.6F, the constant positive v_P indicates mobilization of P_i, which sustains accumulation of FBP (red dashed line) through the stoichiometric coupling of ATP.

To estimate the dynamic fluxes through the trehalose network upon a transition to glucose excess, we used a dynamic [^{13}C]-labeling approach (Chapter 6). Wild-type cells were grown in a glucose-limited chemostat and treated with either 110 mM [^{12}C]-glucose or uniformly labeled [U-$^{13}C_6$]-glucose pulses. The time course of the concentrations and the average carbon labeling enrichments for key intermediates are shown in Fig. 2.7A. For most metabolites up to full enrichment was achieved very rapidly; in contrast, the large trehalose pool was enriched to only 14 % at the end of the experiment. From these data the flux of glucose through the different glycolytic enzymes was estimated based on a hybrid modeling approach [52]. The flux profiles indicated that: (i) fluxes changed rapidly after a glucose pulse, at similar time scales as key metabolites, such as ATP (Fig. 2.7B), (ii) fluxes through Tps1 and Tps2 increased and subsequently decreased between 0 and 5 min and (iii) at its maximum, as much as 28 % of the glucose taken up was branched into trehalose (Fig. 2.7C).

The transient nature of the flux through the trehalose pathway is consistent with the existence of two stable states in glycolysis, i.e. once the system has reached the viable steady state, the need for excessive ATP hydrolysis through futile trehalose cycling has disappeared. Thus, we suggest that trehalose cycling constitutes a transient futile cycle, large enough to push the system's dynamics into the functional steady state.

Different mechanisms contribute to robustness

Finally, we examined the contribution of various aspects of trehalose metabolism to establish proper glycolytic functioning, through random sampling of initial conditions in the full kinetic model (Fig. 2.8). Whereas the combined trehalose cycling and negative (trehalose 6-phosphate mediated) feedback on hexokinase resulted in 100 % viability in the wild-type version of the model, futile cycling of trehalose alone resulted in a regular steady state in 76 % of the sampled cases. Removal of G6P without P_i release (only possible *in silico*) resulted in a functional state in 4 % of the cases. This shows that phosphate recovery is the primary safety mechanism, with hexokinase inhibition also contributing. The reported inhibition of trehalose synthesis by P_i [19] reinforces this picture as low P_i concentrations will relieve inhibition and ensure P_i mobilization. These results provide a strong basis for the (re)interpretation of population-level phenotypes of various mutants in trehalose metabolism and hexokinase (see Chapter 1 and Chapter 7).

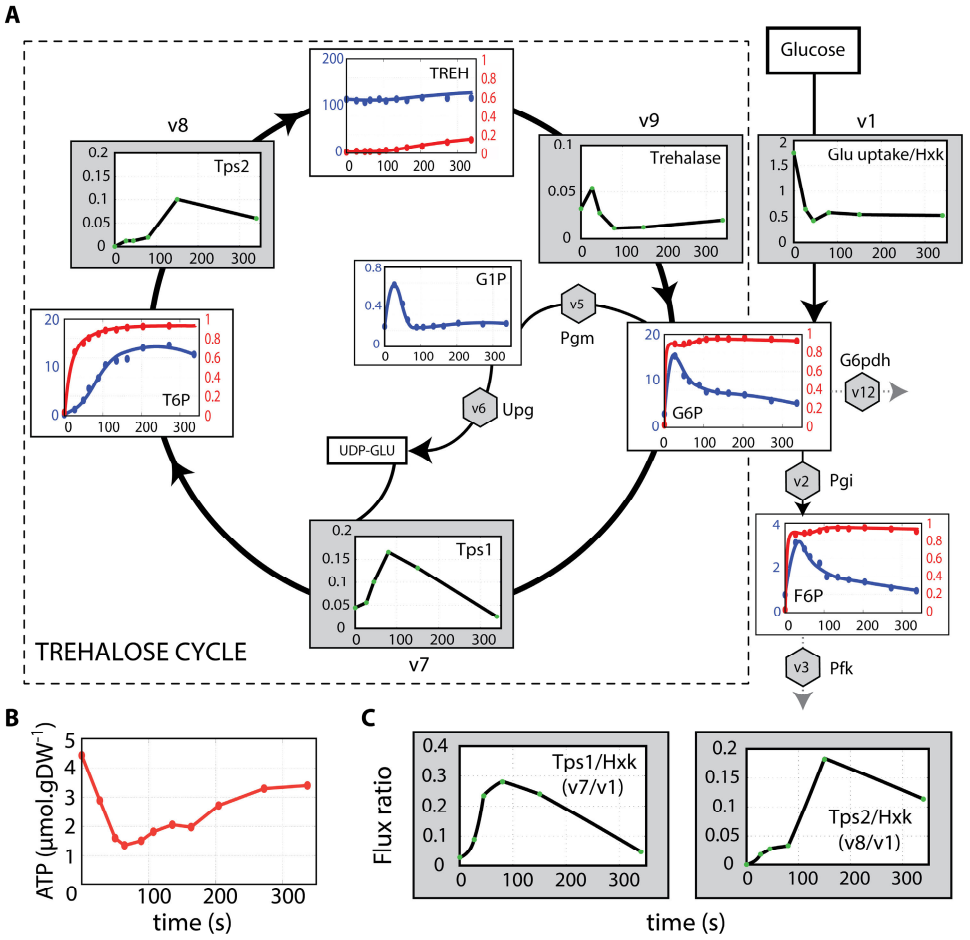

Figure 2.7. **^{13}C tracer enrichment reveals highly dynamic flux distributions through the trehalose cycle.** (A) A selection of data (for complete dataset see Chapter 6), superimposed on the trehalose cycle. White boxes contain metabolite data, with concentrations (µmol.gDW^{-1}) in blue and tracer enrichment (fraction) in red (symbols represent measurements, lines represent model fits); x-axes show time in seconds. Grey boxes show flux profiles (µmol.gDW^{-1}.s^{-1}) of the indicated reactions in time (s). (B) ATP concentration profile show a response time similar to that of flux channeling towards the trehalose pool via the Tps1 reaction. (C) Dynamic flux ratios of Tps1 (v7) and Tps2 (v8) relative to Hxk (v1) show that up to 28 % of glucose is dynamically routed into trehalose metabolism.

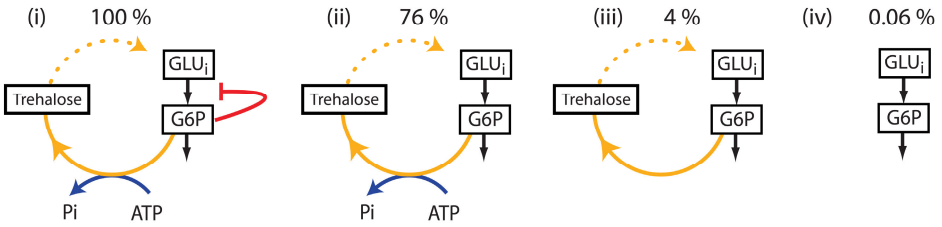

Figure 2.8. Different aspects of trehalose metabolism contribute to the overall probability to reach the functional steady state. Percentage of balanced steady states found with randomly-sampled initial conditions as input for different features of the trehalose cycle.

Startup of glycolysis requires dynamic regulation

From our work a dynamic picture emerges where the organization of glycolysis in an ATP-investing upper and ATP-producing lower part provides a major challenge for robust start-up upon activation. After environmental changes (e.g. nutrition, hormone, drug etc.), proper steering through a dynamic landscape consisting of undesired states requires specialized regulatory mechanisms. Our work shows that phosphate dynamics are an essential determinant of the state that is reached. As existing glycolytic models ignored P_i dynamics, the co-existence of two states in glycolysis was not previously discovered.

The core model demonstrated that mostly generic features of glycolysis give rise to this two state outcome, in particular: (i) its stoichiometry in ATP consumption and production; and (ii) the (universal) equilibrium constants of phosphofructokinase (large; allowing accumulation of FBP) and Gapdh (small; requiring high P_i levels to drive the reaction). In yeast, trehalose metabolism apparently provides protection against the imbalanced state, albeit not 100 % failsafe based on flow cytometry (Fig. 2.4C); the observed failure of wild-type (~7 %) could reflect a trade-off between different aspects of the transition to high sugar, as a higher success rate will require tighter regulation or higher futile cycling that will make startup slower or more costly, respectively.

Other systems, notably mammalian cell types, have adopted alternative mechanisms that may function to prevent glycolytic imbalance. In human cell types, feedback inhibition of hexokinase or glucokinase, either by the product glucose 6-phosphate (muscle) or a glucokinase-regulatory protein (liver), are well-known regulatory mechanisms for glycolysis [53]. Pancreatic beta-cells seem to have no protective mechanism, but have low glucokinase activity that would prevent the upper part of

glycolysis from being too fast. Upon overexpression of hexokinase, these cells exhibit a similar metabolic imbalance to that observed in yeast *tps1Δ* mutants [28], providing relevance for this state in mammalian metabolism.

Our findings have major implications for biotechnological applications and disease. In biotechnology, poor mixing in large-scale fermenters causes dynamic conditions which –often in combination with genetic manipulations– may create conditions in which individual cells behave very different from the measured population average. In disease, cancer in particular, the regulation of glycolysis has recently regained great interest due to the Warburg effect, characterized by an enhanced glycolytic flux and lactate production [54]. Our work provides systems-level insight into the dynamic regulation of glycolysis. As an example, feed-forward activation of pyruvate kinase (PK) by FBP is impaired in the PKM2 splice variant that replaces the original PKM1 protein in many cancer cells [55]. Such feed-forward activation of pyruvate kinase by FBP, observed from bacteria to man, could act as an additional safety mechanism to prevent a metabolic imbalance in glycolysis: FBP activation would help to accelerate the lower part of glycolysis if FBP starts to accumulate. Indeed in all our models, removing the positive feedback on pyruvate kinase enhanced the probability to reach imbalance. Intriguingly, PKM2 expression in tumors coincides with an alternative phosphoglycerate mutase activity that instead of ATP produces P_i from PEP [56]. Such an activity would fit with the role of P_i release to ensure robust functioning of glycolysis. Interfering with protective mechanisms against the metabolic imbalance state in tumor cells, or perhaps, counter-intuitively, enhancing glucose uptake rather than inhibiting it, may provide rationales for sophisticated treatment strategies.

Appendix A | Core model of glycolysis

We developed a core model to understand the main properties of the biochemically detailed kinetic model. The core model also shows the co-existence of two states as the detailed model and explains (1) why the lack of feedback on FBP is required for an imbalanced state, (2) how FBP can accumulate while ATP and P_i are at steady state, (3) the relationship between phosphate homeostasis and an imbalanced state and (4) the disappearance of an imbalanced state upon enhanced activity of the ATPase or glycerol branch. A schematic representation of the core model is depicted in Fig. A.1. The corresponding differential equations are:

$$\dot{FBP} = v_1(ATP) - v_2(ATP, FBP, P_i) - v_5(FBP) \quad \text{(EA.1)}$$

$$\dot{ATP} = -2v_1(ATP) + 4v_2(ATP, FBP, P_i) - v_3(ATP) \quad \text{(EA.2)}$$

$$\dot{P_i} = 0 - 2v_2(ATP, FBP, P_i) + 2v_5(FBP) + v_3(ATP) + v_4(P_i) \quad \text{(EA.3)}$$

We made the dependencies of the reaction rates on the involved substrates and products explicit, e.g. $v_1(ATP)$ indicates that reaction 1 is sensitive to ATP (we will usually exclude the dependencies below). Note that the synthesis reaction of FBP, implemented as a simplified kinetic description of the glucose transporter and hexokinase, is insensitive to FBP, which mimics the situation of a *tps1Δ* mutant strain where regulation of Hxk is absent and, moreover, phosphofructokinase (Pfk) is kinetically insensitive to its product, FBP, in yeast [57].

Stable and attracting states

We are interested in showing that this system, given suitable kinetics, can reach two states; one of the stable solutions is a normal steady state and the other corresponds to an imbalanced state, in which FBP continuously accumulates while P_i and ATP remain constant. The definition of a steady-state or the equilibrium of a dynamical system is where all derivatives are equal to 0 (in this case

$\dot{FBP}=0, \dot{ATP}=0$ and $\dot{P_i}=0$). Equilibria can be attracting or repelling, which means that the system evolves towards the equilibrium or away from it (in the figures attracting equilibria are shown as closed dots while repelling equilibria are shown as open dots). The imbalanced state is technically not a steady state or equilibrium, since FBP is continuously increasing and therefore $\dot{FBP} > 0$. However, the other metabolites are in steady state ($\dot{ATP}=0$ *and* $\dot{P_i}=0$) and some of these imbalanced states are attracting. [1] The system can evolve towards these attracting imbalanced states and therefore they are biologically relevant.

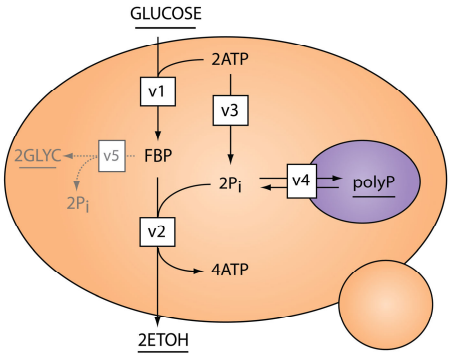

Figure A.1. Depiction of the core model of glycolysis, representing *tps1Δ* mutants. Underlined metabolites are held fixed. Rates of reactions are denoted by a "v" with the reaction number as an index. polyP denotes phosphate storage. The glycerol branch, shown in grey, is omitted from the analysis detailed in the main text and Fig. A.2.

The normal steady-state

A steady state of the entire system, i.e. when $\dot{FBP}=0, \dot{ATP}=0$ and $\dot{P_i}=0$, is only possible if $v_4=0$, because $2\dot{FBP}+\dot{ATP}+\dot{P_i}=v_4$ (the sum $2FBP+ATP+P_i$ depicts the total phosphate content of the system). The rate of phosphate exchange (v_4) is 0, because the whole system does not consume or

[1] Moreover, mathematically a straightforward variable transformation φ -> FBP/(K+FBP) would result in φ=1 and dφ/dt = 0 when FBP goes to infinity and all requirements for a true fixed point (or equilibrium point) would be met. Yet, in biology, it is FBP that continuously accumulates.

produce phosphate, whereas in the imbalanced state phosphate is continuously mobilized with $v_4 \neq 0$. Since v_4 depends on P_i only, $v_4 = 0$ defines the steady-state concentration of P_i, which we denote by P_T. Since $v_4 = 0$ implies a linear combination of differential equations is 0, the steady state concentrations of FBP and ATP can be calculated from two more nullclines:

$$\dot{ATP} = -2v_1(ATP) + 4v_2(ATP, FBP, P_T) - v_3(ATP) = 0 \quad \text{(EA.4)}$$

$$\dot{P_i} = -2v_2(ATP, FBP, P_T) + 2v_5(FBP) + v_3(ATP) + v_4(P_T) = 0 \quad \text{(EA.5)}$$

These two equations allow for a graphical exploration of the steady states of the system in the (ATP,FBP)-plane, which we shall illustrate below.

The imbalanced state

One of the curious features of the imbalanced state is that while ATP and P_i attain a steady state value, FBP accumulates. We will show with the core model how this is possible and that the phosphate that accumulates as a component of FBP, leads to a relation between $\dot{FBP}$ (the FBP accumulation rate) and v_4 in the imbalanced state. FBP accumulates in the imbalanced state (denoted by $FBP_{\to\infty}$), therefore, since FBP is a substrate for reaction 2 and 5, the corresponding enzymes will quickly become saturated with FBP and consequently become insensitive to its concentration. If we write the resulting rate equations as $\hat{v}_2(ATP, P_i) = v_2(ATP, FBP_{\to\infty}, P_i)$ and $V_{5,max} = v_5(FBP_{\to\infty})$, we obtain the following conditions for the imbalanced state:

$$\dot{FBP} = v_1(ATP) - \hat{v}_2(ATP, P_i) - V_{5,max} > 0 \quad \text{(EA.6)}$$

$$\dot{ATP} = -2v_1(ATP) + 4\hat{v}_2(ATP, P_i) - v_3(ATP) = 0 \quad \text{(EA.7)}$$

$$\dot{P}_i = -2\hat{v}_2\left(ATP, P_i\right) + 2V_{5,\max} + v_3\left(ATP\right) + v_4\left(P_i\right) = 0 \qquad \text{(EA.8)}$$

This analysis demonstrates why the insensitivity of v_1 to FBP is a key feature of the imbalanced state; if v_1 would be sensitive to FBP this inhibition would prevent the accumulation of FBP ($\dot{FBP} > 0$ would not hold), and a regular steady state would result. We can use these equations for a graphical exploration of the imbalanced states in the (ATP, P_i)-plane, which we shall illustrate below. Furthermore, in the imbalanced state, we have:

$-1/2\dot{ATP} - 1/2\dot{P}_i = v_1 - \hat{v}_2 - V_{5,max} - 1/2v_4 = \dot{FBP} - 1/2v_4 = 0$ (since $\dot{ATP} = \dot{P}_i = 0$), and therefore $\dot{FBP} = 1/2v_4$. It is logical that the FBP accumulation occurs at half the rate at which phosphate is released from the vacuole, because FBP contains two phosphate groups per molecule.

We can conclude from this section that in the imbalanced state ATP and P_i can reach a steady state while FBP accumulates with a rate equal to half the vacuolar export rate of phosphate, and this can only occur when feedback inhibition on v_1 is lacking (as in yeast glycolysis). In our detailed kinetic wild-type model inhibition on Pfk by FBP is still lacking, but T6P inhibition on Hxk serves to slow down substrate supply for Pfk, making the imbalanced state in the wild-type less likely to occur (Chapter 3, Fig. 3.4).

The importance of phosphate homeostasis

The above insights highlight an important feature of phosphate homeostasis which is central to the imbalanced state. At the normal steady state, there is no net exchange of P_i between cytosol and the vacuole, whereas a key feature of the imbalanced state is the continued import of P_i into the cytosol from the vacuolar storage pool; a process which sustains the accumulation of FBP. Most models of glycolysis do not include P_i as a free variable, but rather completely ignore it or keep it fixed at a measured value. In these cases, there is no moiety conservation of phosphate, because either reactions are not phosphate-balanced or there is an infinite source of phosphate. Such models are unlikely to show an imbalanced state, as the Gapdh reaction will have unlimited P_i. Recent models with P_i as a free variable, such as in two lactic acid bacteria [58] or in muscle [59], do have a conserved moiety of total phosphate; consequently, glycolytic imbalance can potentially occur, but only if exchange of phosphate with either vacuolar storage or external environment is possible.

Without such exchanges, continuous accumulation of FBP cannot occur; imbalance in glycolysis would result in a complete depletion of ATP and P_i, and a stop in FBP accumulation.

A kinetic parameterization of a core model that displays imbalanced states or steady states depending on initial conditions

In the previous section, we carried out an initial analysis of the core model in both a regular steady state and an imbalanced state. In this section, we will present a kinetic parameterization of the core model that will either end up in the imbalanced state or steady state depending on the initial conditions. In Table A.1, the rate equations and the kinetic parameters are summarized.

In Fig. A.2, the dynamics of the core model are shown for two different sets of initial conditions (specified in Table A.1). The phase plane plots (Fig. A.2, top panels) show the balanced and imbalanced state as intersections of the graphs $dP_i/dt = 0$ and $dATP/dt = 0$. Calculations for the phase plane plots were facilitated by the use of a variable transformation, $\phi = FBP/(FBP + K_{M,LG,FBP})$ (where LG = lower glycolysis). This variable transformation ensured that all time derivatives of internal metabolite concentrations were equal to zero in the balanced and imbalanced state – to simplify numerical analysis – and that saturating FBP concentrations are defined by $\phi = 1$. The phase plane plots were constructed by solving the $dP_i/dt = 0$ and $dATP/dt = 0$ for ϕ (using Mathematica with the Solve function) for different concentrations of ATP. The flow diagrams were created by calculating the time derivatives for P_i and ATP for different concentrations of P_i and ATP and subsequently using the Mathematica function ListStreamPlot.

In one case (Fig. A.2B), the system evolves towards a regular steady state where all the concentrations become constant. Note that phosphate becomes equal to the concentration in the vacuole, which was set to 10 mM (Table A.1). In the second case (Fig. A.2A), only ATP and Pi reach a steady state while FBP accumulates. Phosphate reaches a level below 10 mM, resulting in the net export of phosphate from the vacuolar compartment, i.e. $v_4 > 0$. In addition, the ATP level drops to a lower value than that of the regular steady state, which is also in agreement with the experimental data. The initial condition-dependent behavior, shown in Fig. A.2, illustrates the co-existence of two stable states in the core model, as was found in the detailed model (Chapter 2, Fig. 2.2 and Chapter 3, Fig. 3.4).

Table A.1. Kinetic parameterizations of the core model of yeast tps mutants[§]

Rate equations	
"Transporter +Hxk +Pfk"	$v_1 = V_{max,1} \frac{ATP}{ATP\left(1+\frac{ATP}{K_{1,i,a}}\right)+K_{1,a}}$
"Lower glycolysis"	$v_2 = V_{max,2} \frac{FBP}{FBP+K_{2,f}} \frac{\frac{(a_T - ATP)}{K_{2,ADP}} \frac{P_i}{K_{2,p}}}{\left(1+\frac{ATP}{K_{2,ADP}}\right)\left(1+\frac{P_i}{K_{2,p}}\right)}$
"ATPase"	$v_3 = k_3 ATP$
"Vacuole phosphate export"	$v_4 = k_4 (P_T - P_i)$
"Glycerol branch"	$v_5 = V_{max,5} \frac{FBP}{FBP+K_{5,FBP}}$
Kinetic parameters[§]	
"Transporter +Hxk +Pfk"	$V_{max,1} = 10, K_{1,i,a} = 3, K_{1,a} = 0.1$
"Lower glycolysis"	$V_{max,2} = 10, K_{2,f} = 1, K_{2,ADP} = 0.1, K_{2,p} = 2, a_T = 5$
"ATPase"	$k_3 = 10$
"Vacuole phosphate export"	$k_4 = 0.3, P_T = 10$
"Glycerol branch"	$V_{max,5} = 1^*, K_{5,f} = 1$
Initial conditions	
Regular steady state	$FBP = 2, ATP = 1, P_i = 10$
Imbalanced state	$FBP = 0.01, ATP = 0, P_i = 0.01$

[§]Even though this is a core model and not all parameters can be identified with real constants, all affinity constants and maximal rate constants have been assigned realistic values. Units: concentrations are in mM (per liter cytosol) and time in minutes. *In Chapter 2 and Fig. A.2 the model without the glycerol branch (i.e. $V_{max,5} = 0$) is used.

Graphical exploration of the steady states

In the steady state we have the condition $2\dot{FBP} + \dot{ATP} + \dot{P_i} = v_4(P_i) = 0$ which implies $P_i = P_T$. Therefore we can show the isoclines $\dot{P_i} = 0$ and $\dot{ATP} = 0$ in the plane $P_i = P_T$ to determine the concentrations of ATP and FBP in the steady state (Fig. A.2B). A similar analysis can be done for the imbalanced state (Fig. A.2B). In the latter case, the concentration of FBP is set to infinity such that the rate equations become saturated and are not dependent on FBP, as explained above. The steady state

concentrations for P_i and ATP can then be determined from the $\dot{P}_i = 0$ and $\dot{ATP} = 0$ nullclines (Fig. A.2A).

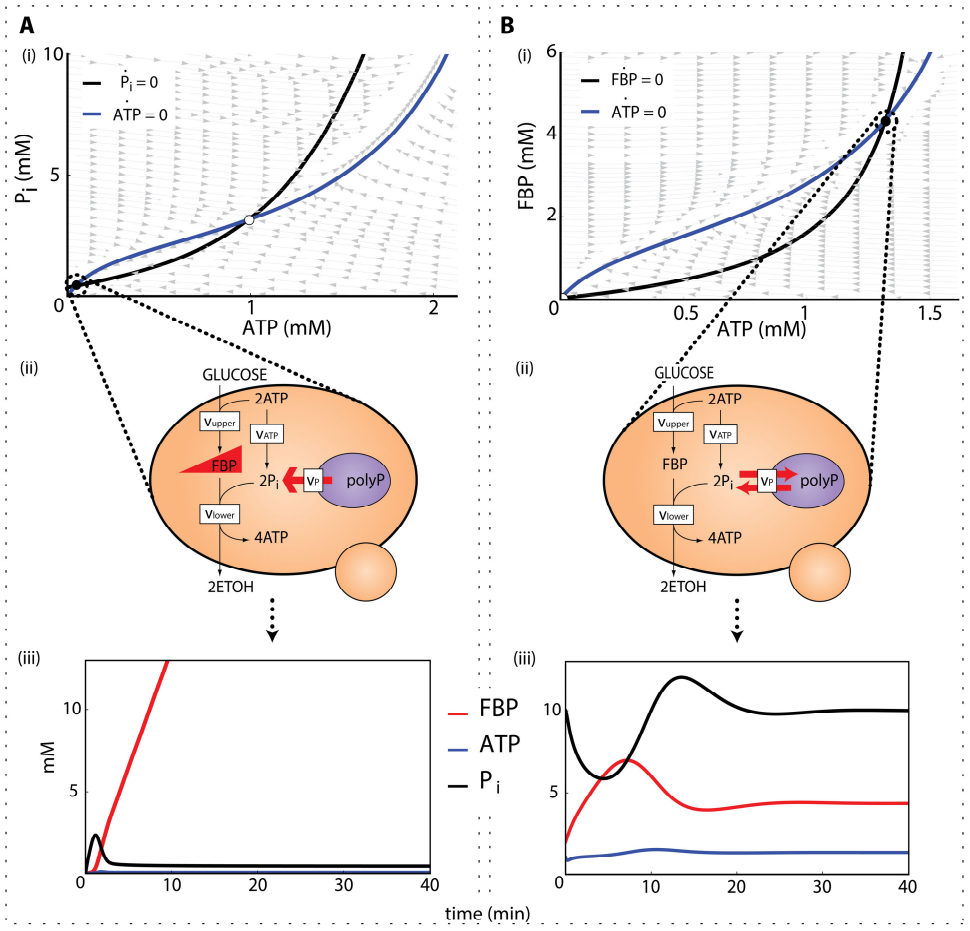

Fig. A.2. Nullcline plots indicate states where the concentrations of FBP, ATP and/or P_i are balanced. (A) In the imbalanced state FBP is saturatingly high and therefore we can find the imbalanced states in the plane FBP = infinity. (i) The intersection of the nullclines $\dot{ATP} = 0$ and $\dot{P}_i = 0$ show the imbalanced state where ATP and P_i are balanced. (ii) In this state P_i mobilized from the vacuolar stores sustains the continued accumulation of FBP (iii). (B) Steady states are found where the nullclines of $\dot{ATP} = 0$ and $\dot{FBP} = 0$ intersect under the condition that $P_i = 10$.

The glycerol branch and the ATPase reaction are both rescue mechanisms in the core model

In the literature several mechanisms that lead to the "rescue" of the *tps1Δ* mutant, i.e. the disappearance of the metabolic imbalance, are described (summarised in Chapter 1). Here we illustrate one well-described rescue mechanism (enhanced activity of the glycerol branch) and a newly discovered one: increased ATPase activity. In Figure A.3, the response of the core model to either an increase in ATPase activity (Fig. A.3A and B) or increased glycerol branch activity (Fig. A.3C and D), at conditions that normally result in an imbalanced state, is shown.

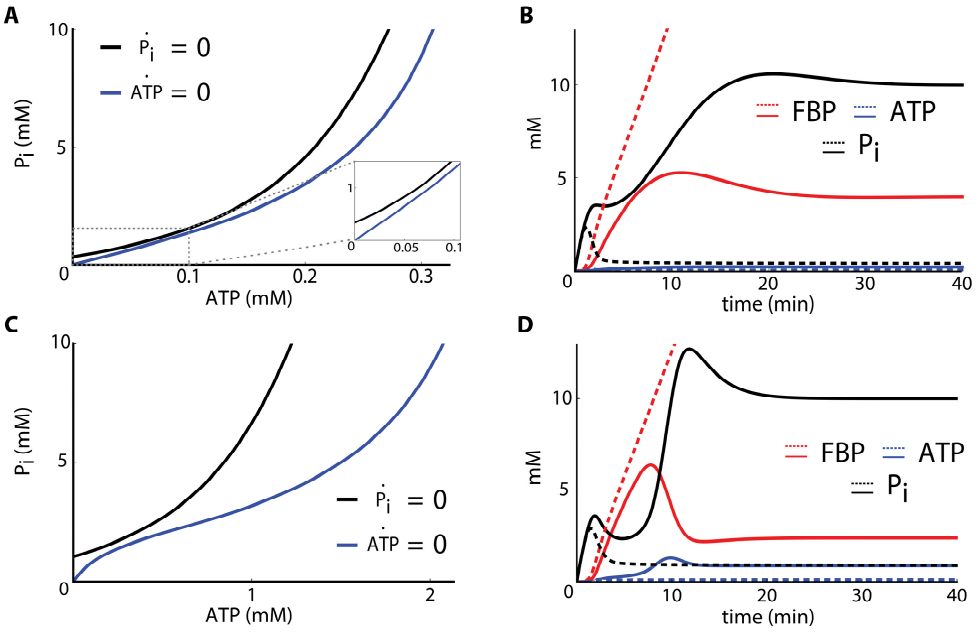

Fig. A.3. Enhancement of ATPase or glycerol branch activity leads to disappearance of the metabolic imbalance. (A) When ATP hydrolysis is increased (6 fold) the intersection of the nullclines at saturating FBP disappears, consequently an imbalanced state no longer exists. Although not visible in (A), a steady state exists with $\dot{ATP} = \dot{P_i} = \dot{FBP} = 0$. This steady state is shown as solid lines in (B), for initial values that would lead to an imbalanced state when k_{ATPase} is low (dashed lines). (C) and (D) Increasing the maximal activity of the glycerol branch from 1 to 2 mmol.L^{-1}. min^{-1} similarly removes the imbalanced state.

3 Kinetic model of glycolysis

Meike T. Wortel, Johan H. van Heerden & Bas Teusink

INTRODUCTION

In the Chapter 1 we summarized the primary mechanistic interpretations of the trehalose cycle's role in the regulation of glycolysis. The summary highlighted several paradoxical results which has made the regulatory function difficult to understand. In this thesis we used a kinetic model of glycolysis to explore putative regulatory contributions in the context of the entire glycolytic pathway, taking into account systemic properties which can be missed when looking at trehalose pathway components in isolation.

This chapter provides details on the kinetic model of glycolysis that informed many of the theoretical insights presented in this thesis. We started by updating an existing model, originally published by Teusink *et al.* [41], modifying rate equations with parameter values that were recently determined under *in vivo*-like conditions [60]. To explore the consequences of a defective trehalose cycle, we defined a simplified representation of this pathway and included feedback inhibition on Hxk. In addition, we defined phosphate as a free variable and included a non-cytoplasmic phosphate sink.

We show that the model can reproduce the most relevant metabolic features of the *tps1Δ* phenotype (ATP and P_i depletion, FBP accumulation and a low glycolytic flux). In addition, we demonstrate the existence of initial condition-dependent bistable behaviour for both tps1Δ (TPS) and WT formulations of the model. Depending on initial conditions, we find that the tps1Δ model could also achieve normal glycolytic function, similar to the WT model, while the WT model could end up in a *tps1Δ*-like state. As the metabolic phenotype of *tps1Δ* mutants is expected to be incompatible with growth, we took this observation to suggest the possibility that two physiologically distinct phenotypes, viable and non-viable, could appear in a population after a sudden glucose challenge.

MODEL DETAILS

Method

The kinetic model was implemented and analysed using Mathematica 9.0 (Wolfram Research). Time simulations were performed with the NDSolve function. A steady state is defined as a state, characterized by the metabolite concentrations, where all time derivatives of internal metabolite concentrations are equal to zero. Steady states were calculated by solving these equalities with the FindRoot function, where metabolite concentrations after 250 simulation minutes, were used as initial inputs.

The detailed kinetic model is available as a digital supplement in SBML (Systems Biology Markup Language) format. In addition, an interactive Web application is provided at www.falw.vu/~mworte/tpsmodel/ [2] and can be used to explore the effects of variations in several parameters on the detailed kinetic model.

Mimicking T6P-mediated hexokinase inhibition

Firstly, we introduced a proxy for the inhibition of Hxk by T6P. Since most of the study deals with the mutant case where this inhibition is actually absent, we only incorporated this feedback loop in a coarse-grained fashion, to have a representation of wild type to benchmark against. Since T6P is not explicitly defined in the model and the magnitude of change in the G6P pool is similar to that of T6P dynamics [61], we used the G6P levels as a proxy to simulate the inhibition of Hxk by T6P (E3.1). Several different values are reported for the T6P inhibition constant of Hxk [24]. We decided to use the average of 0.04 mM and 0.1 mM (see [24] for details), i.e. 0.07 mM (Table S1). The rate equation for Hxk becomes:

$$v_{Hxk} = \frac{v_{max,Hxk}\left(\frac{ATP \cdot GLU_i}{k_{ATP} \cdot k_{GLU_i}} - \frac{ADP \cdot G6P}{k_{eq,Hxk} \cdot k_{ATP} \cdot k_{GLU_i}}\right)}{\left(\frac{ADP}{k_{ADP}} + \frac{ATP}{k_{ATP}} + 1\right)\left(\frac{G6P}{k_{i,G6P}} + \frac{G6P}{k_{G6P}} + \frac{GLU_i}{k_{GLU_i}} + 1\right)} \quad \text{(E3.1)}$$

After the introduction of Hxk inhibition, the V_{max} of the transporter (Table S3.1) was increased in order to restore the flux to the originally published level. This adjustment is in agreement with the

[2] At the time of writing, the Wolfram CDF player does not launch properly in Google's Chrome browser. To use the application, Mozilla Firefox or Microsoft Internet Explorer is recommended.

observation made by Teusink and colleagues, that the glucose transport rate was most likely underestimated by the zero-*trans* influx assay employed [41]. Additionally, we improved the trehalose and glycogen branches by making the fluxes dependent on the G6P concentration (defined as k*G6P) (Table 3.1). Although our implementation of feedback on Hxk is a simplification of trehalose branch mediated inhibition, it represents a design that is also compatible with other glycolysis systems, such as in mammalian muscle and brain cells, were Hxk is directly and strongly inhibited by G6P [62–65].

Introducing inorganic Phosphate as a free variable

Because phosphate dynamics is a key feature of the *tps1Δ*-mutant's phenotype, we included phosphate (P_i) as a free variable. P_i exchange with the vacuole, which functions as an intracellular store [40, 66], is modelled as a diffusion reaction with an equilibrium concentration of P_i in the cytosol of 10 mM, identical to the value originally fixed in the model (E3.2). This ensures that P_i is a dynamic variable, but reaches the original 10 mM at any global steady state. Since the phosphate concentration (stored as polyphosphates) in the vacuole is expected to be much higher (up to 20 % dry weight, see [67]) than the cytosolic concentrations, we did not model the vacuolar pool and kept it as a fixed external metabolite. The rate constant (k_{Phosex}) (see E3.2) for this equation directly influences the rate of FBP accumulation in the TPS model (Fig. 3.2). Consequently, we chose the rate constant such that the FBP accumulation was in agreement with data from Hohmann *et al.* [24] , in the regime where the rate of accumulation was maximal (Table 3.1).

$$v_{\mathrm{Phosex}} = k_{\mathrm{Phosex}} \cdot (P_T - P_i) \tag{E3.2}$$

In addition, we adjusted the rate equation for Gapdh to include P_i and assumed a K_m of phosphate of 1 mM (E3.3).

$$v_{\mathrm{Gapdh}} = \frac{C_{\mathrm{Gapdh}} \left(\frac{v_{\mathrm{max,Gapdh,f}} \cdot \mathrm{GAP} \cdot \mathrm{NAD} \cdot P_i}{k_{\mathrm{GAP}} \cdot k_{\mathrm{NAD}}} - \frac{v_{\mathrm{max,Gapdh,r}} \cdot \mathrm{BPG} \cdot \mathrm{NADH}}{k_{\mathrm{BPG}} \cdot k_{\mathrm{NADH}}} \right)}{(P_i + 1) \left(\frac{\mathrm{BPG}}{k_{\mathrm{BPG}}} + \frac{\mathrm{GAP}}{k_{\mathrm{GAP}}} + 1 \right) \left(\frac{\mathrm{NAD}}{k_{\mathrm{NAD}}} + \frac{\mathrm{NADH}}{k_{\mathrm{NADH}}} + 1 \right)} \tag{E3.3}$$

Introducing allosteric activation of Pyruvate kinase

The activation of Pyk by FBP has been shown be important in regulating lower glycolytic flux [68] and since FBP potentially accumulates in the *tps1Δ*-mutant, we adjusted the Pyk rate equation accordingly (E3.4). We retained the originally measured V_{max} values from [41] and implemented the other parameters as reported by [68] (Table 3.1).

$$v_{Pyk} = \frac{v_{max,Pyk} \cdot \frac{PEP}{k_{PEP}} \left(\frac{PEP}{k_{PEP}} + 1 \right)^{n-1}}{k_{PEP} \left(L_{0,Pyk} \left(\frac{\frac{ATP}{k_{ATP}} + 1}{\frac{FBP}{k_{FBP}} + 1} \right)^{n} + \left(\frac{PEP}{k_{PEP}} + 1 \right)^{n} \right)} \frac{ADP}{(ADP + k_{ADP})} \qquad \text{(E3.4)}$$

Increasing V_{max} of Pyruvate decarboxylase

Lastly, we addressed the observation that pyruvate accumulation under certain conditions is caused by an insufficient V_{max} of Pdc [41], which should be increased to reflect experimental measurements. We therefore increased the V_{max} of Pdc 6.1 fold (Table 3.1), as originally suggested by Teusink *et al.* [41] , which did indeed resolve this behaviour.

Initial metabolite concentrations

The original model was used for predictions of steady state profiles. In this work we were interested in the transient dynamics of the model and therefore we had to make some additional adjustments. Prior to perturbation with a glucose pulse, ethanol will not be present or will be very low, and consequently the ethanol concentration is set to 0 (in the original model, ethanol was fixed at 50 mM); this adjustment had a negligible influence on steady-state fluxes. For the simulations, we used initial metabolite values from a study by Fendt *et al*. [46]. Specifically, we used metabolite data for *S. cerevisiae* cells grown in batch cultures with excess galactose as carbon source, and sampled during mid-logarithmic growth (Table 3.2); this condition closely resembles our own experimental setup where cells were always pre-grown on galactose as sole carbon source (see Chapter 4).

Metabolite values were converted to mM (L cell volume^{-1}) concentrations, using a cell volume of 2 ml per gram dry weight (gDW). This conversion factor is very similar to the value arrived at by van Eunen *et al.* [60], and is calculated by assuming a single cell volume of 3 x 10^{-14} L (as in [60]) and a single cell weight of 1.5 x 10^{-11} gDW.cell^{-1} [69]. Missing metabolite values were calculated using the published steady-state flux distribution map in [46] and the rate equations from our kinetic model.

The sum of AMP, ADP and ATP has also been adjusted to the measurements from [46] (see Table 3.2).

Table 3.1. Parameter adjustments made to the detailed kinetic model of Teusink et al. [41]

Parameters	New Value	Original Value	Unit
$v_{max,Glt}$	198	97.264	mM min^{-1}
$k_{i,G6P,Hxk}$	0.07		mM
$k_{trehalose}$	2.32		min^{-1}
$k_{glycogen}$	5.8		min^{-1}
n_{Pyk}	4		
$L_{0,Pyk}$	60000		
$k_{PEP,Pyk}$	0.19	0.14	mM
$k_{ADP,Pyk}$	0.3	0.53	mM
$k_{FBP,Pyk}$	0.2		mM
$k_{ATP,Pyk}$	9.3	1.5	mM
$v_{max,Pdc}$	1062.58	174.19	mM min^{-1}
k_{Phosex}	0.1		min^{-1}
P_T	10		mM
AXP	3.1	4.1	mM
EtOH	0	50	mM
GLU_o	110	50	mM

Table 3.2. Initial values used in the kinetic model based on [46]

Metabolite	Initial value (mM)
GLU_i	0.087
G6P	3.085
F6P	0.752
FBP	0.836
BPG	0.111
P3G	0.825
P2G	0.138
PEP	0.140
PYR	0.884
ACE	0.047
TRIO (DHAP+GAP)	0.518
NADH	0.044
P_i	10
ATP	2.06
ADP	0.870
AMP	0.165

*****This value was not obtained from the Fendt and Sauer dataset [46], but corresponds to a steady state value reported by [70].

RESULTS

The new model largely reproduces and improves on the original model

The effect of the modifications introduced into the new model was evaluated by comparing the steady-state metabolite concentrations and fluxes to the original [41] model (Fig. 3.1). In general steady state profiles were very similar; the only clear exception was the steady state concentration of PYR, which accumulated to high concentrations in the original model. With the changes introduced here, PYR reached steady state levels that were more realistic and in line with physiological values [46, 71].

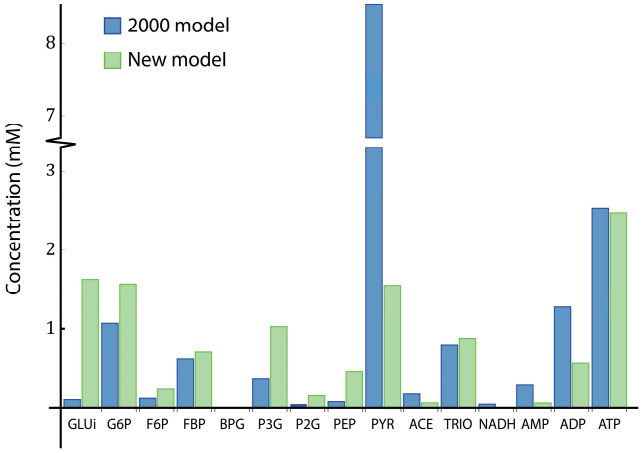

Figure 3.1. Steady-state metabolite levels of the metabolites for the original model [41] **and our adapted model with 110 mM extracellular glucose.** The fluxes through upper glycolysis are 88 (2000 model) and 86 mM min^{-1} in the model presented here, with the fluxes through lower glycolysis at 138 and 133 mM min^{-1} respectively (see Chapter 2, Fig. 2.1 for glycolysis scheme). The difference in intracellular glucose is due to the increase of the transporter V_{max} and the compensation by G6P inhibition of Hxk, the decrease in PYR concentration is due to the increased V_{max} of pdc and the difference in the total of AMP, ADP and ATP is a due to adjustments according to the Fendt and Sauer dataset [46] (Table 3.2). The levels of BPG are very low, but similar.

Simulating the *tps1Δ* phenotype

To mimic the *tps1Δ* mutant, we set the rate constant of the trehalose branch to 0, ensuring that the mass balance definitions of P_i, ATP and G6P to reflect this, and removed the feedback inhibition of G6P on Hxk. Simulations of the *tps1Δ* mutant with this version (TPS) of our model showed canonical metabolite profiles (Fig. 3.2A). While the fluxes within the higher and lower glycolysis modules become equal, the fluxes around FBP and the triose phosphates (TRIO) are unbalanced (Fig. 3.2B), causing the accumulation of FBP; we called this state an imbalanced state.

Rate of FBP accumulation in TPS model is proportional to P_i inflow

A key feature of the *tps1Δ* phenotype is the continued accumulation of FBP at low ATP and P_i concentrations. This behaviour indicates that cells are able to access alternative phosphate pools either from the extracellular space or from vacuolar phosphate stores, but clearly at a rate that is insufficient to support the glycolytic flux. Our choice to model the phosphate store as a "vacuolar compartment" is motivated by previous experimental observations [23, 40] that reported phosphate mobilization mainly from the vacuolar polyphosphate pool and not from the extracellular pool. The introduction of a phosphate exchange reaction allowed us to reproduce experimentally observed

accumulation of FBP. We found that the rate of phosphate import determines the rate of FBP accumulation. We used this observation to determine the rate constant for the exchange reaction based on a qualitative match between FBP accumulation in our model and experimentally determined FBP profiles (Fig 3.3).

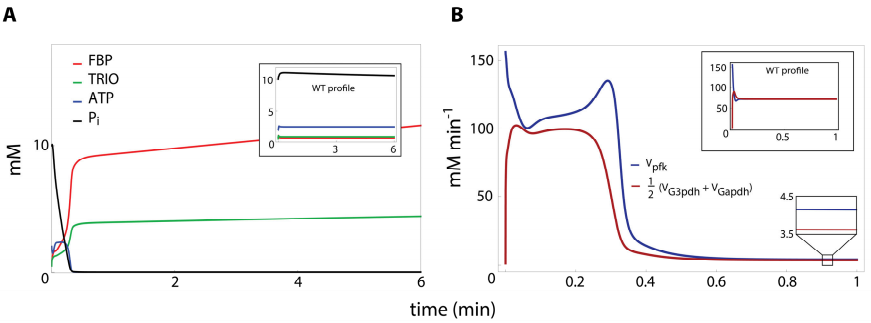

Figure 3.2. *In silico* phenotype of the *tps1Δ* mutant. Insets are profiles of wildtype model simulations. (A) Metabolite profiles of simulations of the TPS model. The *tps1Δ* mutant phenotype is simulated by setting the flux towards trehalose to 0, and eliminating the feedback on hexokinase. In the TPS model, FBP accumulates, while ATP and P_i are almost depleted. (B) Flux profiles of simulations of the TPS model around FBP and the triose phosphates (GAP + DHAP). The production of FBP by Pfk, and the triose phosphates (TRIO) by Ald is higher than the consumptions by Gapdh and G3pdh, causing a steady increase in FBP and the triose phosphates; this state is called an imbalanced state. In the wildtype model (inset), the production and consumption fluxes are equal, and the system reaches a normal steady state.

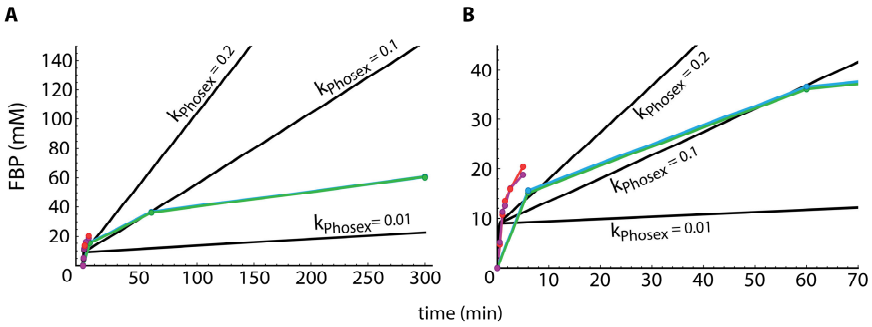

Figure 3.3. FBP dynamics in the TPS model are dependent on the rate of phosphate exchange. Long (A) and short (B) time simulations of FBP for different values of k_{Phosex} (black lines). The coloured dots and lines show previously published experimental measurements [21]. Eventually FBP accumulation slows down, presumably because of polyphosphate depletion in the vacuoles [40] (A, blue and green lines).

Initial condition-dependent outcomes and basins of attraction

Exploration of the dynamical behaviour of this system revealed bistable behaviour. We found that in both the TPS and WT variations of the model, two outcomes were possible. For the TPS model a normal steady state, with no FBP accumulation, high ATP and P_i levels and a high glycolytic flux, could be achieved with the same parameter set under different initial conditions (Chapter 2, Figure 2.2A). The same behaviour was seen for the WT model, where specific initial conditions led to the imbalanced state (Figure 3.4).

We found that initial phosphate concentrations had a significant impact on the outcome of model simulations, with high values leading to steady state solutions in the TPS model and low values leading to an imbalanced state in the WT model. We extended our evaluation by looking at the combined effects of differences in initial FBP and P_i concentrations on simulation outcomes. Whether initial conditions result in a balanced (normal steady state) or imbalanced state is shown in plots with basins of attraction (Figure 2.2A and Figure 3.4). The basins were calculated with time simulations of 250 minutes. The condition for a balanced (regular) steady state was: FBP concentration is not increasing in the last 10 % of the time simulation (using 7 significant digits) and the concentration of P_i is more than 0.5 mM. The latter criterion was defined to avoid classification of a zero-flux state as a steady state (which would be the case if phosphate becomes 0); initial conditions that did not fulfil these requirements were labelled as leading to the imbalanced state. The borders of the basins were calculated by finding the initial concentration of P_i on the separatrix between the basins for the balanced and imbalanced state, for several initial concentrations of FBP. From a predetermined interval of initial P_i concentrations, where the extremes lead to different states, the middle was classified as leading to a balanced or imbalanced state. This was repeated for the half of the interval that has extremes which lead to different states, until the size of the interval was less than 0.1 mM; the middle of this interval was then taken as the divider between the basins. Initial condition values for variables other than those depicted in figures were taken from Table 3.2.

SUMMARY

Biological circuits capable of producing bistable behaviours have been associated with the appearance of distinct phenotypic states, such as in the development and differentiation of many eukaryotic cells [43, 72] or spore formation in some bacteria [42]. More recently, bistability in metabolic signalling circuits have also been implicated in the appearance of distinct metabolic states in populations of otherwise isogenic cells [36, 73]. In this regard, we wondered whether the identified bistability produces to two phenotypically distinct subpopulations in an experimental setting.

In Chapter 4, we describe the experimental methods used to explore the physiological consequences of the identified bistability. We present evidence that two metabolic states indeed appear in both wild-type and *tps1Δ* mutant populations of *S. cerevisiae* following glucose pulse perturbations.

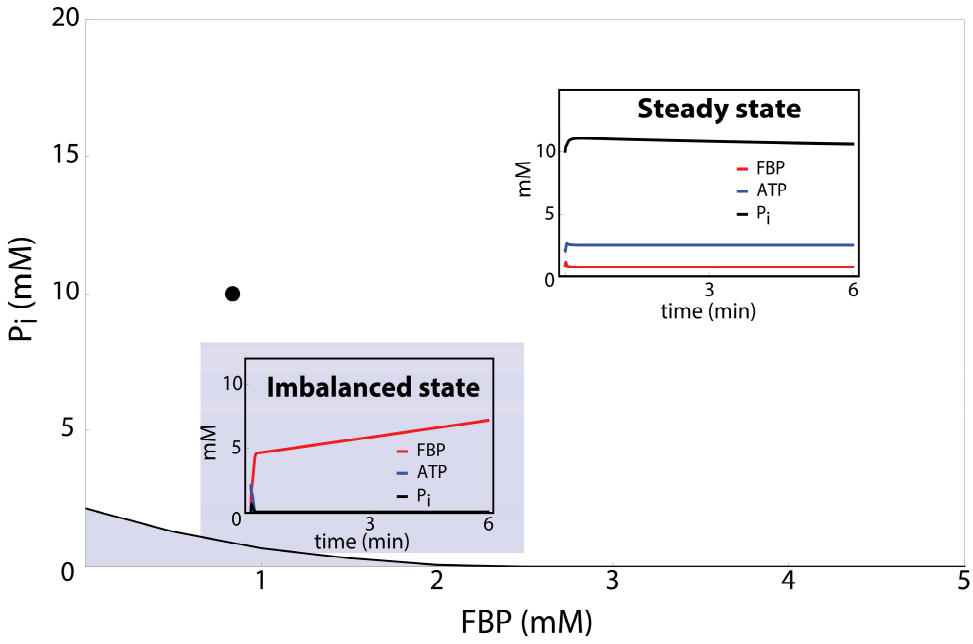

Figure 3.4. Basins of attraction in the wild type formulation of model with simple feedback of G6P on Hxk. The basin is much smaller than in the TPS model (Chapter 2, Fig. 2.2). The bistability is not an artefact of a model without feedback, but also occurs in a model with a simple feedback. Experimental data (Chapter 2, Fig. 2.4C) suggests an underestimation of the *in vivo* size of the basin of attraction in WT cells; a discrepancy that is not unexpected given the simplified approximation of the trehalose pathway in our model.

4 Identification and characterization of phenotypic subpopulations

Johan H. van Heerden, Yves J.M. Bollen, Tom G. O'Toole & Bas Teusink

INTRODUCTION

The kinetic model described in Chapter 3 exhibited initial-condition dependent behaviour, with two possible outcomes at high extracellular glucose concentrations. A regular steady state, with balanced fluxes and metabolite concentrations was found to co-exist with a second state characterised by low ATP and P_i concentrations and a low overall pathway flux; the second state arise as a consequence of a flux imbalance between the upper- and lower-glycolytic parts. Our analysis showed that a trehalose pathway is required to avert this imbalance, but this is not guaranteed under all conditions. Furthermore, the metabolic features of the imbalanced state suggested that it would be incompatible with growth. As many other bistable phenomena have been shown to underlie the appearance of distinct phenotypic states, we wondered whether the two metabolic states predicted by our model would also appear in *S. cerevisiae* populations challenged with a sudden increase in glucose supply.

In this chapter we present experimental evidence demonstrating that two metabolic subpopulations, viable and unviable, do indeed appear after glucose perturbations. We show that without a functional trehalose cycle the majority of cells end up in the imbalanced state; this is the primary fate of *tps1Δ* mutants. However, we also find that other factors can influence the fate of cells and suggest a hypothetical framework that could consolidate our experimental findings with the initial condition-dependent behaviour of the glycolysis model.

MATERIALS AND METHODS

Strains, media and growth conditions

S. cerevisiae strains based on the BY4743 background (MATa/α his3Δ1/his3Δ1 leu2Δ0/leu2Δ0 LYS2/lys2Δ0 met15Δ0/MET15 ura3Δ0/ura3Δ0) were used to characterize growth behaviour and subpopulation dynamics (Table 4.1). The W303-1A background was used to evaluate the effects of Hexokinase 2 (Hxk2) overexpression (Table 4.1). All growth experiments were performed at 30 °C using a defined mineral medium (CBS) (see [60] for reference) with required amino acid supplements, buffered to pH 5 (30 mM Sodium-Citrate/Citric Acid buffer) and supplemented with either 2 % galactose (CBS-GAL) or 2 % glucose (CBS-GLU); where other compounds were added, details are provided in the text. CBS plates were made by addition of 1 % agarose to the growth medium. For all plating experiments, plates were incubated for 2-3 days at 30 ˚C. Medium lacking a carbon source (CBS-C) was used as a wash and resuspension buffer throughout.

Strain constructions

All yeast transformations were performed according to [74]. The pYES-PACT1-pHluorin plasmid described in [75] was kindly supplied by G. Smits. The plasmids for Hxk2 overexpression described in [31] were kindly supplied by J. Thevelein.

Microtitre growth experiments

Growth behaviour in response to different carbon sources and various perturbing agents was monitored using 96-well microtitre plates. All inoculums, unless stated otherwise, were derived from single colony isolates. Glycerol stocks were streaked out onto YEP + 2 % galactose agar plates (1 % Yeast Extract, 2 % Peptone, 2 % agar) and incubated at 30 °C. After 2-3 days, single colonies were isolated directly from the plates and resuspended in CBS-C. Optical densities (OD_{600}) were adjusted to be in the order of 0.1. Each suspension (biological replicate) was divided such that it could be subjected to all permutations within a single experiment. Once carbon sources, and where applicable other perturbing agents, were added, microtitre wells were filled with 300 µl of prepared culture and growth was monitored as a change in optical density (OD) at 600 nm (OD_{600}), using either a SpectraMax Plus384 (Molecular Devices) or Multiskan Go (Thermo Fischer Scientific) microplate spectrophotometer. All experiments were done with at least 2 biological replicates per condition. All growth profiles are presented as the average of biological replicates, unless stated otherwise.

Table 4.1. *S. cerevisiae* strains used in this work

Strain	Genotype	Source
BY4743 (WT)	MATa/α his3Δ1/his3Δ1 leu2Δ0/leu2Δ0 LYS2/lys2Δ0 met15Δ0/MET15 ura3Δ0/ura3Δ0	EUROSCARF
tps1Δ	BY4743; Mat a/α; his3Δ1/his3Δ1; leu2Δ0/leu2Δ0; lys2Δ0/LYS2; MET15/met15Δ0; ura3Δ0/ura3Δ0; YBR126c::kanMX4/YBR126c::kanMX4	EUROSCARF
WTpHl	MATa/α his3Δ1/his3Δ1 leu2Δ0/leu2Δ0 LYS2/lys2Δ0 met15Δ0/MET15 ura3Δ0/ura3Δ0; pYES-PACT1-pHluorin (URA3)	This study
*tps1Δ*pHl	BY4743; MATa/α his3Δ1/his3Δ1 leu2Δ0/leu2Δ0 LYS2/lys2Δ0 met15Δ0/MET15 ura3Δ0/ura3Δ0; YBR126c::kanMX4/YBR126c::kanMX4; pYES-PACT1-pHluorin (URA3)	This study
W303-1A (WT)	MATa; leu2-3,112; trp1-1; can1-100; ura3-1; ade2-1 his3-11,15	J. Thevelein
W303-1A +YEp-Hxk2	MATa; leu2-3,112; trp1-1; can1-100; ura3-1; ade2-1 his3-11,15; YEp-Hxk2 (URA3)	This Study
W303-1A +YEp-Pgk/Hxk2	MATa; leu2-3,112; trp1-1; can1-100; ura3-1; ade2-1 his3-11,15; YEp-Pgk/Hxk2 (URA3)	This Study

Population level pHluorin measurements

Pre-cultures of pHluorin [75] expressing cells (see Table 4.1) were inoculated into CBS-GAL and grown overnight to an OD_{600} of 0.8 - 1. Cells were collected by centrifugation, washed twice with ice cold CBS-C and resuspended to an OD_{600} of approximately 1. Cell suspensions (200 µl) were transferred to black polystyrene clear-bottom 96-well microtitre plates (Greiner Bio-One) and pHluorin fluorescence emission was measured at 510 nm using an Omega Fluostar microtitre plate spectrofluorometer (BMG LABTECH GmbH), with excitation bands of 10 nm centred around 390 and 470 nm, respectively. Glucose was added to a final concentration of 2 %, by automated injection.

Calibration curves were constructed exactly as described in [75]. Background fluorescence for a WT culture not expressing pHluorin was measured in triplicate and subsequently subtracted from all

measurements. The background corrected ratio of emission intensity ($Em510_{390ex}/Em510_{470ex}$) was converted to pH by a function derived from the constructed calibration curve.

pHluorin Micropscopy

Sample preparation and data acquisition

Tps1Δ cells were grown, harvested and washed as above, and kept on ice until the addition of carbon sources. After addition of either 2 % glucose, 2 % galactose or 2 % galactose + 2 mM glucose, cells were incubated on a shaker for 30 min at 30 °C, while microscope slides were prepared with 1 % agarose pads. Agarose was dissolved in CBS-C. Once set, 20 µl of cell culture was pipetted directly onto the agarose and sealed with a cover slip and Valap (a mixture of equal amounts of vaseline, lanolin and paraffin wax).

pHluorin fluorescence images were collected on a Nikon Ti-E inverted microscope using a CFI Plan Apochromat 60x oil-immersion objective (Nikon Instruments, Tokyo, Japan). pHluorin was excited using either a 30 mW 405 nm diode laser or a 90 mW 488 nm diode laser from an Agilent MLC400 laserbox (Agilent Technologies, USA). Both lasers were attenuated to 7 % of their maximal power using an acousto-optical tunable filter. Emission light was selected using a 525 nm filter with 45 nm band width (Semrock, USA) and recorded on a cooled back-illuminated EmCCD-camera (iXon DU897, Andor, UK) using exposure times of 100 ms and an EM Gain of 100 V.

Image processing and data analysis

Images were processed and analyzed using ImageJ version 1.45s [76]. General background correction was applied by the built-in function, with a rolling ball radius of 50 pixels and smoothing enabled. False-colour images were generated from the ratio of emission intensities resulting from excitation at 405 and 488 nm ($Em525_{405ex}/Em525_{488ex}$). These images allowed us to visually confirm that distinct metabolic states, as predicted by our kinetic model (Chapter 2, Fig. 2.4), could be distinguished.

pHluorin Flow Cytometry

Sample preparation

WT and *tps1Δ* cells were cultured, harvested and washed as before. Carbon sources (WT: 2 % GLU or 2 % GAL; *tps1Δ*: 2 % GLU, 2 % GAL or 2 % GAL + 2.5 mM GLU) were added approximately 45 min prior to data acquisition. In addition, signals for cells suspended in CBS-C (unperturbed) were also collected approximately 45 min after resuspension.

A second set of experiments were performed to evaluate whether the presence of ethanol leads to the enrichment of the functional steady state fraction of the population when challenged with glucose. Single colonies were picked directly from a galactose plates and resuspended in CBS-C. Suspensions were perturbed as before with either 2 % GLU, 2 % GAL, 2 % GLU + 40 mM Ethanol (EtOH) or 2 % GAL + 1 mM GLU. Samples not expressing pHluorin were always included to estimate background fluorescence signals.

Data acquisition

Flow cytometry data were acquired on a CyAn ADP 9-Color flow cytometer (Beckman Coulter, Miami Lakes, FL). pHluorin was excited by a 50 mW 405 nm laser and a 25 mW solid state 488 nm laser, respectively, and emission was detected through a 530/40 nm filter. Laser voltages were set at the minimum value that displayed the entire unperturbed WT population on a linearly scaled bivariate plot. The acquisition limit was 10^6 events per sample.

Data analysis

Raw data files (.fcs) were processed and analysed using Matlab R2012b. Data were extracted from FCS (flow cytometry standard) files using the fcsread.m function, available in the Matlab File Exchange repository (http://www.mathworks.nl/matlabcentral/fileexchange/8430-flow-cytometry-data-reader-and-visualization/content/fcsread.m). The channel-specific average background values were calculated from samples not expressing pHluorin and subtracted from each individual data point. Next, a general filter was applied to exclude data points with low signals. In the first set of experiments (Chapter 2, Fig. 2.4C) this threshold was 25-times the channel-specific background signal. For the second set of experiments (Fig. 4.6) this was 5-times the channel-specific background signal. This difference is a consequence of lower overall signal (including background) in the second set of experiments. The chosen thresholds resulted in an average of approximately 200 000 events being retained for each sample, in both experiments. Fluorescence signals for each event were calculated as the ratio of emission intensity resulting from excitation at 405 and 488 nm ($Em530_{405ex}/Em530_{488ex}$). Frequency data (bins = 101) for each sample were normalized to sample-specific total post-filter events and expressed as percentages (Chapter 2, Fig. 2.4C and Fig. 4.6).

RESULTS

Identification and description of glucose tolerant *tps1Δ* subpopulations

Despite a robust phenotype, we found that a small fraction of cells within a *tps1Δ* population was able to tolerate glucose and persist. Glycerol stocks were inoculated into CBS-GAL and grown to OD_{600} 0.8 - 1. Cells were harvested by centrifugation, washed and resuspended in CBS-C. Ten-fold serial dilutions were prepared and either spotted (50 µl) or streaked out (100 µl) onto CBS-GAL and CBS-GLU plates.

Using CBS-GAL colony forming unit (CFU) frequencies as a viability reference, CFU counts on CBS-GLU plates from 9 biological replicates and 4 independent experiments yielded a mean glucose-tolerance frequency of 1 in 4524 cells with a standard deviation of 2540 (see Fig. 4.1A for a representative result). Spotting of 10-fold serial dilutions confirmed tolerance frequencies to be in the range of 1 in 10^3-10^4 (Chapter 2, Fig. 2.3A). This behaviour manifested as a significantly extended lag phases for *tps1Δ* cultures grown on glucose in liquid cultures (Chapter 2, Fig. 2.3B).

To confirm that these cells were indeed *tps1Δ* mutants and not the result of contamination, single colonies were picked and the Tps1 locus (Accession number: YBR126C; see Table S4.2 for primer sequences), which contains a Geneticin resistance (KanMX) cassette, was PCR amplified (USB® FideliTaq™ 2X PCR Master Mix, according to manufacturer's instructions). Results confirmed the displacement of the Tps1 coding region by KanMX (Fig. 4.1B). In addition, tolerance to 200 µg.ml^{-1} G418 (Cayla-Invivogen, Fr) was confirmed in liquid cultures.

Table 4.2. Primer sequences used to confirm the genotype of WT and *tps1Δ* colony isolates.

Primer #	Primer Name	Sequence	Description
1	Tps1_ORF_Fwd	5'-GCCATGGACAAACTGCACTG-3'	Upstream of Tps1 ORF
2	Tps1_ORF_Rev	5'-CGTTATGCGGTGTGAACAGC-3'	Downstream of Tps1 ORF
3	KanR_Int_fwd1	5'- CTTGACAGTCTTGACGTGCG-3'	Specific for KanR coding sequence
4	KanR_Int_rev1	5'-CGACCAGCATTCACATACGA-3'	Specific for KanR coding sequence
5	KanR_Int_fwd2	5'-TCGTATGTGAATGCTGGTCG-3'	Specific for KanR coding sequence

A second possibility, that these glucose tolerant colonies were revertants, i.e. consequence of secondary mutations which rescue the phenotype, was excluded by evaluating the heritability of the glucose-tolerance phenotype through propagation (Fig. 4.2 shows an overview of the scheme). Cultures were inoculated from glycerol stocks (2x *tps1Δ*, 1x WT) and pre-grown in CBS-GAL, and as before, *tps1Δ* glucose tolerance frequencies on plates were calculated: *tps1Δ* replicate A (TA) = 1 in 4827, *tps1Δ* replicate B (TB) = 1 in 5517. Next, we picked 4x *tps1Δ* and 1x WT glucose-tolerant colonies (i.e. from CBS-GLU plates), resuspended them in CBS-C and streaked out ten-fold dilutions onto CBS-GAL plates. After 3 days at 30 °C, two colonies per original glucose-tolerant isolate were picked and resuspended in CBS-C. Ten-fold dilutions were prepared and either spotted as 50 µl suspensions or streaked out (100 µl) onto CBS-GAL and CBS-GLU plates. Results showed that 75 % (3 out of 4) of the original glucose-tolerant isolates again produced subpopulations with tolerance frequencies similar to the glycerol stock derived populations (Chapter 2, Fig. 2.3C and Fig. 4.2), arguing strongly for a non-genetic origin. All colonies retained tolerance to G418 (assessed by growth in the presence of 200 µg.ml^{-1} G418). In the case where glucose tolerance is a consequence of genetic changes (e.g. revertants) it will be transmitted to the progeny of glucose-tolerant isolates.

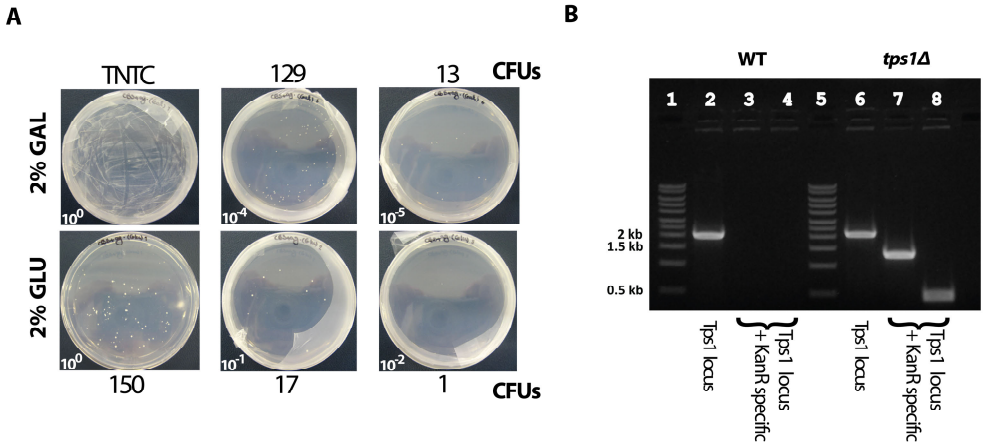

Figure 4.1. Glucose tolerant *tps1Δ* colonies appear on plates. (A) Serial dilution plating shows that a small fraction of individuals from a *tps1Δ* population is able to persist in the presence of 2 % glucose. Enumeration of Colony Forming Units (CFUs) on Galactose vs. Glucose plates allow for the calculation of subpopulation sizes. (B) Glucose tolerant *tps1Δ* colonies contain a KanR casette at the Tps1 locus, confirming the primary phenotype of these cells. Lanes 1 & 5, Size ladder; Lanes 2 & 6, primers 1 & 2 (tps1 locus); Lanes 3 & 7, primers 3 &4 (KanR specific); Lanes 4 & 8, primers 2 & 5 (KanR specific + tps1 locus). See Table 4.2 for definition of primer numbers and associated sequences.

Noteworthy is the observation that 1 out of the original 4 isolates appeared to have acquired tolerance at the genetic level (or some other heritable entity), as all the progeny derived from it no longer exhibited significant glucose-sensitivity; this result is not completely unexpected as *tps1Δ* glucose tolerance was historically interpreted as the consequence of reversion [44]. Importantly, and maybe surprisingly, our results demonstrate that glucose-tolerance emerges spontaneously and in most cases exhibits reversibility, suggesting it is a consequence of phenotypic plasticity rather than genetic mutation.

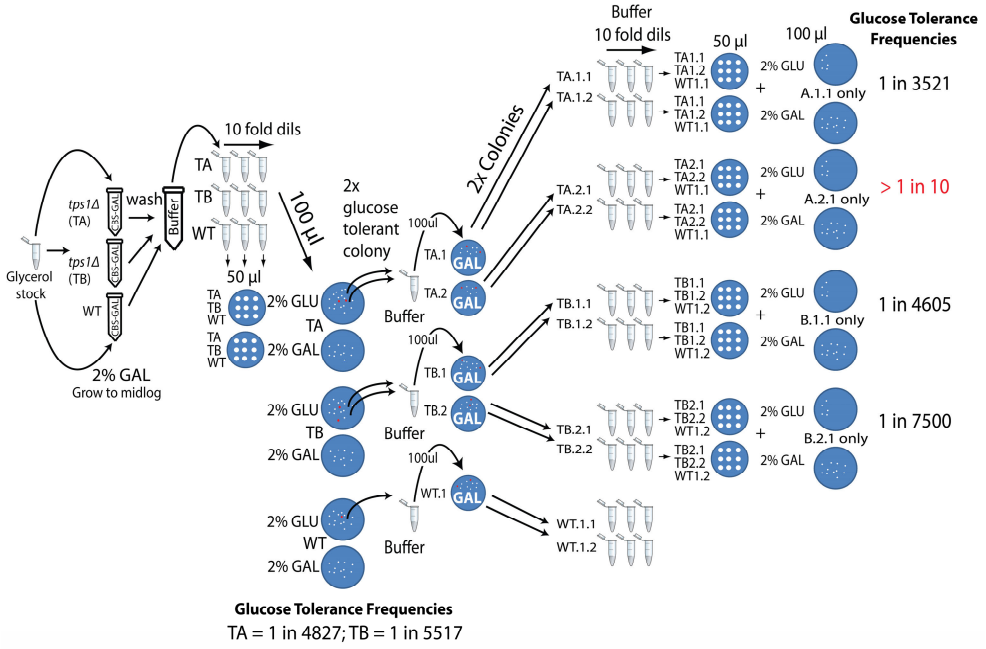

Figure 4.2. Propagation demonstrates that *tps1Δ* glucose tolerance is non-genetic. Shown is the propagation scheme used to assess the heritability of glucose tolerance. Only one of four glucose tolerant colonies (TA.2) showed heritable tolerance. Tolerance for the remaining three colonies appears to be non-genetic in nature, with similar subpopulation structures appearing after a single transition on galactose.

Environmental conditions affect glucose tolerances of *tps1Δ* populations

We hypothesized that the existence of glucose tolerant subpopulations reflects phenotypic plasticity, which arises from the co-existence of two stable states in glycolysis (Chapter 3). In a scenario where transition outcomes are dependent on initial conditions, one could expect that alterations in environmental conditions might affect the size of such glucose tolerant subpopulations, and hence of the lag phases in liquid culture.

Previous work has shown that the glucose sensitivity phenotype can indeed be reduced by addition of respiratory inhibitors such as antimycin A [32] to the growth medium. Microtitre growth monitoring confirmed that the addition of increasing concentrations of antimycin A (Table 4.3) did indeed improve the growth of *tps1Δ* cultures (Fig. 4.3A), reflected by a decrease in the lag phase. However, inclusion of controls revealed that the observed effect could be ascribed mainly to ethanol, the solvent (Table 4.3) in this case (Chapter 2, Fig. 2.5B).

Table 4.3. Overview of *tps1Δ* glucose tolerance improving medium additions

Additive	Solvent	Final concentrations used	Effect on growth	
			tps1Δ	**WT**
Antimycin A	99 % Ethanol	WT: 1, 2 and 20 µg.ml-1 *tps1Δ*: 2, 10, 20 µg.ml-1	Increased concentration correlated with decreased lag phase (Fig. 4.3A)	Increased concentration slightly inhibits growth
Ethanol	Not applicable	4.3 mM; 21.5 mM; 43 mM	Increased concentration correlated with decreased lag phase (main text Fig. 2.5B)	No observable effect
Formic Acid	dH20	4 mM; 10 mM	Increased concentration correlated with decreased lag phase (Fig. 4.3B)	No observable effect

This result was initially unexpected and surprising, but could be consolidated with improved growth described for *tps1Δ* mutants with an enhanced glycerol flux [23]; ethanol has been demonstrated to stimulate the glycerol-3-phosphate dehydrogenase flux through an increase in NADH availability [50]. Interestingly, improved growth in the presence of antimycin A was originally shown to be a consequence of an enhanced glycerol flux and inferred to be caused by increased NADH availability; our results suggest, however, that it is the presence of low concentrations of ethanol rather than antimycin A which underlies the effect. Our interpretations were further substantiated by the substitution of ethanol (and antimycin A) by formic acid (FA, Table 4.3), which resulted in a similar improvement of growth (Fig. 4.3B). Formic acid is oxidised by an endogenous formate

dehydrogenase to CO_2 and NADH [77] and inclusion of FA in the growth medium has been shown to stimulate the formation of glycerol through enhanced NADH availability [77].

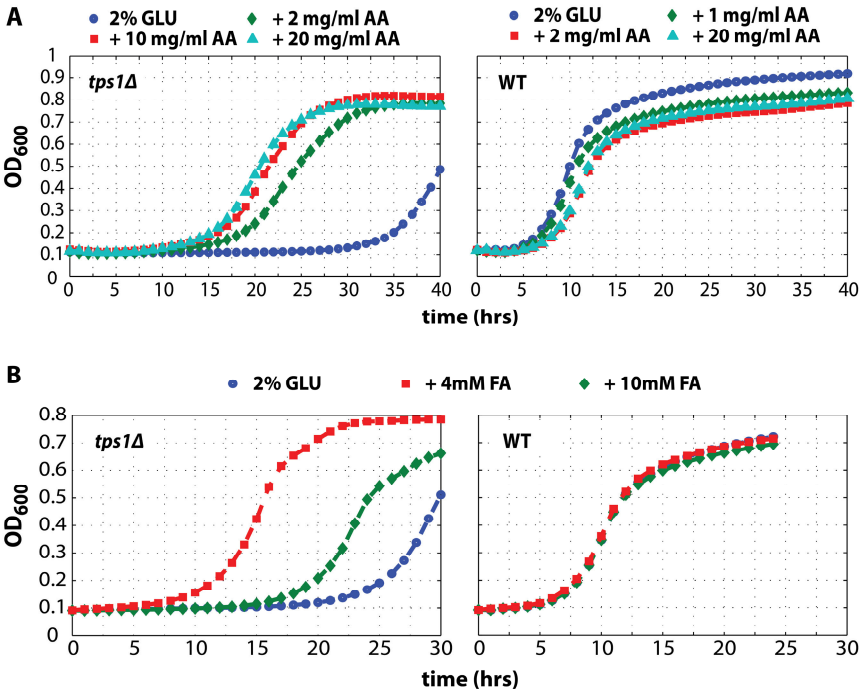

Figure 4.3. Antimycin A and Formic acid additions lead to changes in lag phase duration. (A) Antimycin A (AA) addition to glucose medium markedly reduces the observed lag phase of *tps1Δ* cultures, confirming increased glucose tolerance frequencies, as was previously reported in literature [31]. Antimycin A appears to have a slight inhibitory effect on WT cells, in the presence of glucose. Shown are the average growth profiles of 3 biological replicates. (B) Addition of low concentrations of formic acid (FA) significantly reduces lag phases in the presence of glucose, similar to ethanol (Chapter 2, Fig. 2.5B). This observation provides further evidence of a NADH-mediated effect and suggests that the observed antimycin A effect is a consequence of small amounts of ethanol (the solvent). FA had no effect on WT growth.

Growth dynamics of *tps1Δ* populations reflect subpopulation structures

The growth behaviour described above strongly indicates that changes in the viable fraction of a population underlie growth dynamics, specifically the length of observed lag phases. To further confirm this interpretation, we looked towards previous work, which showed a systematic inhibition of *tps1Δ* growth by low concentrations of glucose in the presence of excess galactose [35]. Cultures

pre-grown in CBS-Gal were harvested, washed and resuspended in CBS-C. Two-fold dilutions were prepared and 50 µl cell suspensions were spotted onto CBS-Gal plates with increasing amounts of glucose. The results confirmed that increasing amounts of glucose correlated with a systematic reduction in the number of viable *tps1Δ* individuals (Fig. 4.4A). WT populations, on the other hand, did not exhibit this behaviour. Additionally, plating experiments showed an approximately 100-fold increase in *tps1Δ* viability when 40 mM ethanol was added to CBS-GLU plates (Fig. 4.5A), providing evidence that the shorter lag phases observed in the presence of ethanol are a consequence of improved viability.

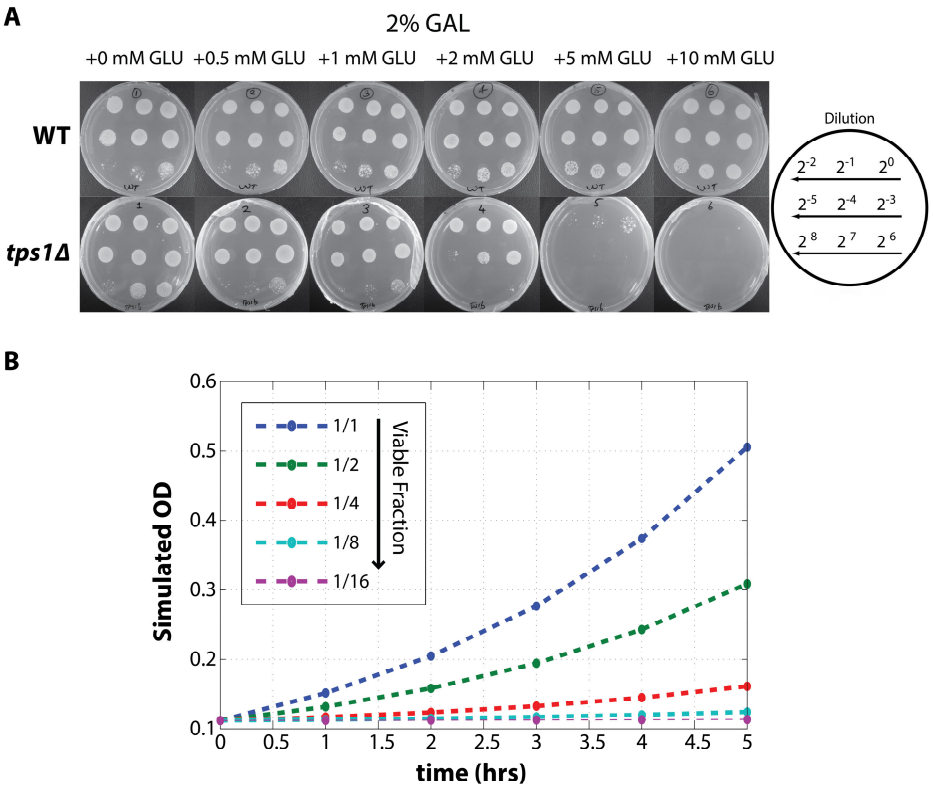

Figure 4.4. Subpopulation size displays glucose dose dependence and translates to differences in observed lag phases. (A) Two-fold serial dilutions show that increasing concentrations of glucose lead to a systematic reduction in the number of viable cells. These results highlight the existence of glucose tolerant and sensitive cells within a *tps1Δ* population, even at low glucose concentrations. Shown here is a representative result. 50 µl per dilution was spotted, with an undiluted OD_{600} of approximately 0.05. (B) A growth model demonstrates how such a systematic reduction in the viable fraction of the population, in response to glucose, manifests as an increase in the observed lag phase.

To illustrate the effect of reduction in population viability on growth dynamics, we simulated the growth of cultures with a fixed inoculum size, but decreasing fractions of viable individuals. We employed a simple exponential growth model in the form $X(t) = X_0 + Xv_0.e^{\mu t}$, with X_0 as the inoculum size and Xv_0 as the number of growing (viable) cells. We took the growth rate (μ) to be equal to the growth rate measured for WT populations.

These results (Fig. 4.4B) reproduce the effect of population viability on the observed growth dynamics and provide an explanation of previously described [35], but not understood, growth behaviour. Importantly, these results confirm environment-dependent glucose sensitivity within *tps1Δ* populations and provide direct evidence for a relationship between population substructures and observed growth behaviours.

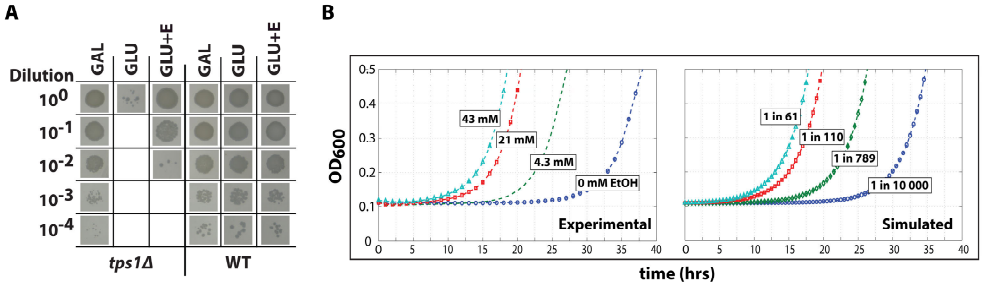

Figure 4.5. Ethanol addition leads to an increase in *tps1Δ* glucose tolerance. (A) Addition of 40 mM EtOH to CBS-GLU plates enhances glucose tolerance of *tps1Δ* populations with an approximately 100-fold increase in viability. Shown are ten-fold dilutions of *tps1Δ* and WT suspensions spotted (50 µl) onto CBS-GAL (GAL), CBS-GLU (GLU) and CBS-GLU + 40mM EtOH (GLU+E) plates. The experiment was repeated twice for *tps1Δ* suspensions, with similar results. (B) Using the insights gained from our growth model, we can estimate the fraction of initially viable individuals in the presence of different concentrations of ethanol. In the right panel we show experimental data (with ethanol concentrations as indicated) and in the right panel we reproduce the ethanol-dependent growth profiles, by simulating growth with different fractions of viable subpopulations at t = 0, as indicated.

Using these insights we were able to reproduce the observed growth profiles of t*ps1Δ* cultures in ethanol supplemented CBS-GLU, allowing us to calculate the approximate fractions of viable cells in these populations (Fig. 4.5B). Importantly, the ability to reproduce *tps1Δ* growth profiles using growth rates estimated from WT cultures (growing on glucose) also precludes the possibility that improved growth is a consequence of a subpopulations solely utilizing ethanol.

Cytoplasmic pH distinguishes distinct metabolic subpopulations

Demonstration of different population structures in response to glucose concentration gradients (Fig. 4.4A) led us to ask whether we could visualize and distinguish distinct metabolic subpopulations. We looked towards intracellular pH (pH_i) as global indicator of metabolic status. We based our decision on the observations that (i) a relation between pH_i and growth rate has been shown [75, 78], suggesting that pH could provide a proxy for metabolic status and (ii) *tps1Δ* mutants, when challenged with glucose, are unable to maintain pH homeostasis due to insufficient ATP levels [40].

We first confirmed the previously described intracellular acidification of *tps1Δ* cultures when challenged with glucose [40]. Results showed a clear difference in the pH responses of *tps1Δ* and WT cells following a glucose pulse (Chapter 2, 2.4A). After an initially similar response, *tps1Δ* cultures display sustained acidification, and after 25 min exhibit a population level pH_i of approximately 1.5 pH units below that of WT cultures. When grown on galactose (Chapter 2, 2.4A) the pH_i of *tps1Δ* and WT cultures is indistinguishable.

Having established that pH_i clearly distinguished between *tps1Δ* populations challenged with glucose and those growing on galactose, we employed fluorescence microscopy to firstly evaluate whether distinct metabolic states could be visualized for individual cells. The collected images confirmed that distinct metabolic states could be distinguished (see Chapter 2, Figure 2.4B for an example).

Next, a high throughput flow cytometry approach was used to characterize population structures under various conditions (Chapter 2, 2.4C and Fig. 4.6). The first set of experiments evaluated both WT and *tps1Δ* population structures in response to 2 % Glucose, 2 % Galactose or a combination of 2 % Galactose + 2.5 mM Glucose (*tps1Δ* only). Samples suspended only in wash buffer were used to determine population structure prior to sugar perturbation. In both the WT and *tps1Δ* populations a bimodal distribution was observed post-perturbation (Chapter 2, Fig. 2.4C), indicating two subpopulations. Low 405 nm/ 488 nm ratios indicate a low pH and vice versa. For *tps1Δ* suspensions exposed to glucose the majority of cells belonged to the low pH peak, confirming this peak as diagnostic of the imbalanced metabolic state. In contrast, WT suspensions primarily displayed a higher pH peak after glucose addition. However, approximately 7 % of WT cells failed to recovery pH, with values corresponding to the imbalanced state.

A second set of experiments were performed to determine whether ethanol led to an enrichment of the peak associated with the viable state (higher ratio peak); as expected from microtitre growth (Fig. 4.5B) and plating experiments (Fig. 4.5A). As before, population distributions were bimodal and the addition of 40 mM Ethanol to glucose perturbed cultures resulted in

enrichment of the higher ratio peak (Fig. 4.6). Due to differences in the pre-data acquisition calibration of the flow cytometer, signal resolution was not optimal in the second set of experiments. While the resolution was sufficient for the identification of two peaks, significant overlap meant that relative peak sizes could not be reliably estimated.

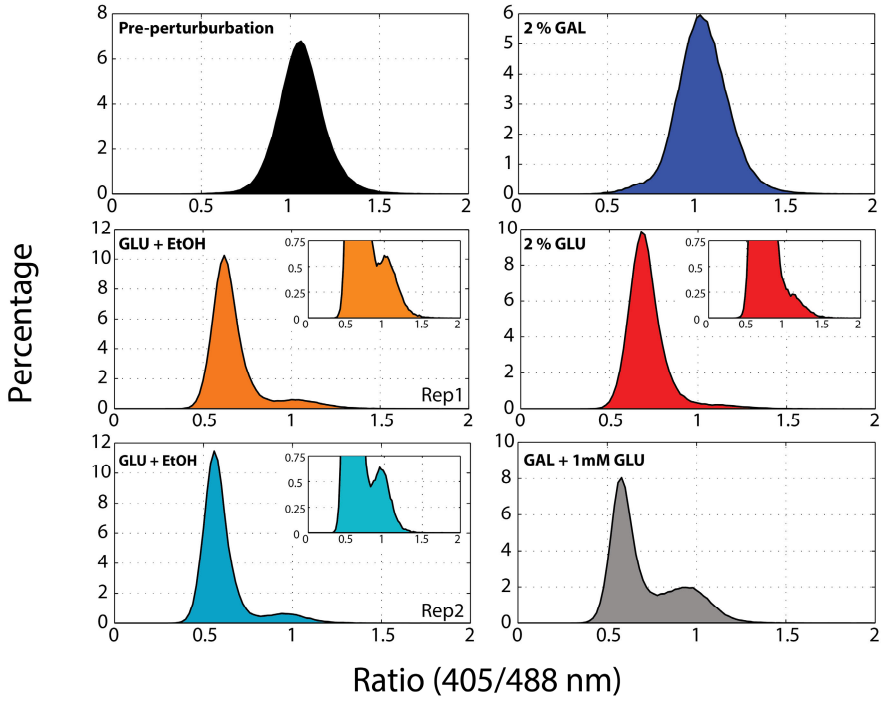

Figure 4.6. Flow cytometry acquired pHluorin emission ratio frequencies for *tps1Δ* cell suspensions. Shown are normalized frequency distributions in response to different perturbations, as indicated (Materials and Methods for details). The top left panel shows a population distribution prior to perturbation. Lower ratio values are associated with lower pH_i's and vice versa for higher ratios. Insets show that the peak associated with the functional steady state (right peak) is visibly enriched when *tps1Δ* cells are perturbed with 2 % GLU in the presence of 40 mM EtOH (compare GLU + EtOH vs. GLU; note that two independent experiments with EtOH are shown). Lastly, addition of 1 mM of GLU in the presence of 2 % GAL (bottom right panel) leads to the appearance of a large peak associated with the imbalanced state (left peak).

Tps1Δ cells remain viable for several hours following a glucose perturbation

Having shown that the growth behaviour exhibited by *tps1Δ* populations can be explained by a small number of individuals that are able to persist and replicate after a glucose pulse perturbation, another relevant question relates to the fate of the cells trapped in the imbalanced state. What are

the physiological consequences of the metabolic disturbances underlying the imbalanced state? At low ATP and P_i concentrations, a low glycolytic flux and a significantly lower cytoplasmic pH, do cells remain viable, but are unable to replicate, or do they ultimately die? To answer these questions, we assessed the ability of glucose-perturbed *tps1Δ* populations to resume growth on galactose after increasing lengths of exposure to glucose. *Tps1Δ* cells were pre-grown in CBS-GAL and harvested during mid-logarithmic growth. Cells were resuspended in CBS-C (to an OD of ~1) and perturbed with 2 % glucose. Before glucose addition a sample was taken and dilution-plated to get an initial CFU count (i.e. viability before glucose perturbation). At regular time intervals after the perturbation, samples were taken, diluted by a factor 10^3 and plated onto CBS-GAL plates (note: a 10^3 dilution ensured that extracellular glucose became negligible when 100 µl samples were spread out on plates). Additionally OD was measured at each sampled time point. Our results show that cells remain viable for a significant period of time following a glucose pulse (Fig. 4.7).

The viable fraction, assessed by the ability to resume growth on galactose, was stable for around 7 h following a glucose pulse, after which a slow and steady reduction in viability is observed. This behaviour is fully consistent with metabolic data, which show that cells remain metabolically active (and thus not dead), for several hours following a pulse, evidenced by continued FBP accumulation (see e.g. [21]), presumably until all intracellular phosphate stores are depleted [40].

While flow cytometry data clearly indicated that a fraction (~7 %) of WT cells also end up in the imbalanced state (Chapter 2, Fig. 2.4C) we were unable to demonstrate their fate using the approach outlined here. An important caveat is that it is easy to resolve growing cells against a background of non-growing cells (as in the *tps1Δ* case), but the opposite scenario is much more difficult with the resolution provided by this method. Based on the metabolic features of the imbalanced state, we do, however, expect their fate to be the same as that of the imbalanced fractions of *tps1Δ* populations, i.e. they will eventually lose viability.

Wild-type cells overexpressing hexokinase 2 display reduced viability

Simulations with the full kinetic model showed that WT cells can also become trapped in the imbalanced state (Chapter 3, Fig. 3.4), but that the trehalose cycle functions to minimize the probability of this state being reached. Analyses showed that an increase in Hxk2 activity, either by reduction or removal of T6P-mediated inhibition (Chapter 2, Fig. 2.8) or by increasing the V_{max} for this reaction, increases the probability that the WT model will end up in the imbalanced state. As discussed in Chapter 1, the effects of Hxk2 overexpression in WT cells had previously been investigated [31]. However, with the insights generated in the current study, we used the strains detailed in [31] to assess whether Hxk2 overexpression in WT impacts the viability of WT cells. Again

population level growth behaviour was monitored in a 96-well microtitre plate alongside CFU counts, which provided a direct measure of viability. Experiments were repeated twice, with similar results (Fig. 4.8).

We found that increased levels of Hxk2 resulted in (i) small but reproducible increases in lag phases when cells are grown on glucose (Fig. 4.8A) and (ii) a reduction in the number of colony forming units (CFUs) on glucose plates (Fig. 4.8B). However, overexpression of Hxk2 had an unexpected effect on the galactose tolerance of cells, resulting, similarly, in a Hxk2 dose-dependent reduction in CFUs when plated on galactose plates. In line with the methodology elsewhere in this work we decided to normalize all glucose CFU counts to the within strain galactose CFU counts, in an attempt to account for the more general effect that Hxk2 overexpression has on viability. Importantly, we still found that increased Hxk2 levels leads to a reduction, albeit more modest than before normalization, in population viability in the presence of glucose (Fig. 4.8C).

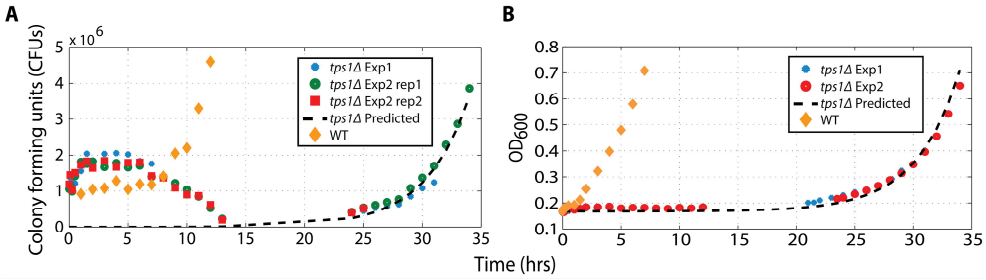

Figure 4.7. *Tps1Δ* populations maintain viability several hours after a glucose pulse perturbation. (A) Shown are the dilution-corrected CFU counts on CBS-GAL plates after a glucose pulse perturbation for both *tps1Δ* and WT populations. The dashed black line indicates the predicted CFU counts for the *tps1Δ* population, generated by an exponential growth equation. For the growth model, we assumed an initial viable population (t=0) of 1 in 3000 individuals (derived from the measured CFU counts) and a growth rate calculated for the *tps1Δ* curve between 30 h and 34 h. The initial (t=0) CFU counts represent viability prior to glucose exposure. The experiment was repeated twice for *tps1Δ*, with 2 technical replicates included in the second run. A single experiment was performed for WT. (B) Measured OD's for time points displayed in (A). The dashed black line depicts the predicted OD evolution of a *tps1Δ* population with the same parameters used for CFU predictions. Note, that while OD-based growth was modeled with the same growth parameters, a baseline equal to the initial OD x 99.97 % (i.e. at t = 0 only 1 in 3000 OD units represent the initial growing population) is added to predicted values.

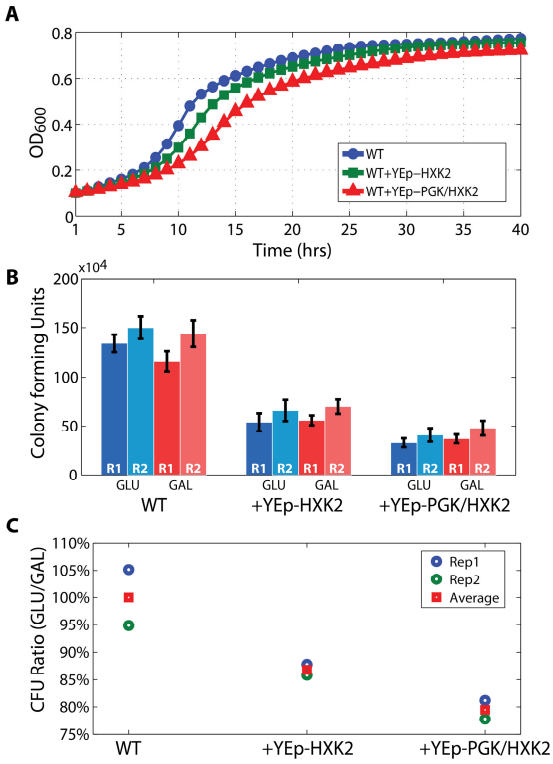

Figure 4.8. Overexpression of Hxk2 leads to a reduction in WT viability. Shown are growth and CFU data for WT and two Hxk2 overexpression strains [31]. (A) Growth on 2 % glucose is characterized by a small increase in the lag phase. (B) CFU counts show a reduction in viability for Hxk2 overexpression strains relative to WT, on both 2 % glucose and 2 % galactose plates (n=11 per biological replicate and condition; R1 and R2 designate biological replicates). (C) Normalizing GLU to GAL CFU counts still shows a Hxk2 dose-dependent reduction in viability. Shown are strain-specific average and replicate GLU/GAL CFU ratios, all scaled relative to the WT average (set to 100 %).

These results indicate that overexpression of Hxk2 (a well-known global regulator of carbohydrate metabolism [79]) has effects not confined to glucose metabolism only, making unambiguous interpretations difficult. Even with this unexpected complication, we do, however, consider these results to provide support for our own predictions and to be consistent with the metabolite profiles shown in [31], which can be explained by a small increase in the imbalanced state fraction of the population. As an aside, this result provides an important caution for the comparative strategies often employed when interpreting genetically modified phenotypes.

SUMMARY

Motivated by the discovery that the initiation of glycolysis can lead to either a functional steady state or a growth-incompatible imbalanced state (Chapter 3), we attempted to determine experimentally whether two such states appear in real populations. We found that a small fraction of *tps1Δ* cells was indeed able to persist in the presence of glucose and that this tolerance was non-genetic in nature. This glucose tolerant subpopulation was highly reproducible in size, with approximately 1 in 10^3 - 10^4 individuals able to survive glucose challenges. Population-level growth profiles could be quantitatively consolidated with estimated subpopulation fractions. Furthermore, we showed that the sizes of the viable and unviable fractions corresponded quantitatively with metabolic subpopulations, using pH_i readouts as a proxy for metabolic status. We also showed that subpopulation sizes could be manipulated by addition of ethanol or formic acid addition to the growth medium, or by directly altering Hxk2 expression levels. Whereas ethanol and formic acid additions are interpreted to stimulate phosphate turnover and consequently alleviate a flux bottleneck at Gapdh, Hxk2 overexpression will have the opposite effect, by increasing upper-glycolytic activity.

Taken together these results provide strong evidence for the theoretically demonstrated bistable behaviour of glycolysis and shows that the startup of glycolysis is not guaranteed, even when all regulatory components are present.

In any population, individual cells are likely to differ from each other in their exact metabolic state. The initial-condition dependent-behaviour of the glycolysis model can be consolidated with our experimental findings, if one assumes that a population of cells is characterized by individuals that all differ slightly in their exact metabolic state. Such differences are not a consequence of genetic alterations, but arise through spontaneous fluctuations in metabolic intermediate and enzyme concentrations.

In Chapter 5, we will provide further substantiation of this interpretation by simulating non-genetic population heterogeneity through the random sampling of enzyme capacities (V_{max}) and initial metabolite concentrations from continuous probability distributions.

5 Simulating spontaneous metabolic variation through random sampling of initial conditions

Johan H. van Heerden, Meike T. Wortel and Bas Teusink

INTRODUCTION

In Chapter 4 we showed that a sudden increase in glucose supply leads to the spontaneous appearance of two metabolically distinct states in a population of otherwise genetically identical *S. cerevisiae* cells. Importantly, we showed that the sizes of these subpopulations could be manipulated through variables that impact upper and lower-glycolytic flux capacities. These results, combined with the initial condition-dependent bistable behaviour of the large kinetic model (Chapter 3), were interpreted to suggest that cell-to-cell differences in key metabolic parameters could explain the appearance of these subpopulations. However, our initial analyses demonstrated this for large and probably physiologically unrealistic differences in initial P_i and FBP concentrations (Chapter 2, Fig. 2.2A and Chapter 3 Fig. 3.4). We hypothesized that such variations might be more subtle *in vivo*, and that the appearance of two metabolically distinct subpopulations can be explained by the combined effect of small continuously distributed variations in all metabolic variables, rather than large fluctuations in one or two variables. In this chapter we use the kinetic model, as detailed in Chapter 3, to explore this idea and evaluate the relationship between more modest, but system wide, variations in initial conditions and the probability of obtaining a regular steady state in the kinetic model.

METHODS

Simulating population heterogeneity

To simulate cell-to-cell metabolic heterogeneity, we took enzyme expression levels and metabolite concentrations as two likely sources of inter-individual metabolic variation in a population. The extent to which the levels of individual metabolite pools or glycolytic enzymes vary between individual cells has not been described in great detail. For yeast, some efforts have been made to quantify inter-individual noise in protein levels [45] and this was found to be significant even for highly abundant proteins (such as metabolic enzymes) which showed coefficients of variation of > 10 %. Additionally, it was found that protein abundance variation typically followed a Gaussian distribution [45]. Information on single-cell variation in metabolite levels, on the other hand, is very scarce. Detection of metabolites at a single cell level is technically challenging and many of the available techniques are not suitable for high-throughput parallel detection of multiple species [80]. However, recently Ibañez *et al*. [81] provided some insight into cell-to-cell differences for several glycolytic intermediates. Data was presented semi-quantitatively and no variation measures (e.g. standard deviation or CV) were reported, but inter-individual differences in glycolytic metabolite pools were clearly present.

Due to a lack of quantitative data for metabolite variability, and for practical purposes, we assumed Gaussian distributions for both enzyme expression levels (represented by V_{max} values) and initial metabolite concentrations. Variance was set such that the probability of a sampled value deviating more than 20 % from the reference value is less than 1 in 10^3; this equals a coefficient of variation (CV, i.e. a mean-normalized standard deviation) of 6.1 % (3.29 standard deviations = mean ± 20 %, for Gaussian distributions).

We randomly drew more than 10^6 unique V_{max} and initial metabolite concentration sets. To additionally evaluate the effect of ethanol on the probability of reaching a steady state, we repeated this sampling at varying ethanol concentrations: 0, 4.3, 10, 21.5, 30, 43, 50, 62.5, 75, 100, 200 and 500 mM.

The randomly drawn sets were then used as initial condition inputs for the kinetic model. For each set, we performed a numerical time simulation for 250 minutes and evaluated the system to check whether a regular or an imbalanced state was obtained. An imbalanced state was defined when the final FBP concentration was higher than the concentration at 90 % of the evaluation time (indicating long term accumulation). In addition, to score a viable state, P_i concentration > 0.5 mM was used to avoid incorrectly identifying zero flux states as vital steady states; a scenario which would arise when no P_i is available to drive FBP accumulation. Based on the evaluation outcome each randomly drawn data set was categorized and saved.

Random sampling, time simulations and steady state evaluations were performed using Mathematica 9.0 (Wolfram Research).

Linear Discriminant Analysis

Using the output from the random sample evaluations we explored the effect of initial conditions and ethanol concentration on the probability of reaching a regular steady state, by means of linear discriminant analysis (LDA, [82]). LDA seeks to find a linear combination of variables that can optimally distinguish between independent sample classes and as such reveals meaningful correlations between variables and class labels.

From the saved initial condition sets (see above), 5000 samples (sets) were randomly drawn, for both imbalanced and regular steady state solutions, at each ethanol concentration. This yielded a data set with 28 variables (14 initial metabolite and 14 V_{max} values) and 24 independent classes (2 groups: imbalanced vs. steady state, at 12 different ethanol concentrations, see above). The discriminant analysis was performed with the lda function of the MASS package in the R (version 2.14.2) statistical environment [83]. All parametric assumptions (distribution normality,

homogeneity of variance, independence of observations) of the LDA method were confirmed to be met.

RESULTS

Steady state evaluations of randomly sampled initial states

Approximately 1 in 10^3 of the randomly sampled initial condition sets produced steady state solutions for the TPS model, similar to experimentally observed glucose tolerance frequencies for *tps1Δ* populations (Chapter 4). The *in vivo* effect of ethanol was also reproduced well, with increasing amounts of ethanol correlating with increased percentages of steady state solutions (Chapter 2, Fig. 2.5C). While experimental results showed that a significant fraction of WT populations ended up in an imbalanced (low pH) state, we did not find any imbalanced state solutions from the randomly sampled initial condition sets for the WT model. This could be due to the simplified approximation of the trehalose pathway in our wild-type model or conservative estimates of cell-to-cell variability for metabolite and enzyme levels. We know from available experimental data that the implemented variability in enzyme levels is conservative [45], but we were uncertain as to the expected degree of variability for metabolite pools. Increasing the CV (to 15 %) did indeed result in small percentage (~2 %) of imbalanced state solutions for WT models (data not shown).

Evaluation of variable contributions to steady state outcomes

The linear discriminant analysis revealed that 99 % of the achievable between-group separations (inter-group differences) could be explained by the first linear discriminant, with the second discriminant accounting for 0.4 % of the separation. The standardized variable loadings (Chapter 2 , Fig 2.5A and Table 5.1) clearly show that the variables with the largest loadings (the magnitude of these coefficients indicates the relative contribution to the discriminant function) on the first two discriminants represent a contrast between parameters and metabolites that are key in determining upper- and lower-glycolytic flux capacities (Table 5.1).

Table 5.1. Variable loadings for the first two discriminant functions

Variable	LD1	LD2
GLUi	-0.001	-0.031
P (energy status)*	0.256	-0.080
G6P	0.156	-0.021
F6P	0.043	-0.004
FBP	0.086	-0.041
BPG	0.008	-0.044
P3G	0.047	-0.001
P2G	0.002	-0.010
PEP	0.012	0.061
PYR	-0.001	-0.022
ACE	0.003	0.013
TRIO (DHAP+GAP)	0.026	-0.019
NADH	0.000	-0.006
P_i	**0.499**	-0.158
V_{max}Glt	**-0.696**	0.362
V_{max}Hxk	**-0.792**	-0.300
V_{max}Pgi	-0.286	0.159
V_{max}Pfk	**-0.356**	0.134
V_{max}Ald	0.095	0.092
V_{max}G3pdh	0.157	**0.734**
$V_{max}Gapdh_{fwd}$	**0.446**	0.256
$V_{max}Gapdh_{rev}$	-0.011	-0.027
V_{max}Pgk	0.025	-0.018

Table 5.1. Continue

Variable	LD1	LD2
V_{max}Pgm	0.035	0.038
V_{max}Eno	0.131	-0.067
V_{max}Pyk	0.043	-0.040
V_{max}Pdc	-0.001	-0.013
V_{max}Adh	-0.030	0.122

Shown in bold are the 5 largest loadings for the first discriminant and the largest loading on the second discriminant. *****P represents a summary term reflecting the high energy phosphate pool (ATP, ADP and AMP), see [41] for explanation.

Evaluating group centroids[3] (Fig. 5.1A) clearly confirms that the first discriminant captures differences between imbalanced-state and steady-state samples. Imbalanced-state samples correlate with higher V_{max}Glt, V_{max}Hxk, V_{max}Pfk values (indicating higher upper glycolytic flux capacities) and reduced values for V_{max}Gapdh and P_i (i.e. reduced lower glycolytic flux capacities) while vital steady-state samples display converse correlations.

Interestingly, the 2nd discriminant appears to mainly reflect ethanol-dependent differences between steady-state samples (Fig. 5.1A). When looking at the variable loadings for this discriminant, V_{max}G3pdh stand out (Table 5.1). Combined, these data suggest that the increased regular steady state frequencies associated with increased ethanol concentrations (Chapter 2, Fig. 2.5C) is correlated with G3pdh activity. In Chapter 4, we suggested that the mechanism by which ethanol (and formate) addition improves growth of *tps1Δ* on glucose can be explained by the stimulatory effect of excess NADH on the glycerol flux. Evaluation of steady states shows that higher ethanol concentrations are indeed correlated with higher G3pdh rates and increased NADH concentrations at steady state (Fig. 5.1B).

Figure 5.1C shows, in a simplified two parameter scenario, how different combinations of V_{max} values of Hxk and G3pdh can lead to either steady state or imbalanced state outcomes. Steady-state solutions can be achieved by e.g. an increase in the G3pdh V_{max}, a decrease in the Hxk V_{max} or a combination of both. In addition, it is illustrated how the addition of ethanol enlarges the size of the

[3] A centroid refers to the class average of the discriminant function.

parameter space that results in a regular steady state solution, thereby increasing the probability that a steady state can be reached.

SUMMARY

In Chapter 3, we illustrated how different combinations of initial P_i or FBP concentrations lead to bistable outcomes in our kinetic model. One caveat, however, was that fairly large changes were required to produce the non-typical outcomes: imbalanced state for WT model and steady state for TPS model.

Metabolism is considered relatively noise free due to high metabolite and enzyme levels. While available experimental evidence demonstrates clearly that enzyme levels and metabolite concentrations vary between individual cells, these differences are unlikely to be of the magnitude seen for low copy number systems such as transcription cascades (protein abundance estimates indicate CV values of between 10 and 20 % for glycolytic enzymes [45]). However, we showed how small distributed changes across all metabolites and enzymes, a scenario likely for a population consisting of millions of individuals, can explain the bistable outcomes observed, both in our model and experimentally. In populations consisting of millions of individuals, metabolic outliers can appear when deviations in key metabolic variables converge to generate qualitatively different responses to an environmental perturbation. Importantly, these results provide a novel framework that demonstrates how small amounts of metabolic noise can to lead phenotypic heterogeneity, through complex interactions and interdependencies in metabolic networks; a model that is distinct from other frameworks such as fluctuation induced bistable switching (FIBS), which has previously been linked to the emergence of phenotypic heterogeneity (e.g. antibiotic resistance in *E. coli*) in microbial populations [48].

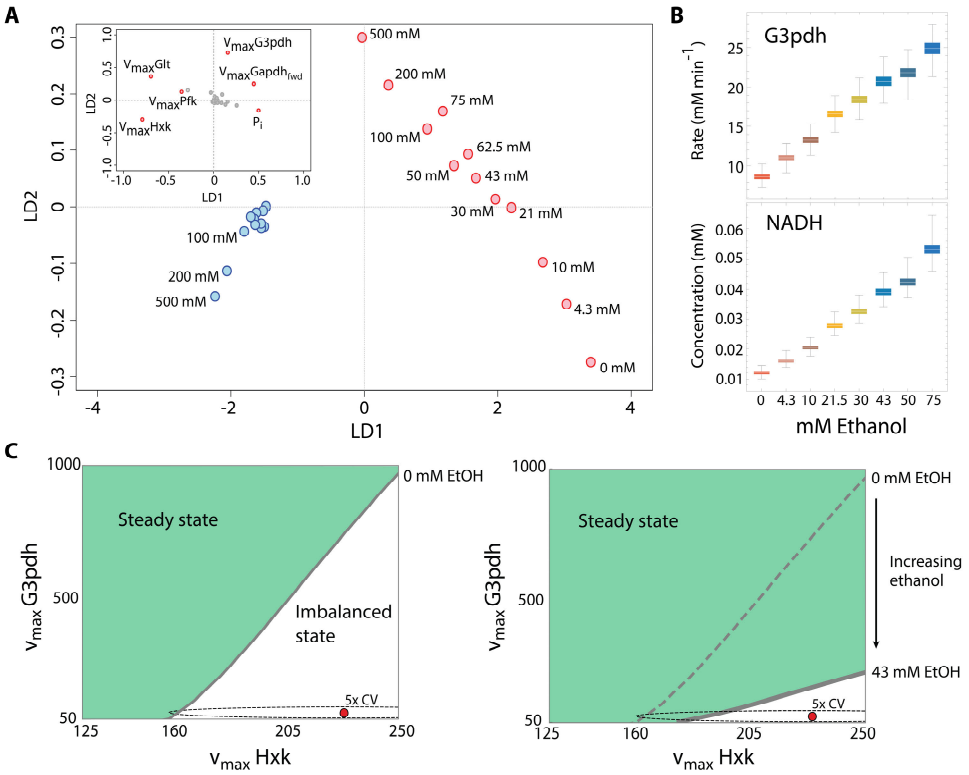

Figure 5.1. Linear discriminants separate sample classes and highlight class-determining variables. (A) Centroids for each independent sample class, when plotted, highlight a clear separation between imbalanced-state (blue circles) and steady-state samples (red circles), which is captured by the first linear discriminant (LD1). The second discriminant (LD2) highlights ethanol-dependent differences between steady-state samples. Ethanol concentrations are indicated next to each steady-state sample (and shown only for imbalanced-state samples associated with the three highest ethanol concentrations). The inset shows the most important variable loadings for the two discriminant axes (also see Fig. 3A, main text). (B) Randomly sampled data, shown as boxplots, that lead to steady state solutions reveal an ethanol-dependent increase in the steady-state G3pdh rate (i.e. flux towards glycerol) and NADH concentration. (C) Shown is the relationship between different combinations of G3pdh and Hxk vmax values and the outcome of model simulations (steady state, green area or imbalanced state, white area). The red dot indicates the values of these parameters in the model. The addition of ethanol leads to a larger range of Hxk and G3pdh values that produce a regular steady state (right panel) – i.e. upon random sampling of these two parameters, within a range 5x coefficient of variation (CV; ± 30 %, indicated by the dashed ellipse), we will see a higher percentage of regular steady states.

6 Trehalose cycle flux estimations by ^{13}C tracer enrichment

Johan H. van Heerden, S. Aljoscha Wahl, Joseph J. Heijnen and Bas Teusink

INTRODUCTION

In the previous chapters we showed that the initial condition-dependent bistable behaviour exhibit by the kinetic model of glycolysis manifests as two distinct phenotypic subpopulations in *S. cerevisiae* cultures. In the absence of a trehalose pathway (*tps1Δ*), most cells are unable to transition to high glucose, but success could be significantly improved by stimulation of a flux towards glycerol. Our kinetic models showed that an increase in ATP hydrolysis (futile cycling) produced a similar result (Chapter 2) and we realized that the stoichiometry of the full trehalose pathway constitutes such a futile cycle. With the cycling of glucose via trehalose, at the cost of ATP and simultaneous recovery of P_i, a large flux towards trehalose could serve to steer glycolysis towards the functional steady state, or at least could significantly increase the probability to reach it.

Our core model (Chapter 2, Appendix A) showed how such a mechanism would function to balance ATP-consumption and production with phosphate availability when the glucose influx suddenly increases. However, the prevailing opinion is that compared to glycolysis, the flux capacity of this pathway is not sufficient to have a significant effect [17, 33, 34, 84].

Due to the bistable dynamics of the system, we hypothesized that a high flux would only be required temporarily; once the system has reached the regular steady state, the need for excessive ATP hydrolysis (and consequential P_i recovery) disappears.

To evaluate this hypothesis, we set out to estimate dynamic flux changes through the trehalose pathway when glucose supply suddenly increases. Using a [^{13}C]-enrichment strategy we quantified both metabolite pool sizes and their labelling patterns over a period of approximately 5 minutes following a glucose pulse. An analytical method by Abate *et al*. [52] allowed us to estimate dynamic flux profiles from the obtained data.

Our results strongly substantiate the hypothesis that trehalose cycling constitutes a temporal futile cycle, which is large enough to guide the system towards the regular steady state after a glucose pulse perturbation.

MATERIALS AND METHODS

Strain, Media and Reference cultivation

The haploid prototrophic *Saccharomyces cerevisiae* strain CEN.PK 113-7D [85] was cultured in an aerobic glucose-limited chemostat using a low-salt defined medium [71] containing: 8.25g L^{-1}glucose, 0.39 g L^{-1}ethanol and 0.05 g L^{-1} silicone antifoaming agent (BDH, UK), yielding a steady-

state biomass concentration of 4.0 g_{DW} L^{-1} (DW, dry weight). Ethanol was added to suppress spontaneous oscillations [86].

The continuous culture was performed in a 7.0 L bioreactor with 4.0 L working volume (Applikon, Schiedam, the Netherlands) at a dilution rate of 0.1 h^{-1}. Temperature was set to 30 ˚C and pH was kept constant at 5.0 by automated addition of 4.0 M KOH (aq). Air was sparged through the culture at a rate of 2.0 L.min^{-1} and stirring was set to 800 rpm. Steady-state conditions were assumed when, after five volume changes, dissolved oxygen, off-gas composition and biomass concentration were stable.

Biomass dry weight was measured, in triplicate, by filtering 5.0 ml broth samples through pre-weighed and pre-dried 0.45 µm cellulose membranes (Supor®-450, Gelman Sciences, Ann Arbor, MI, USA). Next, the membranes were washed with 10.0 ml demineralized water and placed at 70 ˚C to dry (24 hours), before being weighed.

Glucose pulse perturbations

Glucose pulse perturbations were performed by coupling a Bioscope reactor [86] to the chemostat culture; this facilitated multiple sequential perturbations without disturbing the steady state reference culture in the chemostat. The Bioscope flow was calibrated to a rate of 0.475 mL.min^{-1}, which allowed for a total sampling time of 5 min 37 s with samples after: -0 s, 27 s, 50 s, 64 s, 89 s, 107 s, 135 s, 163 s, 204 s, 272 s and 337 s. The culture was perturbed by the addition of 110 mM glucose to the broth flow when entering the Bioscope (see Fig. 6.1 for an illustration of the experimental setup). The sampling time was chosen based on *a priori* expectations of flux dynamics through central carbon metabolism and represents a trade-off between resolving rapid and slow enrichments of the various metabolite pools. Within our system, the main challenge was to ensure that the tracer was sufficiently propagated to the large trehalose pool, whilst maintaining some degree of resolution for the much smaller and rapidly labelled upper glycolytic metabolite pools. The experiments were performed in duplicate from the same chemostat culture for both a, ^{12}C glucose perturbation (for concentration measurements) and a perturbation with uniformly labelled ^{13}C (U-$^{13}C_6$) glucose (for labelling enrichment measurements).

Sample extractions, processing and analysis were performed as in [71] and is briefly described below.

Metabolite extraction and sample storage

Tubes with 100 % methanol (5 mL) were taken from the cryostat (-40 ˚C) and 1 mL of broth was sampled directly into this quenching solution. The biomass is separated from the quenching solution

by centrifugation. To remove the broth supernatant an additional washing step is included. In case of concentration measurements, ^{13}C extract was added. The washed pellet is then extracted by the addition of 5 ml of 75 % (v/v) boiling ethanol. Samples were immediately vortexed and placed in a waterbath at 95 ˚C for 3 min and then returned to the cryostat. Ethanol was evaporated using a RapidVap N2 (Labconco, US). The dried residues were stored at -80 ˚C until further processing.

Metabolite concentration and mass isotopomer quantifications

Mass isotopomer fractions as well as concentrations of glucose 6-phosphate (G6P), fructose 6-phosphate (F6P), glucose 1-phosphate (G1P), fructose 1,6-bisphosphate (FBP), trehalose 6-phosphate (T6P), uridine-diphospho-glucose (UDP-GLU), and 6-phosphogluconate (6PG) were determined using anion- exchange liquid chromatography mass spectrometry (LC-MS) [71]. The concentration of ATP was determined by ion-pair reverse-phase LC-MS [71]. Additionally, G6P, F6P, FBP, T6P and Trehalose (TREH) were measured, as methoxime-trimethylsilyl derivatives, by gas chromatography (GC)–MS. The intracellular concentrations were determined based on Isotope dilution (ID)-MS [71]. Where applicable, metabolite values determined by more than one platform were combined.

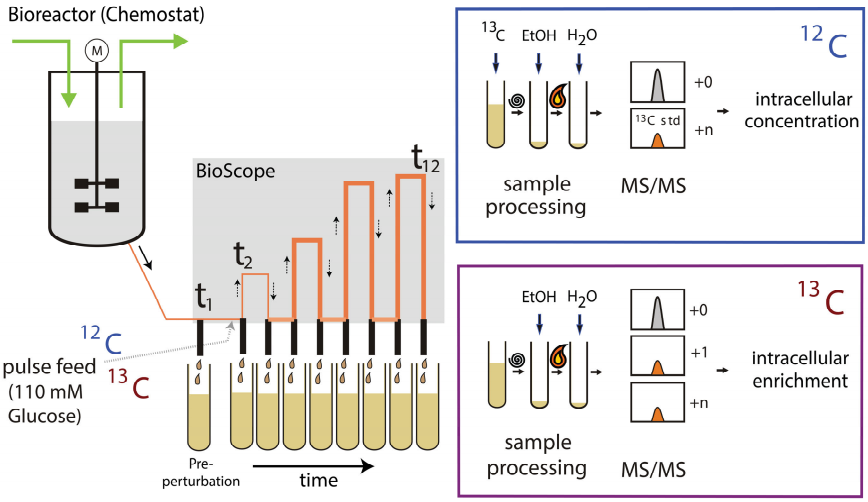

Figure 6.1. Schematic illustration of the isotope labelling experimental setup used for glucose pulse perturbations, sample collection and processing. See text for details.

Hybrid modelling approach

In a 'classical' kinetic modelling approach, the flux is a function derived from an enzyme mechanism (e.g. Uni-uni). A flux (v) is influenced by the concentrations (c) of the substrate(s), products(s) and inhibitors(s)/activator(s) and the enzyme-kinetic properties (α) (e.g. maximal activity, substrate affinity). In general, v is a non-linear function of concentrations $c$and parameters α:

$$v(c,\alpha) \tag{E6.1}$$

However, it is often difficult, if not impossible, to accurately describe in vivo reaction mechanisms due to the complex, or unknown, nature of allosteric regulations and other physicochemical variables. Therefore, the reaction mechanism function (which requires several kinetic assumptions) is replaced by an approximation of the result: the flux value in time. The flux is defined as a continuous piece-wise affine (PWA) function with switch-times (time points between which linear functions are used) and flux values at the switches. E.g. the uptake reaction rate v_1 can be described by (three switches):

$$v_1(t) = \begin{cases} v_{1,t_0} \dfrac{v_{1,t_1} - v_{0,t_0}}{t_1} t & t \le t_1 \\ v_{1,t_1} + \dfrac{v_{1,t_2} - v_{1,t_1}}{(t_2 - t_1)}(t - t_1) & t_1 < t \le t_2 \\ v_{1,t_2} + \dfrac{v_{1,t_3} - v_{1,t_2}}{t_3 - t_2}(t - t_2) & t_2 < t \le t_3 \end{cases} \tag{E6.2}$$

This function has four parameters, $\Theta_1 = (v_{1,0}, v_{1,1}, v_{1,2}, v_{1,3})^T$.

With these flux functions, the balance equations for the concentrations and the labelling can be formulated similarly to the kinetic modelling approaches. In the approach, the labelling enrichment is simplified and represented as C-molar ^{13}C enrichment. Thus, each metabolite has a concentration and one ^{13}C enrichment fraction. The balances are derived from the defined stoichiometric network (see Table 6.1 for overview). As an example, the F6P pool has an influx from G6P (Pgi, v2) and an efflux towards FBP (Pfk, v3). The concentration change can be described by the respective in- and out-fluxes:

$$\frac{dc_{\mathrm{F6P}}}{dt} = v_2 - v_3 \tag{E6.3}$$

For the C-molar labelling enrichment (x_{F6P}), the labelling state of the substrate and the pool itself has to be taken into account:

$$c_{\mathrm{F6P}} \frac{dx_{\mathrm{F6P}}}{dt} = x_{\mathrm{G6P}} v_2 - x_{\mathrm{F6P}} v_3 \tag{E6.4}$$

Note that the concentration of the pool has an impact on the labelling enrichment dynamics – the equation systems E6.3 and E6.4 have to be solved simultaneously.

The simplification of the labelling state to C-molar enrichment requires assumptions in the case of bi-molecular reactions, e.g. the split of trehalose into two glucose moieties. Here, it is assumed, that the labelling enrichment is equally distributed over the two glucose (in this case G6P as intracellular glucose is not balanced) moieties:

$$\begin{aligned} c_{\mathrm{G6P}} \frac{dx_{\mathrm{G6P}}}{dt} = {} & x_{\mathrm{Glc,ext}} v_1 - x_{\mathrm{G6P}} v_2 + x_{\mathrm{F6P}} v_{2\mathrm{bwd}} - x_{\mathrm{G6P}} v_5 \\ & - x_{\mathrm{G6P}} v_{12} + 2x_{\mathrm{TREH}} v_9 + \left(x_{\mathrm{G1P}} v_{5\mathrm{bwd}} \right) \end{aligned} \tag{E6.5}$$

This is justified for the small observed metabolic network especially, when uniformly labelled glucose is used and the C6 units stay intact within the considered reactions.

Network architectures

For the estimation of flux dynamics, two alternative networks were defined (see Table 6.1 for stoichiometric definitions). The first represented a minimal network that included only measured components. The second network was an extension of the first and included a glycogen cycle. The latter was defined to evaluate the potential influence of glycogen cycling on the ^{13}C-enrichment dynamics of the UDP-GLU and G1P pools. Although the glycogen pool was not measured, cycling between UDP-GLU and G1P, through this pool, was simulated by including a large (initially unlabelled) glycogen sink (see Fig. 6.3 for a graphical illustration of these two architectures).

Estimation of fluxes

In short, each measurement (concentration as well as enrichment) y_{i,t_k}, can be compared with the model predicted value (result of the integration of E6.4, E6.5):

$$\begin{aligned} \varepsilon_1 &= y^c_{G6P,t_1} - c_{G6P}(\theta, t_1) \\ \varepsilon_2 &= y^x_{G6P,t_1} - x_{G6P}(\theta, t_1) \\ &\vdots \\ \varepsilon_{j-1} &= y^c_{Treh,t_n} - c_{Treh}(\theta, t_n) \\ \varepsilon_j &= y^x_{Treh,t_n} - x_{Treh}(\theta, t_n) \end{aligned} \tag{E6.6}$$

In a successful regression, the parameters $\Theta = \left(v_{1,t_0}, v_{1,t_1}, v_{1,t_2}, v_{1,t_3}, \ldots, v_{m,t_0}, \ldots, v_{m,t_n} \right)^T$ (as defined in E6.2 for one flux) are estimated such, that the (random) deviation between prediction and all measurements $\varepsilon = \left(\varepsilon_1, \ldots . \varepsilon_j \right)^T$ is minimal:

$$\hat{\theta} = \arg\min_{\theta} \varepsilon^T \, \Sigma_y^{-1} \, \varepsilon \tag{E6.7}$$

To estimate the accuracy of the determined flux profiles, linearized error propagation of the regression model in eqn. E6.6 was applied. The parameter covariance matrix is calculated by:

$$\Sigma_\theta = \left(\frac{dy}{d\theta} \Sigma_y^{-1} \frac{dy^T}{d\theta} \right)^{-1} \tag{E6.8}$$

The covariance matrix (Σ_y) represents the measurement accuracy of concentration as well as the labelling measurements. The diagonal of the covariance matrix (Σ_θ) contains the variances of the estimated parameters.

The results are displayed in Fig. 6.2, and are based on the following assumptions: The enrichment is measured with a standard deviation of 2 % (absolute deviation of each measurement point). This value is based on previous repetitive experiments (~0.5 % technical deviation of repetitive measurements) and measurements of natural labelled samples where the expected distribution can be calculated.

Concentrations are measured with 5 % standard deviation – the absolute standard deviation is estimated based on the average concentration. This assumption is based on the ID-MS protocol that relies on isotope ratios (see references within [71]). Because of additional sample preparation steps, the deviation is higher than for enrichment measurements.

Table 6.1. Description of metabolic reaction network used to estimate fluxes between upper-glycolytic and trehalose pathway enzymes

	Reaction Name	Catalysed transition	C-atom transitions*
Upper Glycolysis	Glucose Feed (v0)	Feed → Extracellular glucose	#ABCDEF → #ABCDEF
	Glucose Transport / Hexokinase (v1)	Extracellular glucose → G6P	#ABCDEF → #ABCDEF
	Phosphoglucose isomerase (v2)	G6P ← → F6P	#ABCDEF ← → #ABCDEF
	Phosphofructokinase (v3)	F6P → FBP	#ABCDEF → #ABCDEF
	Aldolase/Glycolysis Sink (v4)	FBP → External Sink	#ABCDEF → #ABCDEF
Trehalose pathway§	Phosphoglucomutase (v5)	G6P ← → G1P	#ABCDEF ← → #ABCDEF
	UDP glucose pyrophosphorylase (v6)	G1P → UDP-GLU	#ABCDEF → #ABCDEF
	Trehalose 6-phosphate synthase (v7); tps1	G6P + UDP-GLU → T6P	#ABCDEF + #abcdef → #ABCDEFabcdef
	Trehalose 6-phosphate synthase (v7) (alternative, dependent only on G6P fragment); tps1	G6P → T6P	#ABCDEF → #ABCDEF
	Trehalose 6-phosphate phosphatase (v8); tps2	T6P →TREH	#ABCDEFabcdef → #ABCDEFabcdef
	Trehalose 6-phosphate phosphatase (v8) (alternative, dependent only on G6P-derived T6P enrichment); tps2	T6P → TREH	#ABCDEF → #ABCDEF
	Trehalase (v9)	TREH → G6P	#ABCDEFabcdef → #ABCDEF + abcdef
	Trehalase (v9)	TREH → External Sink	#ABCDEF → #ABCDEF

Table 6.1. Continue

	Reaction Name	Catalysed transition	C-atom transitions*
Glycogen cycle ‡	Glycogen Synthase (v10)	UDP-GLU -> Glycogen	#ABCDEF → #ABCDEF
	Glycogen Phosphorylase (v11)	Glycogen (sink) -> G1P	#ABCDEF → #ABCDEF
PPP	Glucose 6-phosphate dehydrogenase (v12)	G6P → 6PG	#ABCDEF → #ABCDEF
	6-Phosphogluconate dehydrogenase/Pentose phosphate pathway sink (v13)	6PG → External Sink	#ABCDEF → #ABCDEF

*****Letters denote individual carbon atoms. Grey shaded rows indicate reactions which were included in the alternative network, which were used for comparison to the results derived from the minimal network, represented by unshaded rows and presented in the main text (also see Fig. S16). [§] The enrichment of the T6P pool (a disaccharide) can alternatively be estimated as the enrichment of the G6P-derived fragment only. [‡]Although the glycogen pool was not measured, cycling between UDP-GLU and G1P, through this pool, was simulated by including a large glycogen sink. PPP, Pentose phosphate pathway.

The steady-state (pre-pulse) flux value, as well as the flux at the end of the experiment, is not considered in the covariance calculation. Based on the measured data, the steady-state value is not observable. For the last timepoint, most of the metabolites have already reached a steady-state (i.e. unchanging) enrichment, hindering the observability of the last timepoint for the glycolytic flux.

RESULTS

We focused our analysis on an estimation of fluxes through the trehalose cycle and the upper-part of glycolysis (see Fig. 6.3). Based on the acquired data, we defined a minimal network that included concentration and ^{13}C-tracer enrichment data for G6P, F6P, FBP, UDP-GLU, T6P, TREH and 6PG, and concentration data for G1P. The measurement of G1P enrichment is technically difficult – the concentration of G1P is low and there is co-elution with Mannitol-1-phosphate. Flux profiles were estimated using the PWA functions described above, with 4 defined switch times: 27 s, 45 s, 80 s and 150 s. Two additional points at 0 s and 340 s designate the start and the end of the flux estimation time domain, respectively, resulting in dynamic profiles composed of five flux vectors.

In the first instance we used the minimal network (shown in black in Fig. 6.3) and applied parameter estimation to find dynamic flux profiles that reproduce the measurements. We estimated fluxes as net forward rates only (i.e. all backward rates were set to 0). The dynamic flux profiles (Fig. 6.4A) estimated from the minimal network architecture (Fig. 6.3) resulted in good fits for most of the measured data (Fig. 6.4B). Importantly, the simulated labelling and concentration profiles resembled many features of the measured profiles, indicating that the applied metabolic network and modelling approach captures the most relevant mechanisms and dynamics of the *in-vivo*

metabolic activity. Two exceptions should, however, be pointed out. Both the UDP-GLU enrichment and 6PG concentration simulations still deviated from the measured data.

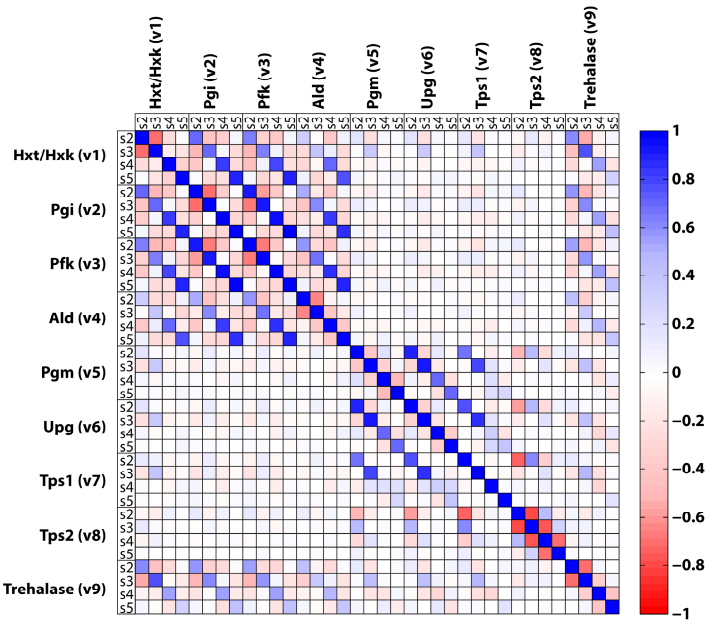

Figure 6.2. Correlation of estimated fluxes. Shown are the correlations for the minimal network (see text and Fig. 6.3) at switch times s2 - s5 (27 s, 45 s, 80 s and 150 s). High correlations are observed for fluxes in a reaction sequence, e.g. Hxk -> Pgi -> Pfk -> Ald as well as for consecutive switch times (e.g. Hxk(s2) and Hxk(s3) are negatively correlated). The trehalose cycle fluxes (especially trehalase) are correlated with Hxk, Pgi and partly also Pfk and Ald.

The discrepancy between the model-derived fit and the measured concentration data for the 6PG pool is not unexpected and can readily be explained. In our network definition, 6PG is derived directly from G6P as opposed to 6-phosphogluconolactone, an intermediate metabolite which we could not measure. Furthermore, we decided to set the efflux rate out of the 6PG pool equal to the influx rate (to reduce the amount of parameters) and consequently the concentration of 6PG remains constant. Although the 6PG concentration does decrease slightly following the glucose pulse, this change is negligible relative to the changes observed in the other larger metabolite pools. In spite of these simplifications, the enrichment dynamics around this pool were sufficiently captured (Fig. 6.4B). Additionally, the fraction of glycolytic flux channelled towards this pool (and therefore towards the pentose phosphate pathway) stabilized at around 12 % (see Fig. 6.4A, flux ratio of v12/v1), similar to previous flux values reported for this branch (referenced in [87]).

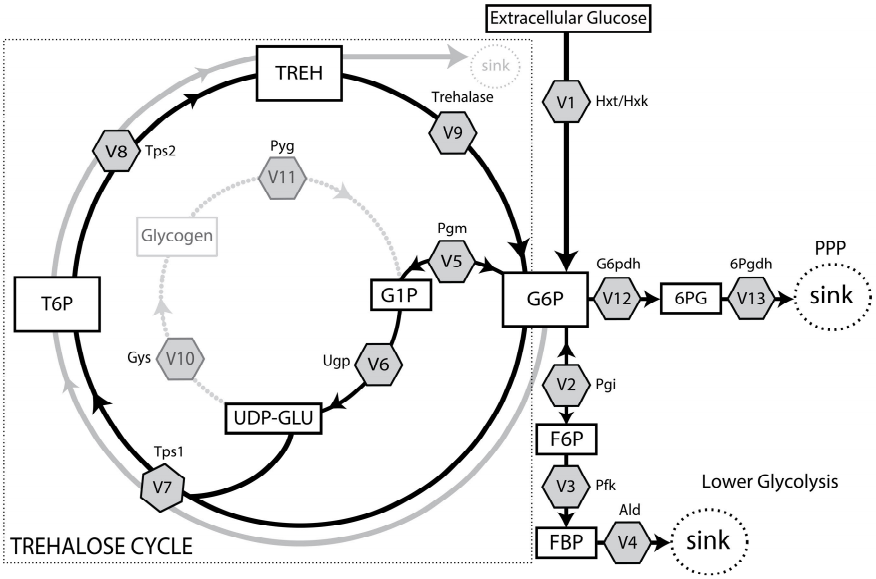

Figure 6.3. Overview of the network architecture(s) used for the estimation of *in vivo* flux profiles. The minimal network is drawn with black arrows; the extension including the glycogen cycle is indicated in grey (dotted). Hexagons represent reactions, (with rates, µmol.gDW^{-1}.s^{-1}), and blacked framed white rectangles represent metabolite pools (with concentrations, µmol.gDw^{-1} and fractional enrichment). Dotted ovals indicate network sinks (i.e. pools which are not balanced in the network). Shown are two flux routes towards the T6P pool, both via v7. The black route is dependent on both the UDP-GLU and G6P pools, whereas the grey route is dependent only on the G6P pool. See text for a detailed explanation.

The deviation between simulation and enrichment data for the UDP-GLU pool is slightly more difficult to explain, but likely results from missing interactions between this pool and other metabolite pools for which information is lacking. Within the minimal network, UDP-GLU is derived from G1P, which in turn is derived from G6P. This linear propagation scheme, however, leads to an overestimation of the rate at which enrichment of the UDP-GLU pool occurs, suggesting that an influx of an additional unlabelled carbon source is required to delay the enrichment rate.

To this end, we introduced the glycogen pool (Fig. 6.3). Glycogen constitutes another large intermediate storage carbohydrate pool [88], which acts as a sink for cycling between UDP-GLU and G1P (UDP-GLU → Glycogen → G1P → UDP-GLU). Introduction of these additional reactions improved the overall fit of the UDP-GLU enrichment data, with very good approximations for data points from 50s onwards; however, a discrepancy remained between the simulation and the 2nd

time point (27s), which we were unable to fully resolve (Fig. 6.4B). The dynamic flux profiles for this network are shown in Fig. 6.4A.

Although there were some minor quantitative differences between the solutions offered by the two network architectures, the qualitative differences (and the functional interpretations which follow) were minimal. A comparison of the dynamic flux profile simulations for these two networks (Fig. 6.4A), show only small differences for the trehalose cycle fluxes. This is of course not wholly unexpected as an additional route for UDP-GLU was introduced by means of the large glycogen pool. Cycling via this pool effectively reduces the rate of carbon enrichment propagation from the UDP-GLU pool towards trehalose. Importantly, however, is that the time-dependent fraction of glycolytic flux branched towards trehalose is functionally the same for both network variations, and accurately captures the dynamics of concentration changes and label enrichment of the relevant metabolite pools (Fig. 6.4B). We find that regardless of whether a glycogen cycle is included or not, the percentage of glycolytic flux channelled towards the trehalose pool is significant, with dynamic profiles being very similar. In the case of the minimal network (without a glycogen cycle), this reaches a maximum of 28 %, while in the network including a glycogen cycle, the Tps1 flux percentage peaks at 27 %.

In Chapter 2 the results obtained from the minimal network are presented, as the inclusion of a glycogen flux, although improving the simulation of UDP-GLU enrichment, had no effect on the functional behaviour of the network. In addition, the glycogen cycle extension introduces more parameters and compared to the number of additional degrees of freedom, the improvement appears small. Thus, given the lack of functional differences between the two network variations, we were confident that the minimal network captured the most relevant mechanisms and dynamics of the *in-vivo* metabolic activity.

SUMMARY

A core model of glycolysis (Chapter 2, Appendix A) showed how an increase in futile cycling activity would function to steer glycolysis towards a balanced steady state. We wondered if the trehalose cycle could fulfil this function, given that the stoichiometry of the full pathway is that of a futile cycle. However, it was uncertain whether the flux capacity of the trehalose pathway would be sufficient to have a regulatory impact on glycolysis. To answer this question, we used a ^{13}C-tracer enrichment strategy to estimate dynamic flux changes through upper-glycolysis and the trehalose cycle, following a sudden increase in glucose.

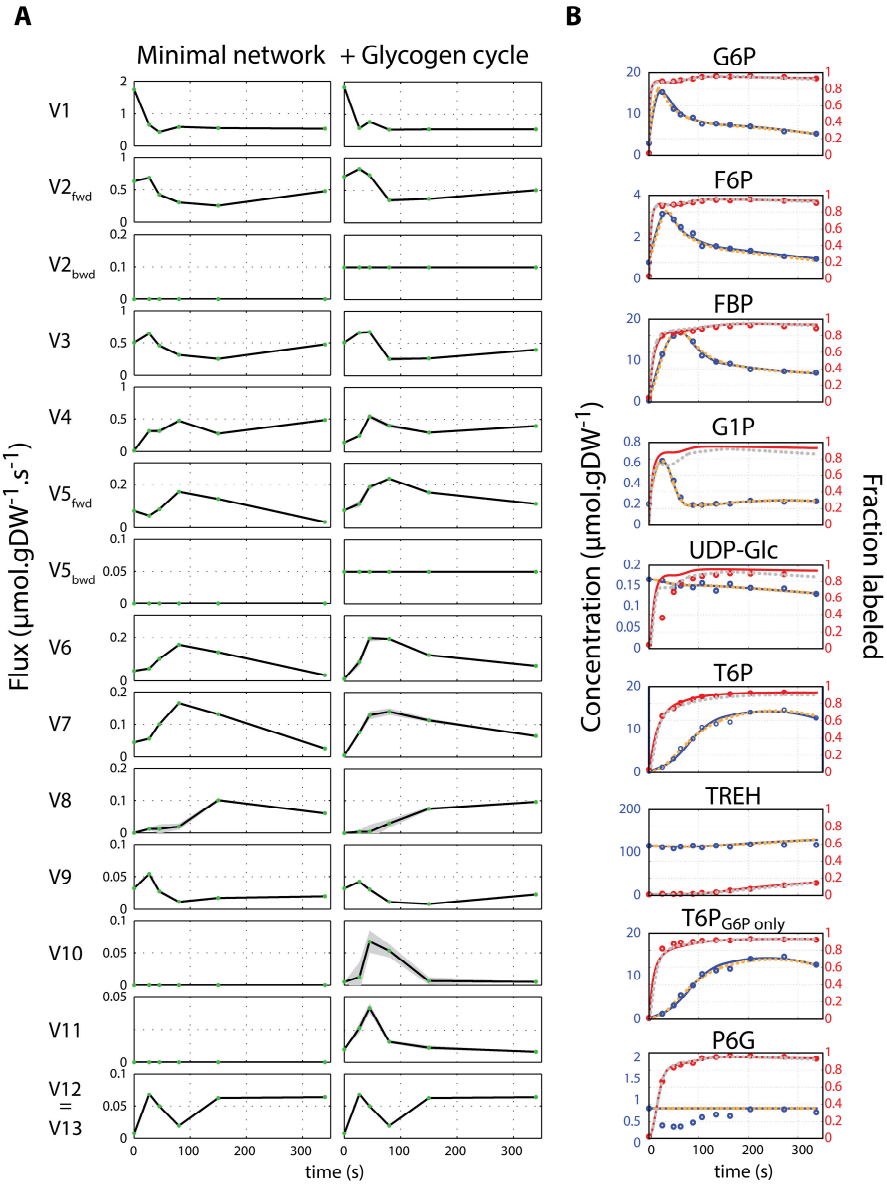

Figure. 6.4. Overview of dynamic flux profiles and resulting metabolite and label enrichment simulations. (A) The time dependent flux profiles for the reactions included in the minimal network and the extension including the glycogen cycle. Estimated standard deviation is indicated by a grey region. The green dots denote the switch times of the piece-wise affine functions (see text above). (B) The metabolite and label enrichment simulations for both networks are very similar and accurately capture measured metabolite (Red circles) and label enrichment (Blue circles) data. Minimal network simulations are shown as solid lines: Red = label enrichment, Blue = metabolite concentrations. The simulation result for the network including a glycogen cycle is shown by dotted lines: Grey = label enrichment, Orange = metabolite concentrations.

The flux profiles of the reactions in our defined system (Fig. 6.3) show that all fluxes are highly dynamic (Fig. 6.4). We find that after a glucose pulse as much as 28 % percent of the uptake flux is channelled towards trehalose; a significant amount that could clearly impact both the overall glycolytic flux and phosphate homeostasis.

By considering the dynamics of upper-glycolytic fluxes relative to those of the trehalose cycle, a more nuanced interpretation of regulatory contributions by trehalose metabolism becomes possible. Here, the temporal offset between Tps1 and Tps2 fluxes is particularly informative. Following the glucose pulse, the Tps1 flux increases rapidly after 27 s (when G6P concentrations are highest), until a maximum is reached at 80 s post-pulse. At this point the Tps2 flux starts increasing rapidly, peaking at 150 s. These profiles indicate that the initial period following the pulse is primarily characterized by the rapid accumulation of T6P (up to 80 s); as reflected by metabolite profiles (Fig 6.4). When the Tps2 flux subsequently increases, T6P accumulation will slow down and P_i recovery will increase. From these results one can infer that the regulatory mechanism embedded in the trehalose pathway probably involves the differential contribution of several processes. Initially, accumulating T6P will serve to slow down the rate of glucose phosphorylation by Hxk, thereby moderating the rapid consumption of ATP. Next, the flux bottleneck at Gapdh - which results from P_i accumulation in upper-glycolytic intermediates - can be reduced by dephosphorylation of T6P. A third aspect of this cycling mechanism is the removal of G6P. Removal of G6P will effectively translate to lower Pgi and Pfk rates (in the regime where these reactions are not substrate saturated), further moderating ATP-consumption by upper-glycolysis.

To test the extent to which these aspects contribute to establishing a balance between upper and lower-glycolytic fluxes, we returned to our detailed kinetic model (Chapter 3). We employed the random sampling approach outlined in Chapter 5, and evaluated steady state outcomes when trehalose cycle features are systematically omitted (Chapter 2, Fig. 2.8). While P_i recovery was found to be the primary mechanism, Hxk inhibition and G6P removal were additionally required to ensure functional steady state outcomes. Together these results provide strong evidence for the (re)interpretation of population level phenotypes of trehalose cycle mutants and rescue mechanisms.

Finally, our results show activation of this pathway to be transient. That this temporary activation can be of regulatory significance can only be understood when the dynamics of glycolysis is considered. The bistable nature of glycolysis means that futile cycling will only be required immediately following a flux increase. Once a new stable state is established, trehalose pathway fluxes can be safely down-regulated; given the energetic consequences of futile cycles, this regulatory model makes a lot of sense.

7 General discussion and perspective

In natural environments, fluctuating conditions are part and parcel of the everyday life of a microorganism. Changes in environmental variables such as temperature, water pressure and nutrient availability all require some degree of physiological and biochemical adaptation, which function to maintain the integrity and competitive fitness of a cell. Often these adaptations are described by comparing differences between one adapted state and another. For this reason, historical emphasis has been on gene and protein expression changes. While specific physiological adaptations are ultimately achieved by rearrangements in metabolic pathways, these changes take time to take effect, which limits their efficacy in response to sudden and unexpected environmental changes. Under dynamic conditions, cells therefore also require mechanisms that can act immediately to regulate metabolic fluxes.

As such, the main aim of this thesis was to advance an understanding of metabolic regulation under dynamic conditions. For this we chose to look at the regulation of glycolysis in response to a sudden increase in glucose availability. While this scenario has been extensively investigated, and metabolite dynamics have been described by many studies [25, 61, 89–92], much less is known about the regulatory mechanisms that coordinate metabolite and flux dynamics in response to sudden changes in glucose availability.

As a case study for dynamic metabolic regulation, the *S. cerevisiae tps1Δ* mutant presented an interesting candidate. This mutant is unable to cope with a sudden increase in glucose availability, with its metabolic phenotype suggestive of a deficit in regulatory mechanisms that maintain an ATP and inorganic phosphate balance, when glucose uptake suddenly increases. First described more than 30 years ago, the mechanistic origin of this mutant's phenotype have been difficult to pinpoint. Various mechanisms have been proposed (summarised in Chapter 1), but to date, none could sufficiently account for the metabolic phenotype.

My thesis reports a study of the mechanistic failure that underlies the *tps1Δ* phenotype, using a combination of theory, modelling and experimentation. We discovered a novel metabolic regulatory mechanism, involving a transient increase in futile cycling through the trehalose pathway. Importantly, the picture that emerged from this work showed that regulatory events can be transient and only relevant immediately following a perturbation. Furthermore, we showed that the outcome of metabolic regulation can be understood as a probabilistic phenomenon; a scenario that adds to current deterministic conceptions about metabolism and its regulation.

In this final chapter, I will briefly revisit some important outcomes, address some potential caveats and elaborate on the consequences of certain findings. These discussion points serve to

highlight not only key insights, but also to emphasize some open ended questions that will require future research to fully resolve.

As with any scientific study, the specific methods employed come with certain caveats that could impact conclusions. While this is usually unavoidable, clearly identifying these will delineate the relevance and extensibility of our findings. As a first discussion point, I will address the kinetic model of glycolysis that served as a theoretical point of departure for much of the experimental work.

Model simplifications and parameterizations

Many of the insights presented in this thesis were derived from mathematical simulations of yeast glycolysis and a consideration of some of its important simplifications and parameterizations is required.

Several kinetic models of glycolysis are available and we opted to start with a model originally published by Teusink et al [41]. This model included detailed kinetic descriptions of all glycolytic reactions, but the recent determination of enzyme kinetics in an *in vivo*-like buffer [60] highlighted the need to update some of the kinetic parameters, and include key allosteric interactions (Chapter 3). In addition, given the features of the system we were interested in, extensions of the model to include a trehalose pathway and phosphate as a dynamic variable were required.

Simplifying the trehalose pathway

In deciding on an implementation of the trehalose pathway, we chose for a simplified approximation (Chapter 2). We defined a flux towards trehalose using a simple mass-action reaction dependent on G6P concentration; additionally the mass balances of ATP, P_i and G6P were modified to include this flux, and we implemented inhibition of Hxk by G6P, as a proxy for inhibition by T6P. Owing to the fact that the first two reactions of the pathway are catalysed by a trehalose synthase enzyme-complex (Chapter 1, Figure 1.3), consisting of the catalytic subunits Tps1 and Tps2, and two regulatory subunits, Tps3 and Tsl1, formulation of a rate equation is not straightforward. While some attempts have been made to characterize the kinetic properties of the two catalytic subunits (Tps1 and Tps2), these have been found to be highly dependent on interactions with regulatory subunits, which in turn are subject to several regulatory signals [18–20]. Our own attempts to formulate a rate equation from existing kinetic characterizations, which could approximate experimentally determined fluxes, were not successful. This failure was not completely unexpected

as it has been shown that almost all of the enzymes in the trehalose pathway are subject to condition-specific post-translational phosphorylation [21], the impact of which is not fully understood. In addition, all existing kinetic descriptions are derived from *in vitro* assays that were performed in reaction buffers with little resemblance to *in vivo* (cytoplasmic) conditions.

Although details of the trehalose pathway have no bearing on the behaviour of our *tps1Δ* model, it did impact our ability to quantitatively consolidate the WT version with experimental results. Here the most obvious discrepancy between our simulations and experimental results is seen in the frequency of imbalanced outcomes for the WT model. While we saw a good match between the predicted and experimental frequencies of SS and imbalanced fractions for *tps1Δ*, our WT model appeared to overestimate the robustness of WT glycolysis. Flow cytometry results (Chapter 2, Fig. 2.4C) showed that approximately 7 % of WT cells end up in the imbalanced state, whereas the small parameter variations included in our random sampling simulations (Chapter 5) produced no such events. Exploration of initial condition-dependence in the WT model showed that very large deviations from the reference state would be required to produce imbalanced outcomes. This mismatch is not entirely surprising, as the kinetic characteristic of the trehalose synthase complex are likely to have an important impact on its *in vivo* efficacy in WT cells.

While our model could not qualitatively reproduce the experimental behaviour of WT cells, it contained sufficient detail to identify the existence of a bistability and gain insight into the factors that determine robustness during a sudden increase in pathway flux. These insights allowed us to make specific predictions that were tested experimentally. For example, our model predicted that an increase in Hxk activity would result in a larger imbalanced fraction of cells, which was validated by overexpression of Hxk in WT cells and (Chapter 4, Fig. 4.8); with hindsight, this is easily understandable without the model.

Whereas the exact implementation of the trehalose cycle only relates to the WT model, the definition of inorganic phosphate (P_i) as a free variable turned out to be essential for a general understanding of pathway dynamics.

Phosphate as a free variable

One of the key features of the *tps1Δ* phenotype is the rapid depletion of P_i while FBP continues to accumulate. Insufficient P_i availability has been interpreted as a primary cause of the apparent imbalance between upper- and lower-glycolytic fluxes, with a flux bottleneck resulting at the level of Gapdh. Importantly, the sustained accumulation of FBP shows that P_i must continue to enter the system, but that this supply is somehow insufficient to restore a high flux through lower glycolysis. To capture this behaviour we redefined phosphate as a free variable (Chapter 3) by including a non-cytoplasmic pool that could be mobilized to support continued FBP accumulation. Here the extracellular space and the vacuole were the two obvious candidates. NMR studies have demonstrated that P_i is predominantly mobilized from vacuoles, while extracellular P_i is left largely untouched [23, 40]. In line with this, we defined a vacuolar phosphate pool that allowed for phosphate exchange, modelled as a simple diffusion reaction, with parameters set such that the rate of FBP accumulation approximately matched available data [24]. With this addition, our model reproduced the continued accumulation of FBP at low P_i and ATP levels (Chapter 2, Figure 2.2).

Importantly, phosphate dynamics turned out to be an essential feature of the bistable behaviour of glycolysis. While we showed that differences in initial phosphate concentration affected which state the system would reach, in both the *tps1Δ* and WT models, it was the capacity to rapidly liberate phosphate that contributed significantly to the robust startup of glycolysis; this was inferred to be one of the functions of trehalose cycle.

Although the flux imbalance that results from insufficient phosphate availability is clearly demonstrated by our model, it is not obvious why *tps1Δ* cells experience a phosphate limitation when an abundance of phosphate is available in the extracellular space.

Phosphate limitation is a consequence of an import bottleneck, not availability

In our model, we found that a very high rate of phosphate mobilization, from the vacuolar pool, led to the disappearance of the imbalanced state (Fig. 7.1). This can easily be understood by considering the situation where phosphate concentration is fixed (equivalent to being mobilized infinitely fast). In this instance phosphate concentrations do not change and never become limiting. Similarly, if the rate of phosphate mobilization is much higher than the rate of consumption by glycolytic reactions, changes in cytoplasmic concentrations will be minor and as such will approximate the situation where phosphate is fixed. This finding suggested that a sudden large influx of P_i would reduce the need to liberate phosphate through ATP hydrolysis and should drive the system to a steady state.

We wondered whether this could be achieved experimentally by changing pre-culturing conditions, such that the initial phosphate uptake capacity of cells is maximized prior to a glucose challenge.

We attempted to enhance initial phosphate uptake by pre-incubating cells under phosphate starvation conditions. At extracellular phosphate concentrations < 100 µM the high affinity transporter, PHO84, should be fully induced [93, 94]. Wykoff *et al.* [95] reported a fourfold increase in uptake capacity when WT cells were pre-incubated under phosphate starvation conditions, with a V_{max} of 19.4 nmol.OD^{-1}.min^{-1} or 2.15 µmol.gDW^{-1}.s^{-1} (assuming 10^7 cells per mL [96] and a dry weight of 15 pg [69] per cell). It is clear that, under these conditions, maximal uptake capacity should be well in excess of the maximal flux measured through the trehalose cycle, which we estimated to be 0.17 and 0.1 µmol.gDW^{-1}.s^{-1} for Tps1 and Tps2, respectively (Chapter 6). Unfortunately, our attempts to enhance phosphate uptake by prior starvation, had no visible effect on the growth behaviour of *tps1Δ* cultures.

Alternatively, overexpression of phosphate transporters could theoretically increase uptake capacity. However, Luyten et al. [23] reported a failure to rescue the *tps1Δ* phenotype by phosphate transporter overexpression. While it is clear that ample phosphate should be available, and uptake capacities should theoretically be sufficient to meet demand by glycolysis, uptake from the medium appears to be limited by some other physicochemical or regulatory constraint. Although we do not have direct evidence for the cause of the apparent bottleneck in phosphate acquisition, the available literature on phosphate transport mechanisms in *S. cerevisiae* provides sufficient information to propose a hypothesis.

Phosphate transport into the cell is tightly coupled to H^+ translocation, and this process is dependent on the maintenance of a proton gradient across the plasma membrane [97]. The disruption of this proton gradient will impede phosphate uptake via the H^+/PO_4^{3-} transport system [98]. Importantly, the plasma membrane H^+-ATPase, PMA1, is responsible for the generation of the proton gradient and the membrane potential that act as the driving force for phosphate uptake [98]. These features, when placed in the context of the pH homeostasis disturbances (Chapter 4) and an absence of glucose-induced activation of the plasma membrane H^+-ATPase [29, 40], provide a reasonable, although admittedly speculative, hypothesis for the apparent lack of phosphate uptake from the medium by *tps1Δ* mutants.

To further explore this hypothesis, overexpression of the K^+/H^+ antiporter system involving the potassium transporters TRK1 and TRK2 could offer an alternative means to augment the maintenance of pH homeostasis [99, 100] and membrane potential [101], and possibly relieve an electrochemical bottleneck that might be impeding phosphate uptake from the medium.

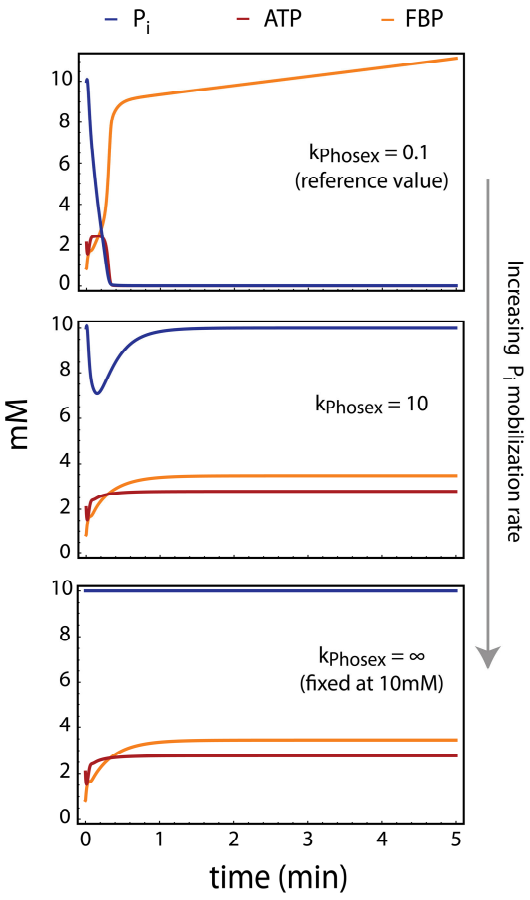

Figure 7.1. Sufficiently fast phosphate mobilization or acquisition eliminates the appearance of an imbalanced state. Shown are the metabolite profiles of P_i, ATP and FBP at three different rates of phosphate mobilization in the *tps1Δ*-version of the large kinetic model.

The link between pH and growth phenotypes

Growth happens on much longer time scales than the metabolic processes for which we originally predicted the bistable behaviour. Having clearly established the presence of a growing and non-growing fraction in *tps1Δ* populations, using plating assays and microtitre growth experiments (Chapter 4), we exploited cytoplasmic pH (pH_i) readouts as a means of linking growth outcomes to the metabolic bistability.

In response to a glucose pulse, *S. cerevisiae* exhibits a rapid and transient drop in cytoplasmic pH [75, 100, 102, 103]. Using a combination of hexose kinase deficient mutants and different substrates, Ramos *et al.* [100] argued that this acidification is largely a consequence of the ATP-driven phosphorylation of hexose sugars in the upper part of glycolysis. Following this initial

acidification, an efflux of H^+ results in alkalization and the restoration pH_i [100]. This restoration is dependent on the activation of the H^+-ATPase (PMA1) proton pump [104, 105], an energetically expensive process that requires ATP [106]. As such, the rapid and sustained depletion of ATP in the imbalanced state will have a significant impact on the ability to drive proton extrusion to restore and maintain pH_i, as shown for *tps1Δ* in this thesis (Chapter 2, Fig 2.2) and previously [40].

Flow cytometry data revealed the glucose-induced appearance of two distinct pH subpopulations, with frequencies corresponding to the viability counts of plating assays. From this we inferred a correlation between pH outcomes and growth phenotypes. While the energetic burden associated with a low pH_i could already explain a significant reduction in growth capacity, the pH-dependence of enzyme activities provides further substantiation for this inference. In this regard, we used pH titrations to measure the enzyme activities for several available purified *S. cerevisiae* glycolytic enzymes, using *in vivo*-like assays [60] (Appendix B). We found large decreases in the activities of all enzymes as pH was lowered. Significantly, at a pH of 6, Gapdh showed a 93 % loss in glycolytic activity (i.e. converting glyceraldehyde-3-phosphate to 1,3-bisphosphoglycerate), relative to the reference at pH 6.94 (Fig. 7.2); no other enzymes tested displayed this degree of sensitivity. This suggested that the lower glycolytic flux (and hence ATP-production capacity) will be severely restricted in the low pH_i subpopulation. Taken together, cells with low ATP and low pH_i are unlikely to recover from the imbalanced state if high glucose conditions persist. ATP is required to restore pH, and without pH recovery Gapdh activity (and consequently ATP-generating capacity) will be extremely low, resulting in a metabolic Catch-22.

The appearance of growing and non-growing subpopulations in response to nutrient transitions has recently also been demonstrated for *E. coli* [36] and *L. lactis* [37]. However, a major difference between our study and these relates to the capacity of the non-growing subpopulation to resume growth when returned to pre-transition conditions. In contrast to the mentioned studies, the non-growing fraction in our population appears to lose viability after a few hours (Chapter 4, Fig. 4.7). Given the quantitative similarity between pH and CFU subpopulation sizes, combined with the energetic burden a low pH poses, there is significant evidence for the interpretation that the low pH subpopulation corresponds to a non-growing subpopulation that loses viability – so, a truly maladapted state.

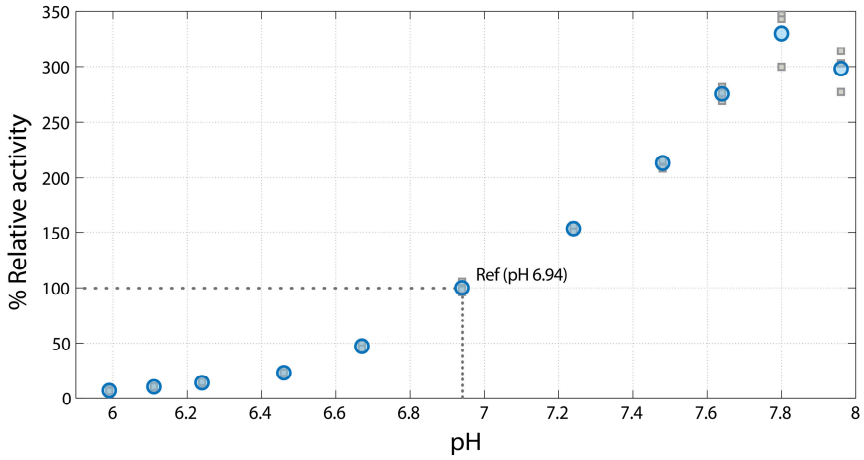

Figure 7.2. Glycolytic Gapdh activity is highly sensitive to changes in pH. Relative to the reference at pH 6.94 (100 % activity), this enzyme displays 93 % activity loss at a pH of 6, resulting in a significant reduction in lower glycolytic flux capacity. Blue circles are the average of three technical replicates, grey squares show data for individual replicates. All data are normalized to the average activity at pH 6.94.

Consolidating population averages and single cell phenotypes: the problem of heterogeneity

When microbial populations transition from utilizing one carbon source to another, a period of reduced growth, called a lag phase, is often seen. Monod originally described this phenomenon in bacteria, and termed it diauxie [107]. For more than 70 years this ubiquitous phenomenon was interpreted to reflect a period during which regulatory mechanisms effect metabolic adaptation to a new carbon source. When population-level measurements are assumed to offer a faithful approximation of the average cell, phenomena such as lag phases can be explained as a period during which *all* cells exhibit reduced growth. However, the current work and several other recent studies [36, 37, 108] show that microbial populations are typically characterized by significant cell-to-cell heterogeneity; a finding that has important implications for the interpretation of mechanisms underlying metabolic regulation and physiological adaptation.

For example, we found that the long lag phases observed for *tps1Δ* cultures could be explained by the differentiation of the population into growing and non-growing subpopulations. Two other recent studies also demonstrated that the lag phase behaviours seen for *L. lactis* [37] and *E. coli* [36] cultures could be explained by the same phenomenon. Non-growing subpopulations appear when fractions of individual cells fail to affect regulatory processes required for adaptation to a second carbon source. In these cases growth rate estimates based on population-level measurements will

underestimate the growth rate of growing cells. In addition, distinct differences in subpopulation phenotypes will likely result in the erroneous interpretations of any other population level measurement, including the nature of mechanisms that regulate metabolism.

Why and how such metabolic subpopulations arise is a topic of active discussion, with different possible explanations, including long-term evolutionary strategies (e.g. bet-hedging) or simple failures in regulation (the current work) (see [36] for an overview of possible explanations). What is clear, however, is that population-level measurements or a focus on phenotypic averages can obscure potentially informative observations (Fig. 7.3).

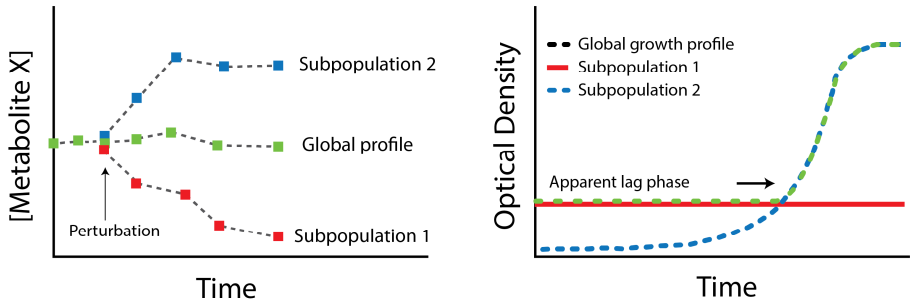

Figure 7.3: Population level measurements can be misleading. Shown is an illustration of how subpopulations can obscure interpretation. In this example an experimental perturbation (indicated by the arrow in the left panel) is applied to a population and a change in the concentration of some metabolite (X) and optical density is followed. In both cases the consequences of the perturbation will likely be incorrectly interpreted if only the average response is measured (also see Fig. 7.4).

The fact that a small fraction of *tps1Δ* cells are able to persist in the presence of glucose was not a novel result, as previous studies provide evidence for this, with plating experiment sometimes showing colonies appearing in the presence of glucose (see e.g. [35, 40]). It is striking, however, that very few studies considered these “outlier” cells as potentially informative. In fact, glucose tolerant *tps1Δ* colonies were discarded as revertants [44]. In this work we demonstrated how an emphasis on such phenotypic outliers could in fact reveal novel aspects of the system being studied. By identifying mechanisms that could act as surrogates for futile cycling through the trehalose pathway, we gained new insights into the functional constraints acting on glycolysis.

Single-cell quantification of most phenotypic features, in a population of cells, will likely generate a continuum of values that can best be described by a probability distribution. While population level measurements could in many instances provide a good approximation of the average phenotype, scenarios involving phenotypically distinct subpopulations (such as the one described in this thesis) pose obvious problems. But perhaps a more subtle consequence of phenotypic distributions is the capacity to consolidate theory with experimental observation. "Outlier" phenotypes might exhibit features that can deviate significantly from theoretical descriptions of metabolic pathway properties. Model parameterizations derived from population-level experimental measurements will be constrained to the average state, not necessarily the operationally optimal state (e.g. maximal flux state). As demonstrated in this work, sampling potential parameter values from probability distributions can generate surprising results that would have been missed if only "population" averages were used.

Re-interpreting the phenotypes of related mutants

In Chapter 1, we provided a brief summary of the many attempts to understand the regulatory deficits of *tps1Δ* mutants. Many of these efforts involved genetic manipulations that targeted components of the trehalose pathway or upper-glycolytic phosphorylation capacity, with results often appearing ambiguous or inconclusive (Chapter 1). In this thesis we presented two major findings that shine new light on previous phenotypic interpretations. The first relates to the discovery of two subpopulations (Chapter 4), and the second to the demonstration that rather than a single feature, several aspects of the trehalose pathway contribute to the robust startup of glycolysis (Chapter 2, Fig. 2.8).

A pitfall of previous interpretations was the expectation of "all-or-nothing" outcomes. We show here that glycolytic regulation can be viewed as a probabilistic process, with specific regulatory mechanisms greatly increasing a cell's chances of coping with dynamic conditions, but not guaranteeing it (also see [36, 37, 108]). We demonstrated that the dependence on or efficacy of regulation by the trehalose pathway is dependent on many other variables. We showed for example that the addition of ethanol or formic acid to the medium significantly reduced the need for phosphate recovery through trehalose cycling. Similarly, within a framework of initial condition-dependence and probabilistic regulatory outcomes, any manipulation that leads to an increase in the regulatory burden should in turn increase the probability of failure.

This predicted effect of an increased regulatory burden was validated by overexpression of Hxk in WT cells (as described in [31]), where we found a clear decrease in viability (Chapter 4, Fig. 4.8). These results supported our model of regulation and suggested that one can interpret the metabolite profiles presented in the original study in a more nuanced way, i.e. that these reflect averages of heterogeneous populations consisting of different fractions of cells in the functional and imbalanced states; where changes in the relative frequencies of each phenotypic state lead to differences in population averages (Fig. 7.4 shows data that demonstrates this scenario). The metabolite profiles reported in [31] appears compatible with this interpretation, where increased Hxk2 expression resulted in metabolite profiles that were intermediate between WT and *tps1Δ* profiles.

The behaviour of *tps2Δ* mutants has also been difficult to interpret. Lacking trehalose 6-phosphatase activity, these cells cannot recover phosphate from T6P. However, when challenged with glucose, these cells do not display the metabolic disturbances seen for *tps1Δ* mutants; an observation that is generally interpreted to contradict a P_i recovery function of the trehalose pathway. However, *tps2Δ* mutants differ in their metabolic behaviour from WT cells, providing clues regarding their capacity to deal with a sudden increase in the glycolytic flux. Above all, with constitutively high T6P concentrations (at least 15-times higher than WT) [24], and well above the K_i of the hexokinases [24], phosphorylation in these mutants will be maximally inhibited when extracellular glucose suddenly increases.

There are several indirect metabolic indications that tps2Δ cells have much lower phosphorylation activities than WT cells. In response to glucose, ATP decreases are significantly reduced, while hexose phosphates accumulate to much lower levels when compared to WT cells. Furthermore, these cells do not display the typical cytoplasmic acidification in response to glucose addition [84]. With the degree and rate of glucose induced acidification dependent on phosphorylation capacity [100], the pH response of *tps2Δ* mutant can be understood in light of a significant reduction in glucose phosphorylation, which is a consequence of constitutively high T6P concentrations. In WT cells, the need to recover phosphate through trehalose cycling comes from the rapid consumption of ATP by Hxk (and Pfk), when the glycolytic flux suddenly increases. With increased Hxk activity, the efficacy of this mechanism is reduced (see above). Similarly, by decreasing the phosphorylation capacity, regulation by the trehalose pathway will become less essential [24]. As such, the *tps2Δ* phenotype can be understood in this context. If Hxk activity is constitutively lower (through e.g. high T6P levels), sudden flux increases will be of a much smaller magnitude and the danger of a metabolic imbalance significantly reduced. A metabolic scenario

corresponding to the one proposed for *tps2Δ* is illustrated in Figure 7.5. By lowering the inhibition constant (Ki_{G6P}) of Hxk by a factor of 10 in the WT model, initial G6P concentrations (recall that we use G6P to approximate inhibition by T6P) lead to much higher initial inhibition and a significantly lower startup flux, thereby reducing the need to recover P_i through futile cycling.

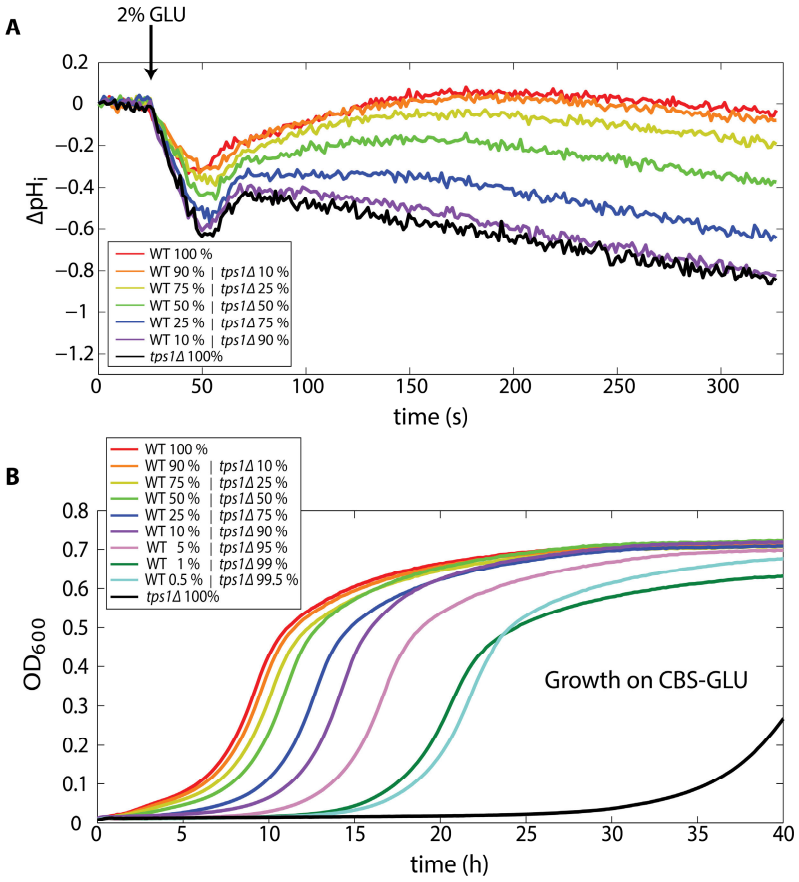

Figure 7.4. Population level measurements reflect proportions of functional (WT-like) and imbalanced (*tps1Δ*-like) states. Shown are (A) pH_i profiles and (B) growth curves, generated by mixing different proportions (indicated as percentages) of WT and *tps1Δ* cells (using OD as a proxy for cell number). pH profiles and growth curves were generated as described in Chapter 4. Cells were pre-grown on 2% GAL, harvested at an OD ~0.8, washed and resuspended in CBS-C. Next, WT and *tps1Δ* suspensions were combined to different proportions and pH_i and growth was measured in response to 2% GLU. In earlier chapters we showed that the majority of WT cells end up in the functional steady state, while the majority of *tps1Δ* cells end up in the imbalanced state. As such, mixtures of WT and *tps1Δ* demonstrate directly how changes in the relative proportions of imbalanced (*tps1Δ*) and functional (WT) states translate to differences in population average measurements.

While the above argument provides an interpretation that can be understood when considering metabolic regulatory nuances, there are also indications that *tps2Δ* cells might already be in a state primed for glucose fermentation. Importantly, this would imply that these cells face a completely different regulatory challenge. Walther *et al.* [84] reported that *tps2Δ* mutants display significantly reduced growth rates when grown on non-fermentable sugars. In plants, T6P is known to be a key signal for glucose-induced catabolite repression via an interaction with Snf1-related protein kinase (SnRK1) [109, 110]. It was suggested that T6P could fulfil a similar role in *S. cerevisiae*, and that the respiratory growth deficits of *tps2Δ* cells could be explained by partial catabolite repression [84]. Support for this interpretation comes from the observation that *tps2Δ* mutants grown on glycerol show a significant reduction in fructose 1,6-bisphosphatase activity [24], a target of glucose repression. This suggests that, besides the constitutive inhibition of Hxk, *tps2Δ* cells might already be partially adapted for growth on glucose.

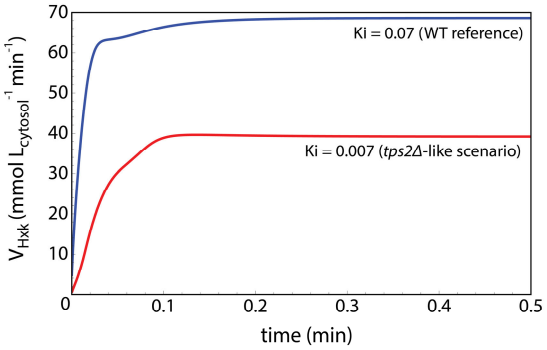

Figure 7.5. High initial inhibition of Hxk can explain the tps2*Δ* *phenotype*. Shown is the consequence of a 10-fold decrease in the G6P inhibition constant (Ki) of Hxk; leading to much higher initial inhibition of Hxk activity, this scenario is similar to the one outlined for *tps2Δ* mutants. The blue and red lines show the Hxk flux profiles for the original model (Ki = 0.07) and a modified version (Ki = 0.007), respectively. All other model parameters were left unchanged.

The failure of WT cells imply a regulatory trade-off

The fact that approximately 7 % of wild-type cells also fail to cope with a sudden increase in glucose indicates that the proper startup of glycolysis is not guaranteed, even when the necessary regulatory components are available. How can this failure be understood? We speculate that the wild-type

failure reflects a trade-off between efficient startup and failsafe regulation. Although cells could reduce the startup risk by always maintaining the trehalose cycle in a high state of activity, effecting tighter control of glucose influx will likely come at a permanent cost of reduced ATP yield (due to futile cycling) and glycolytic flux capacity [111]. From a population perspective a 7 % loss in viability could be justified if the remaining 93 % survives without a permanent sacrifice in capacity.

It has been suggested that maximal growth rate under any one condition comes at the cost of adaptability to different conditions [112]. New *et al.* [108] recently presented results that demonstrate the existence of such a trade-off in *S. cerevisiae* when subjected to different carbon source transitions. They found that populations of different wild strains of *S. cerevisiae* displayed significant anti-correlations between maximal growth on glucose and the time required to resume growth when switched to an alternative different carbon source (i.e. lag phase). All strains could be characterised along a spectrum ranging from (i) specialists, which display maximal growth rates when grown on glucose, but long lag phases when switched to a different carbon source, to (ii) generalists, which display short lag phases when switched to a new carbon source, but suboptimal growth rates on glucose. Additionally, single cell analyses revealed a large degree of heterogeneity in lag phases for any single population. Ultimately, it is concluded that being prepared for sudden environmental changes is costly, due to the maintenance of cellular components that may only be required when conditions change. Any reduction in this cost will yield benefits when conditions are stable, but may lead to regulatory failures for some cells when they have to suddenly adapt to new conditions. Regulatory trade-offs in metabolism may therefore be quite general and a limit to evolution in dynamic environments.

In this regards it is interesting to note that galactose challenges also produced two subpopulations. For both WT and *tps1Δ* populations, a fraction of 7 to 8 % ended up in the low pH (imbalanced) state (Chapter 2, Fig. 2.4C). This finding is somewhat perplexing given the fact that cells were pre-grown on galactose, and therefore presumably already adapted to this carbon source. Although the data at hand does not permit a definitive explanation for this observation, a comparison of glucose and galactose catabolism allow for some speculation.

Why does a galactose challenge lead to subpopulations?

A sudden increase in the glycolytic flux requires specific regulatory mechanisms to avoid an imbalance between ATP consuming and producing steps as the pathway is initiated. Theoretically, however, the potential for such an imbalance is not limited to glycolysis alone.

The danger of the metabolic imbalance in glycolysis is largely dependent on the initial rate of ATP-consuming reactions when substrate uptake suddenly increases. The galactose utilization pathway (Leloir-pathway) displays a very similar ATP-driven auto-catalytic architecture (Fig 7.6). After galactose enters the cell, it is immediately phosphorylated by galactokinase (Gal1) to produce Galactose-1-phosphate (GAL1P). Through a series of additional reactions GAL1P is converted to G6P, converging with glycolysis. While the trehalose pathway functions to balance ATP consumption with production, no such mechanisms have been found for the Leloir-pathway. The absence of such mechanisms suggests that sudden flux increases are unlikely to be of a magnitude that requires specific regulation; unfortunately, high resolution dynamic flux data for the Leloir-pathway is limited, but a study by Ostergaard and colleagues [113] is informative. They showed that a sudden increase in galactose, leads to an immediate 2.5-fold increase in flux and a 2-fold decrease in ATP concentrations, presumably as a result of Gal1 activity. While most cells can clearly deal with this challenge (Chapter 2, Fig. 2.4C), it is quite possible that, in some cells, ATP consumption proceeds too rapidly, resulting in the flux imbalances that lead to the imbalanced state.

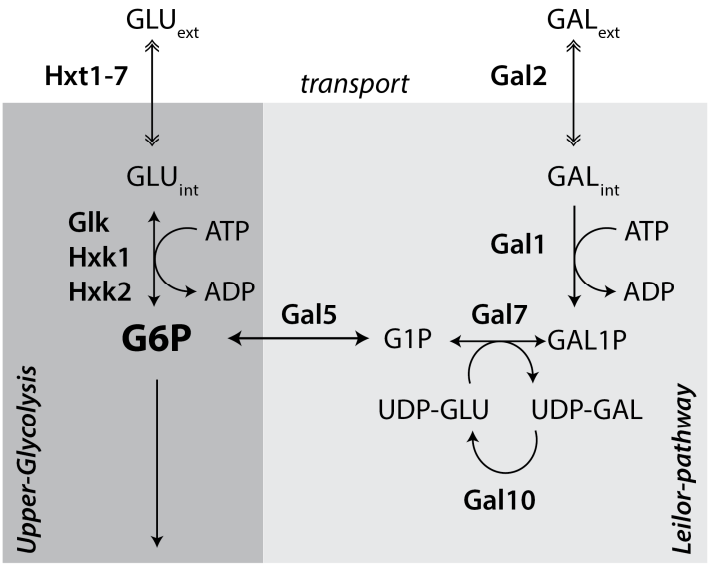

Figure 7.6. Galactose and Glucose metabolism converge at G6P. Shown is a schematic depiction of the reaction sequences that lead from Glucose (GLU) or Galactose (GAL) to Glucose-6-phosphate (G6P). Hxt1-7, Hexose transporters; Glk, Glucokinase; Hxk1/2; hexokinase 1 and 2; Gal2; Galactose permease; Gal1; Galactokinase; Gal7; Galactose-1-phosphate uridyl transferase; Gal10, UDP-glucose 4-epimerase; Gal5, Phosphoglucomutase; GAL1P, Galactose-1-phosphate; G1P, Glucose-1-phosphate.

In this thesis, and in the Ostergaard study [113] , cells were pre-grown on galactose. The Leloir-pathway is subject to glucose repression and is induced in the presence of galactose. This prior adaptation means that the Leloir-pathway would have been fully induced when (washed) cells were challenged with a sudden increase in galactose. The higher the initial flux increases are in the ATP-consuming steps of the pathway, the greater the risk of an ending up in the imbalanced state. As such, prior growth on galactose could have had the unintended effect of sensitizing, rather than protecting, cells against the potential dangers of a flux imbalance.

We chose to use galactose for comparability with previous experiments, but an alternative carbon source would have been informative. In retrospect, the choice of galactose grown cultures as a reference state meant that our plating experiments would not reveal the existence of a non-growing WT subpopulation. With a similar fraction (7 – 8 %) of imbalanced cells appearing in response to both glucose and galactose perturbations (Chapter 2, Fig. 2.4C), all population-level viability estimates – which were normalized to galactose - obscured this phenomenon.

As we did not attempt to repeat experiments with an alternative carbon source, we are unfortunately left with a hypothesis that will have to be validated by future studies. It would be informative to evaluate pH_i distributions of WT populations pre-grown on glucose followed by a galactose perturbation. Cells pre-grown on glucose, exhibit delayed consumption of galactose when suddenly challenged with excess amounts [114]. Although it has previously been shown that under anaerobic conditions such transitions results in an energetic bottleneck that impede growth [114], we expect that, if our hypothesis is correct, a reduction in galactose uptake capacities – under aerobic conditions - should reduce the size of the low pH_i subpopulation in response to a galactose pulse.

Quantifying cell-to-cell metabolic variability

A change in the environment can impact individual cells differently, depending on their specific physiological and metabolic states. In a typical microbial population, often consisting of millions of individuals, minor variations in physiological parameters such as age and size, combine with variability in gene expression and intracellular metabolite concentrations to generate unique states for every single individual.

One of the central themes in this thesis is the idea that metabolic heterogeneity can drive phenotypic diversification under dynamic condition. While phenotypic heterogeneity in populations of otherwise isogenic cells is becoming an established phenomenon [36, 37, 48], cell-to-cell

variability is generally thought to result from stochastic fluctuations in gene expression. We showed, in this work, that variation in metabolite concentrations could partly contribute to the metabolic outcome of sudden glucose perturbations. While a statistical analysis (Chapter 5) showed that the contribution from most metabolite pools was small in comparison to variations in enzyme concentrations, variations in energy status (ATP) and P_i concentration stood out as metabolites that impacted the startup of glycolysis; with P_i as one of the 5 largest overall contributors. While the random sampling approach employed here demonstrated that glycolytic behaviour can be determined by small distributed variations in components, one might wonder how realistic the levels of variation included in our model are. How much evidence is there for cell-to-cell variation in glycolytic enzymes and metabolites?

For central metabolic enzymes, cell-to-cell variability in glycolytic enzymes have been shown to be similar, or even higher, than the variability included in our model [45]; for metabolites the picture is less clear. Very few attempts have been made to quantitatively describe cell-to-cell variability in central metabolic pools. This is largely due to the lack of available methods that allow for metabolite quantification at this resolution. However, using a novel mass spectrometry approach, Ibañez et al [81], demonstrated significant cell-to-cell variability in glycolytic metabolite pools. One major drawback of this approach is its destructive nature, making individual cell tracking impossible.

A potentially promising (and non-destructive) approach to dynamically quantify *in vivo* metabolite concentrations, involves the use of genetically encoded Förster resonance energy transfer (FRET) sensors (see [115] for an overview). These fluorescent sensors are constructed with high specificity for a target metabolite, which upon binding leads to changes in FRET effeciency. Relevant to the findings in this thesis, is the availability of such sensors for ATP and P_i [116, 117]. With the theoretical demonstration that variations in the initial concentrations of these metabolites impact regulatory outcomes, such sensors provide an obvious means to validate this hypothesis. However, most fluorescent proteins (FPs) are sensitive to environmental factors, particularly low pH [118]. This sensitivity presents a general challenge when signals from fluorescent reporter proteins are interpreted, but becomes even more problematic in settings where pH and target metabolite levels changes simultaneously (as in this thesis). While several studies have demonstrated the use of FRET-based biosensors to track the *in vivo* dynamics of key metabolites, including ATP [117, 119], inorganic phosphate (P_i) [116] and Glucose [117], the confounding effect of pH dynamics has unfortunately not been properly characterized.

In light of our findings, we attempted to implement an available FRET-based sensor for ATP [117]. However, pilot measurements confirmed a significant pH-dependent bias (at fixed concentrations of ATP) in population level measurements, with the signal primarily determined by pH. This sensitivity would therefore obscure any inferences regarding cell-to-cell differences in metabolite levels. Further optimization of such sensors will be required in order to reliably implement them for the *in vivo* tracking of metabolite levels.

Without the reliable quantification of intracellular P_i and ATP concentrations, the impact that variations in these pools have on the outcome of glycolytic transitions remains theoretical. What is needed is a direct demonstration of the dependence of glycolytic outcomes on initial ATP and P_i concentrations, following a glucose challenge. We hope that continuous efforts to improve the pH-sensitivity of FPs will provide future studies with the means to validate this hypothesis, using either fluorescent microscopy approaches or flow cytometry based sorting methods.

Intracellular pH variations can also contribute to metabolic outcomes

From the flow cytometry data (Chapter 2, Fig. 2.4C and Chapter 4, Fig. 4.7) it is evident that, initially, populations displayed a continuum of pH states. While these states belonged to a single unimodal distribution, it is conceivable that the states corresponding to the tails of the distribution could exhibit quantitatively different glycolytic capacities due to pH-dependent effects on reaction rates (see above and Appendix B). Although we did not include pH-dependence in our kinetic model, it is likely that cell-to-cell variability in initial pH_i could be another source of variation impacting metabolic outcomes.

It would be informative to monitor growth and pH_i using fluorescent microscopy in combination with microfluidics for sudden sample perturbations. This should provide insight into whether pH_i differences at the time of glucose addition affects the probability of transition outcomes.

Spontaneous metabolic variation: a parsimonious explanation for the occurrence of glucose tolerant *tps1Δ* subpopulations

In this thesis we interpreted the emergence of phenotypic subpopulations as a consequence of metabolic heterogeneity within an isogenic population (Fig. 7.7 illustrates this hypothesis). This scenario offered the simplest interpretation which explains both the physiological (growth) behaviour of populations and the two-state outcome of kinetic model simulations. It is important to emphasize that this outcome does not depend on the existence of a bistability in the model or

experimental populations prior to the addition of glucose; only upon perturbation with glucose a bistability emerges in the model and a bimodal outcome (i.e. two subpopulations) is observed experimentally; this has also been called “responsive diversification” [36].

In this respect, it is relevant to consider alternative frameworks such as fluctuation-induced bistable switching (FIBS) [48], also referred to as stochastic switching. Stochastic switching has been shown to explain the presence of antibiotic tolerant fractions of cells in bacterial populations (Type II persisters). The key difference between “responsive diversification” and FIBS is the fact that phenotypic subpopulations are already present prior to a perturbation; this can be described as “anticipatory diversification”, or bet-hedging. While FIBS would result in the same qualitative outcome (i.e. distinct subpopulations), it is not required to explain our experimental data and would be a more complicated hypothesis, as it requires bistability (i.e. two distinct physiological states) under the initial conditions (i.e. during the pregrowth condition). Hence, in contrast to stochastic-switching induced bistability phenomena, the emergence of two distinct phenotypes (viable and non-viable) is not due to the prior co-existence of two qualitatively different physiological states, as we did not observe bistability in either the model or experimentally prior to glucose addition.

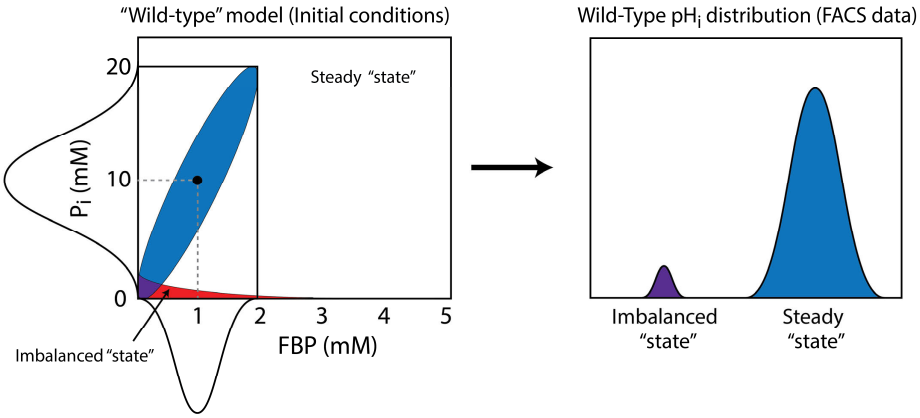

Figure 7.7: Metabolic heterogeneity can explain the emergence of phenotypic subpopulations. The illustration shows how, depending e.g. on the initial concentrations of FBP and P_i (left panel), the model representing wild-type can end up in the imbalanced state (red area) or the steady state (white area). Heterogeneity in initial conditions (depicted as the ellipse), results in subpopulations after the addition of glucose, as demonstrated by the flow cytometry data (Chapter 2, Fig. 2.4C). The purple area represents the set of individuals that end up in the imbalanced state (unviable) after glucose addition; the blue area indicates individuals that will end up in the steady state (viable). The black dot (right panel) indicates the average initial state of the population.

Several recent microbial studies have shown or inferred the appearance of distinct subpopulations following nutrient transitions [36, 37, 108]. This phenomenon may turn out to be quite ubiquitous and part of a general survival strategy adopted by populations of microorganisms faced with uncertain future conditions. Here we demonstrated how spontaneous metabolic variation can be both a curse and blessing, leading, in some cases, to glycolytic imbalances in WT cells, while potentially mitigating the consequences of a trehalose biosynthesis deficiency in *tps1Δ* individuals.

From an evolutionary perspective, non-genetic sources of phenotypic heterogeneity are fascinating, having been demonstrated to be a potentially important adaptive mechanism that enhances the long term fitness of populations [120, 121]. However, in biotechnological or clinical settings this phenomenon can be undesirable, with heterogeneity potentially impacting culture performance or treatment efficacies, respectively. As such, increasing insight into the origins and consequence of non-genetic variability is of practical relevance for the both medical and biotechnological endeavours.

In Conclusion

The two primary take home message of this thesis is that phenotypic variability can arise through processes that do not operate under stochastic regimes, and that the dynamic regulation of glycolysis can be understood as a probabilistic phenomenon. Spontaneously arising phenotypic heterogeneity has potentially important implications for biotechnological applications [122], but also for the biomedical field. The demonstrated role of phenotypic heterogeneity in e.g. antibiotic resistance is particularly relevant for studies which aim to understand the susceptibility of populations of cells to drug treatments [36, 48]. Insight into metabolic mechanisms that generate phenotypic variability could help to inform intervention strategies for diseases with a central metabolic component, such as cancer and diabetes. Antibiotic treatment regimens could also benefit from such insights, as natural resistance by fractions of cells in *E. coli* populations have been linked to non-genetic metabolic heterogeneity [36], where it was found that, depending on culturing conditions, naturally occurring resistant subpopulations could be enhanced or reduced.

It is hoped that the work presented in this thesis has provided new insight into the principles of metabolic regulation. The picture of the regulation of glycolysis that emerges from our work is multi-levelled and dynamic and it was only through a combination of theoretical and experimental approaches that the regulatory role of trehalose metabolism could be understood. From our perspective, it will be interesting to see how ideas on metabolism and its regulation evolve to account for transient regulatory phenomena and probabilistic outcomes.

Appendix B | pH-dependence of enzyme activities

Employing the *in vivo*-like enzyme activity assays described by van Eunen et al. [60], we measured the pH-dependent activities of several commercially available purified *S. cerevisiae* glycolytic enzymes (Table B.2). pH was titrated by adjusting the ratios of buffer components as described in Table B.1. Results are shown in Figures 7.2 and B.1.

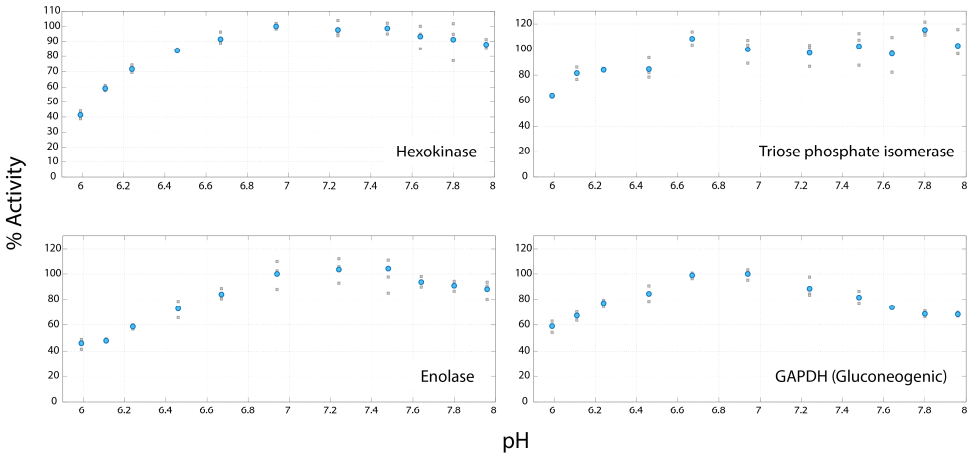

Figure B.1. Glycolytic enzymes display pH-dependent changes in activity. Shown are scaled activity profiles for selected glycolytic enzymes that could be assayed in the glycolytic direction of operation. In addition, the pH-dependent profile for Gapdh operating in the gluconeogenic direction is shown; operating in this direction pH-sensitivity is significantly reduced compared to the glycolytic direction (see Fig. 7.2). All data points were scaled (%) to the average activity at pH 6.94 (100 %). Blue circles show the average of three technical replicates; grey squares show values for individual measurements.

Table B.1. Buffer composition of pH-dependent enzyme activity assays.

	Buffer components					
pH (20 °C)	**1.1M K_2HPO_4 (ml)**	**1.1M KH_2PO_4 (ml)**	**1M NaH_2PO_4 (ml)**	**1M Na_2HPO_4 (ml)**	**dH_2O (ml)**	**$C_5H_8KNO_4$. H_2O (g)**
5.99	0.15	9.85	3.90	0.10	86	14.94
6.11	0.86	9.14	3.44	0.56	86	14.94
6.24	1.47	8.53	3.07	0.93	86	14.94
6.46	2.44	7.56	2.53	1.47	86	14.94
6.67	3.79	6.21	1.89	2.11	86	14.94
6.94	5.37	4.63	1.28	2.72	86	14.94
7.24	6.85	3.15	0.81	3.19	86	14.94
7.48	8.00	2.00	0.49	3.51	86	14.94
7.64	8.80	1.20	0.29	3.71	86	14.94
7.80	9.30	0.70	0.16	3.84	86	14.94
7.96	9.60	0.40	0.09	3.91	86	14.94

	Buffer concentrations (M)			Assay concentrations (M)		
pH (20 °C)	**K^+**	**PO_4^{3-}**	**Na^+**	**K^+**	**PO_4^{3-}**	**Na^+**
5.99	0.847	0.150	0.041	0.282	0.050	0.014
6.11	0.854	0.150	0.046	0.285	0.050	0.015
6.24	0.861	0.150	0.049	0.287	0.050	0.016
6.46	0.872	0.150	0.055	0.291	0.050	0.018
6.67	0.887	0.150	0.061	0.296	0.050	0.020
6.94	0.904	0.150	0.067	0.301	0.050	0.022
7.24	0.920	0.150	0.072	0.307	0.050	0.024
7.48	0.933	0.150	0.075	0.311	0.050	0.025
7.64	0.942	0.150	0.077	0.314	0.050	0.026
7.80	0.947	0.150	0.078	0.316	0.050	0.026
7.96	0.951	0.150	0.079	0.317	0.050	0.026

Table B.2. Summary of purified yeast enzymes tested for pH-dependent glycolytic activity.

Enzyme Name	EC number	Supplier	Catalogue number	Assay concentration (Units/ml)
Hexokinase	2.7.1.1	Roche	11426362001	0.25
Triosephosphate isomerase	5.3.1.1	Sigma	T2507	0.17
Glyceraldehyde-3-phosphate dehydrogenase	1.2.1.12	Sigma	G5537	0.2
Enolase	4.2.1.11	Sigma	E6126	0.16

References

1. **Bar-Even A, Flamholz A, Noor E, Milo R**. 2012. Rethinking glycolysis: on the biochemical logic of metabolic pathways. *Nat. Chem. Biol.* **8**: 509–17.

2. **Keller MA, Turchyn A V, Ralser M**. 2014. Non-enzymatic glycolysis and pentose phosphate pathway-like reactions in a plausible Archean ocean. *Mol. Syst. Biol.* **10**: 725.

3. **Buijs NA, Siewers V, Nielsen J**. 2013. Advanced biofuel production by the yeast Saccharomyces cerevisiae. *Curr. Opin. Chem. Biol.* **17**: 480–8.

4. **Li H, Liao JC**. 2013. Engineering a cyanobacterium as the catalyst for the photosynthetic conversion of CO2 to 1,2-propanediol. *Microb. Cell Fact.* **12**: 4.

5. **Bogorad IW, Lin TS, Liao JC**. 2013. Synthetic non-oxidative glycolysis enables complete carbon conservation. *Nature* **502**: 693–7.

6. **Vander Heiden MG, Cantley LC, Thompson CB**. 2009. Understanding the Warburg effect: the metabolic requirements of cell proliferation. *Science* **324**: 1029–33.

7. **Zhao Y, Butler EB, Tan M**. 2013. Targeting cellular metabolism to improve cancer therapeutics. *Cell Death Dis.* **4**: e532.

8. **Schrauwen P, Timmers S, Hesselink MKC**. 2013. Blocking the entrance to open the gate. *Diabetes* **62**: 703–5.

9. **Bénéteau M, Zunino B, Jacquin MA, Meynet O,** et al. 2012. Combination of glycolysis inhibition with chemotherapy results in an antitumor immune response. *Proc. Natl. Acad. Sci. U. S. A.* **109**: 20071–6.

10. **Pearce EL, Poffenberger MC, Chang C-H, Jones RG**. 2013. Fueling immunity: insights into metabolism and lymphocyte function. *Science* **342**: 1242454.

11. **Werner S, Diekert G, Schuster S**. 2010. Revisiting the thermodynamic theory of optimal ATP stoichiometries by analysis of various ATP-producing metabolic pathways. *J. Mol. Evol.* **71**: 346–55.

12. **Flamholz A, Noor E, Bar-Even A, Liebermeister W,** et al. 2013. Glycolytic strategy as a tradeoff between energy yield and protein cost. *Proc. Natl. Acad. Sci. U. S. A.* **110**: 10039–44.

13. **Chandra FA, Buzi G, Doyle JC**. 2011. Glycolytic oscillations and limits on robust efficiency. *Science* **333**: 187–92.

14. **Teusink B, Walsh MC, van Dam K, Westerhoff H V**. 1998. The danger of metabolic pathways with turbo design. *Trends Biochem. Sci.* **23**: 162–9.

15. **Avonce N, Mendoza-Vargas A, Morett E, Iturriaga G**. 2006. Insights on the evolution of trehalose biosynthesis. *BMC Evol. Biol.* **6**: 109.

16. **Alonso A, Pascual C, Herrera L, Gancedo JM,** et al. 1984. Metabolic imbalance in a Saccharomyces cerevisiae mutant unable to grow on fermentable hexoses. *Eur. J. Biochem.* **138**: 407–11.

17. **Thevelein JM, Hohmann S**. 1995. Trehalose synthase: guard to the gate of glycolysis in yeast? *Trends Biochem. Sci.* **20**: 3–10.

18. **Bell W, Sun W, Hohmann S, Wera S,** et al. 1998. Composition and Functional Analysis of the Saccharomyces cerevisiae Trehalose Synthase Complex. *J. Biol. Chem.* **273**: 33311–9.

19. **Londesborough J, Vuorio OE**. 1993. Purification of trehalose synthase from baker's yeast. Its temperature-dependent activation by fructose 6-phosphate and inhibition by phosphate. *Eur. J. Biochem.* **216**: 841–8.

20. **Trevisol ET, Panek AD, De Mesquita JF, Eleutherio EC**. 2014. Regulation of the yeast trehalose-synthase complex by cyclic AMP-dependent phosphorylation. *Biochim. Biophys. Acta* **1840**: 1646–50.

21. **Oliveira AP, Ludwig C, Picotti P, Kogadeeva M,** et al. 2012. Regulation of yeast central metabolism by enzyme phosphorylation. *Mol. Syst. Biol.* **8**: 623.

22. **Jules M, Beltran G, François J, Parrou JL**. 2008. New insights into trehalose metabolism by Saccharomyces cerevisiae: NTH2 encodes a functional cytosolic trehalase, and deletion of TPS1 reveals Ath1p-dependent trehalose mobilization. *Appl. Environ. Microbiol.* **74**: 605–14.

23. **Luyten K, Albertyn J, Skibbe WF, Prior BA,** et al. 1995. Fpsl, a yeast member of the MIP family of channel proteins, is a facilitator for glycerol uptake and efflux and is inactive under osmotic stress. *EMBO J.* **14**: 1360–71.

24. **Hohmann S, Bell W, Neves MJ, Valckx D,** et al. 1996. Evidence for trehalose-6-phosphate-dependent and -independent mechanisms in the control of sugar influx into yeast glycolysis. *Mol. Microbiol.* **20**: 981–91.

25. **Bonini BM, Van Dijck P, Thevelein JM**. 2003. Uncoupling of the glucose growth defect and the deregulation of glycolysis in Saccharomyces cerevisiae tps1 mutants expressing trehalose-6-phosphate-insensitive hexokinase from Schizosaccharomyces pombe. *Biochim. Biophys. Acta - Bioenerg.* **1606**: 83–93.

26. **Bonini BM, Van Vaeck C, Larsson C, Gustafsson L,** et al. 2000. Expression of escherichia coli otsA in a Saccharomyces cerevisiae tps1 mutant restores trehalose 6-phosphate levels and partly restores growth and fermentation with glucose and control of glucose influx into glycolysis. *Biochem. J.* **350**: 261–8.

27. **Petitjean M, Teste M-A, François JM, Parrou J-L**. 2015. Yeast Tolerance to Various Stresses Relies on the Trehalose-6P Synthase (Tps1) Protein, Not on Trehalose. *J. Biol. Chem.* **290**: 16177–90.

28. **Iynedjian P**. 1998. Glycolysis, turbo design and the endocrine pancreatic B cell. *TiBS* **23**

29. **Walther T, Mtimet N, Alkim C, Vax A,** et al. 2013. Metabolic phenotypes of Saccharomyces cerevisiae mutants with altered trehalose 6-phosphate dynamics. *Biochem. J.* **454**: 227–37.

30. **Blázquez MA, Lagunas R, Gancedo C, Gancedo JM**. 1993. Trehalose-6-phosphate, a new regulator of yeast glycolysis that inhibits hexokinases. *FEBS Lett.* **329**: 51–4.

31. **Ernandes JR, De Meirsman C, Rolland F, Winderickx J,** et al. 1998. During the initiation of fermentation overexpression of hexokinase PII in yeast transiently causes a similar deregulation of glycolysis as deletion of Tps1. *Yeast* **14**: 255–69.

32. **Blázquez MA, Gancedo C**. 1995. Mode of action of the gcr9 and cat3 mutations in restoring the ability of Saccharomyces cerevisiae tps1 mutants to grow on glucose. *Mol. Gen. Genet. MGG* **249**: 655–64.

33. **Gancedo C, Flores C**. 2004. The importance of a functional trehalose biosynthetic pathway for the life of yeasts and fungi. *FEMS Yeast Res.* **4**: 351–9.

34. **François J, Parrou JL**. 2001. Reserve carbohydrates metabolism in the yeast Saccharomyces cerevisiae. *FEMS Microbiol. Rev.* **25**: 125–45.

35. **Neves M, Hohmann S, Bell W, Dumortier F**. 1995. Control of glucose influx into glycolysis and pleiotropic effects studied in different isogenic sets of Saccharomyces cerevisiae mutants in trehalose biosynthesis. *Curr. Genet.* : 110–22.

36. **Kotte O, Volkmer B, Radzikowski JL, Heinemann M**. 2014. Phenotypic bistability in Escherichia coli's central carbon metabolism. *Mol. Syst. Biol.* **10**: 736.

37. **Solopova A, van Gestel J, Weissing FJ, Bachmann H,** et al. 2014. Bet-hedging during bacterial diauxic shift. *Proc. Natl. Acad. Sci. U. S. A.* **111**: 7427–32.

38. **Stelling J, Sauer U, Szallasi Z, Doyle FJ,** et al. 2004. Robustness of cellular functions. *Cell* **118**: 675–85.

39. **DeBerardinis RJ, Thompson CB**. 2012. Cellular metabolism and disease: what do metabolic outliers teach us? *Cell* **148**: 1132–44.

40. **Van Aelst L, Hohmann S, Bulaya B, de Koning W,** et al. 1993. Molecular cloning of a gene involved in glucose sensing in the yeast Saccharomyces cerevisiae. *Mol. Microbiol.* **8**: 927–43.

41. **Teusink B, Passarge J, Reijenga CA, Esgalhado E,** et al. 2000. Can yeast glycolysis be understood in terms of in vitro kinetics of the constituent enzymes? Testing biochemistry. *Eur. J. Biochem.* **267**: 5313–29.

42. **Veening JW, Hamoen LW, Kuipers OP**. 2005. Phosphatases modulate the bistable sporulation gene expression pattern in Bacillus subtilis. *Mol. Microbiol.* **56**: 1481–94.

43. **Wang L, Walker BL, Iannaccone S, Bhatt D,** et al. 2009. Bistable switches control memory and plasticity in cellular differentiation. *Proc. Natl. Acad. Sci. U. S. A.* **106**: 6638–43.

44. **De Winde JH**. 2012. Personal Communication.

45. **Newman JRS, Ghaemmaghami S, Ihmels J, Breslow DK,** et al. 2006. Single-cell proteomic analysis of S. cerevisiae reveals the architecture of biological noise. *Nature* **441**: 840–6.

46. **Fendt S, Sauer U**. 2010. Transcriptional regulation of respiration in yeast metabolizing differently repressive carbon substrates. *BMC Syst. Biol.* **4**: 12.

47. **Raj A, Oudenaarden A Van, van Oudenaarden A**. 2008. Nature , Nurture , or Chance : Stochastic Gene Expression and Its Consequences. *Cell* **135**: 216–26.

48. **Balaban NQ, Merrin J, Chait R, Kowalik L,** et al. 2004. Bacterial persistence as a phenotypic switch. *Science* **305**: 1622–5.

49. **Levy SF, Ziv N, Siegal ML**. 2012. Bet hedging in yeast by heterogeneous, age-correlated expression of a stress protectant. *PLoS Biol.* **10**: e1001325.

50. **Overkamp KM, Bakker BM, Kötter P, Luttik MAH,** et al. 2002. Metabolic engineering of glycerol production in Saccharomyces cerevisiae. *Appl. Environ. Microbiol.* **68**: 2814–21.

51. **Geertman JM, van Dijken JP, Pronk JT**. 2006. Engineering NADH metabolism in Saccharomyces cerevisiae: formate as an electron donor for glycerol production by anaerobic, glucose-limited chemostat cultures. *FEMS Yeast Res.* **6**: 1193–203.

52. **Abate A, Hillen RC, Wahl SA**. 2012. Piecewise affine approximations of fluxes and enzyme kinetics from in vivo 13 C labeling experiments. *Int. J. ROBUST NONLINEAR Control* : 1120–39.

53. **Teusink B, Westerhoff H V, Bruggeman FJ**. 2010. Comparative systems biology: from bacteria to man. *Wiley Interdiscip. Rev. Syst. Biol. Med.* **2**: 518–32.

54. **Koppenol WH, Bounds PL, Dang C V**. 2011. Otto Warburg's contributions to current concepts of cancer metabolism. *Nat. Rev. Cancer* **11**: 325–37.

55. **Christofk HR, Vander Heiden MG, Wu N, Asara JM,** et al. 2008. Pyruvate kinase M2 is a phosphotyrosine-binding protein. *Nature* **452**: 181–6.

56. **Vander Heiden MG, Locasale JW, Swanson KD, Sharfi H,** et al. 2010. Evidence for an alternative glycolytic pathway in rapidly proliferating cells. *Science* **329**: 1492–9.

57. **Teusink B, Westerhoff H V**. 2000. "Slave" metabolites and enzymes. *Eur. J. Biochem.* **267**: 1889–93.

58. **Levering J, Musters MWJM, Bekker M, Bellomo D,** et al. 2012. Role of phosphate in the central metabolism of two lactic acid bacteria--a comparative systems biology approach. *FEBS J.* **279**: 1274–90.

59. **Schmitz JPJ, van Riel NAW, Nicolay K, Hilbers PAJ,** et al. 2010. Silencing of glycolysis in muscle: experimental observation and numerical analysis. *Exp. Physiol.* **95**: 380–97.

60. **Van Eunen K, Bouwman J, Daran-Lapujade P, Postmus J,** et al. 2010. Measuring enzyme activities under standardized in vivo-like conditions for systems biology. *FEBS J.* **277**: 749–60.

61. **Kresnowati MTAP, van Winden WA, Almering MJH, ten Pierick A,** et al. 2006. When transcriptome meets metabolome: fast cellular responses of yeast to sudden relief of glucose limitation. *Mol Syst Biol* **2**

62. **Toews CJ**. 1966. Kinetic studies with skeletal-muscle hexokinase. *Biochem. J.* **100**: 739–44.

63. **Thompson AL, Cooney GJ**. 2000. Acyl-CoA inhibition of hexokinase in rat and human skeletal muscle is a potential mechanism of lipid-induced insulin resistance. *Diabetes* **49**: 1761–5.

64. **Ureta T, Lazo PA, Sols A**. 1985. Allosteric inhibition of brain hexokinase by glucose 6-phosphate in the reverse reaction. *Arch. Biochem. Biophys.* **239**: 315–9.

65. **Liu X, Kim CS, Kurbanov FT, Honzatko RB,** et al. 1999. Dual mechanisms for glucose 6-phosphate inhibition of human brain hexokinase. *J. Biol. Chem.* **274**: 31155–9.

66. **Thomas MR, O'Shea EK**. 2005. An intracellular phosphate buffer filters transient fluctuations in extracellular phosphate levels. *Proc. Natl. Acad. Sci. U. S. A.* **102**: 9565–70.

67. **Kornberg A, Rao NN, Ault-Riché D**. 1999. Inorganic polyphosphate: a molecule of many functions. *Annu. Rev. Biochem.* **68**: 89–125.

68. **Van Eunen K, Kiewiet JAL, Westerhoff H V, Bakker BM**. 2012. Testing biochemistry revisited: how in vivo metabolism can be understood from in vitro enzyme kinetics. *PLoS Comput. Biol.* **8**: e1002483.

69. **Sherman F**. 2002. Getting started with yeast. *Methods Enzymol.* **350**: 3–41.

70. **Theobald U, Mohns J, Rizzi M**. 1996. Dynamics of orthophosphate in yeast cytoplasm. *Biotechnol. Lett.* **18**: 461–6.

71. **Canelas AB, Ras C, ten Pierick A, van Gulik WM,** et al. 2011. An in vivo data-driven framework for classification and quantification of enzyme kinetics and determination of apparent thermodynamic data. *Metab. Eng.* **13**: 294–306.

72. **Ferrell JE, Machleder EM**. 1998. The biochemical basis of an all-or-none cell fate switch in Xenopus oocytes. *Science* **280**: 895–8.

73. **Ozbudak EM, Thattai M, Lim HN, Shraiman BI,** et al. 2004. Multistability in the lactose utilization network of Escherichia coli. *Nature* **427**: 737–40.

74. **Schiestl RH, Gietz RD**. 1989. High efficiency transformation of intact yeast cells using single stranded nucleic acids as a carrier. *Curr. Genet.* **16**: 339–46.

75. **Orij R, Postmus J, Ter Beek A, Brul S,** et al. 2009. In vivo measurement of cytosolic and mitochondrial pH using a pH-sensitive GFP derivative in Saccharomyces cerevisiae reveals a relation between intracellular pH and growth. *Microbiology* **155**: 268–78.

76. **Schneider CA, Rasband WS, Eliceiri KW**. 2012. NIH Image to ImageJ: 25 years of image analysis. *Nat. Methods* **9**: 671–5.

77. **Compagno C, Brambilla L, Capitanio D, Boschi F,** et al. 2001. Alterations of the glucose metabolism in a triose phosphate isomerase-negative Saccharomyces cerevisiae mutant. *Yeast* **18**: 663–70.

78. **Orij R, Urbanus ML, Vizeacoumar FJ, Giaever G,** et al. 2012. Genome-wide analysis of intracellular pH reveals quantitative control of cell division rate by pHc in Saccharomyces cerevisiae. *Genome Biol.* **13**: R80.

79. **Gancedo JM**. 2008. The early steps of glucose signalling in yeast. *FEMS Microbiol. Rev.*

80. **Zenobi R**. 2013. Single-cell metabolomics: analytical and biological perspectives. *Science* **342**: 1243259.

81. **Ibáñez AJ, Fagerer SR, Schmidt AM, Urban PL,** et al. 2013. Mass spectrometry-based metabolomics of single yeast cells. *Proc. Natl. Acad. Sci. U. S. A.* **110**: 8790–4.

82. **Fisher RA**. 1936. The use of multiple measurements in taxonomic problems. *Ann. Eugen.* **7**: 179–88.

83. **Ihaka R, Gentleman R**. 1996. R: A Language for Data Analysis and Graphics. *J. Comput. Graph. Stat.* **5**: 299–314.

84. **Walther T, Mtimet N, Alkim C, Vax A,** et al. 2013. Metabolic phenotypes of Saccharomyces cerevisiae mutants with altered trehalose 6-phosphate dynamics. *Biochem. J.* **454**: 227–37.

85. **Van Dijken JP, Bauer J, Brambilla L, Duboc P,** et al. 2000. An interlaboratory comparison of physiological and genetic properties of four Saccharomyces cerevisiae strains. *Enzyme Microb. Technol.* **26**: 706–14.

86. **Mashego MR, van Gulik WM, Vinke JL, Visser D,** et al. 2006. In vivo kinetics with rapid perturbation experiments in Saccharomyces cerevisiae using a second-generation BioScope. *Metab Eng* **8**: 370–83.

87. **Voit E**. 2003. Biochemical and genomic regulation of the trehalose cycle in yeast: review of observations and canonical model analysis. *J. Theor. Biol.* **223**: 55–78.

88. **Aboka FO, Heijnen JJ, van Winden W a**. 2009. Dynamic 13C-tracer study of storage carbohydrate pools in aerobic glucose-limited Saccharomyces cerevisiae confirms a rapid steady-state turnover and fast mobilization during a modest stepup in the glucose uptake rate. *FEMS Yeast Res.* **9**: 191–201.

89. **Theobald U, Mailinger W, Baltes M, Rizzi M,** et al. 1997. In vivo analysis of metabolic dynamics in Saccharomyces cerevisiae: I. Experimental observations. *Biotechnol. Bioeng.* **55**: 305–16.

90. **Theobald U, Mailinger W, Reuss M, Rizzi M**. 1993. In vivo analysis of glucose-induced fast changes in yeast adenine nucleotide pool applying a rapid sampling technique. *Anal Biochem* **214**: 31–7.

91. **Visser D, van Zuylen GA, van Dam JC, Eman MR,** et al. 2004. Analysis of in vivo kinetics of glycolysis in aerobic Saccharomyces cerevisiae by application of glucose and ethanol pulses. *Biotechnol. Bioeng.* **88**: 157–67.

92. **Wu L, van Dam J, Schipper D, Kresnowati MTAP,** et al. 2006. Short-term metabolome dynamics and carbon, electron, and ATP balances in chemostat-grown Saccharomyces cerevisiae CEN.PK 113-7D following a glucose pulse. *Appl. Environ. Microbiol.* **72**: 3566–77.

93. **Lagerstedt JO, Zvyagilskaya R, Pratt JR, Pattison-Granberg J,** et al. 2002. Mutagenic and functional analysis of the C-terminus of Saccharomyces cerevisiae Pho84 phosphate transporter. *FEBS Lett.* **526**: 31–7.

94. **Levy S, Kafri M, Carmi M, Barkai N**. 2011. The competitive advantage of a dual-transporter system. *Science* **334**: 1408–12.

95. **Wykoff DD, Rizvi AH, Raser JM, Margolin B,** et al. 2007. Positive Feedback Regulates Switching of Phosphate Transporters in S. cerevisiae. *Mol. Cell* **27**: 1005–13.

96. **Wykoff D, O'Shea E**. 2001. Phosphate transport and sensing in Saccharomyces cerevisiae. *Genetics*

97. **Persson BL, Lagerstedt JO, Pratt JR, Pattison-Granberg J,** et al. 2003. Regulation of phosphate acquisition in Saccharomyces cerevisiae. *Curr. Genet.* **43**: 225–44.

98. **Giots F, Donaton MC V, Thevelein JM**. 2003. Inorganic phosphate is sensed by specific phosphate carriers and acts in concert with glucose as a nutrient signal for activation of the protein kinase A pathway in the yeast Saccharomyces cerevisiae. *Mol. Microbiol.* **47**: 1163–81.

99. **Valle E, Bergillos L, Ramos S**. 1987. External K+ affects the internal acidification caused by the addition of glucose to yeast cells. *J. Gen. Microbiol.* **133**: 535–8.

100. **Ramos S, Balbín M, Raposo M, Valle E,** et al. 1989. The mechanism of intracellular acidification induced by glucose in Saccharomyces cerevisiae. *J. Gen. Microbiol.* **135**: 2413–22.

101. **Navarrete C, Petrezsélyová S, Barreto L, Martínez JL,** et al. 2010. Lack of main K+ uptake systems in Saccharomyces cerevisiae cells affects yeast performance in both potassium-sufficient and potassium-limiting conditions. *FEMS Yeast Res.* **10**: 508–17.

102. **Thevelein JM, Beullens M, Honshoven F, Hoebeeck G,** et al. 1987. Regulation of the cAMP level in the yeast Saccharomyces cerevisiae: the glucose-induced cAMP signal is not mediated by a transient drop in the intracellular pH. *J. Gen. Microbiol.* **133**: 2197–205.

103. **Kresnowati MTAP, Suarez-Mendez C, Groothuizen MK, van Winden WA,** et al. 2007. Measurement of fast dynamic intracellular pH in Saccharomyces cerevisiae using benzoic acid pulse. *Biotechnol. Bioeng.* **97**: 86–98.

104. **Serrano R**. 1983. In vivo glucose activation of the yeast plasma membrane ATPase. *FEBS Lett.* **156**: 11–4.

105. **Goossens A, de La Fuente N, Forment J, Serrano R,** et al. 2000. Regulation of yeast H(+)-ATPase by protein kinases belonging to a family dedicated to activation of plasma membrane transporters. *Mol. Cell. Biol.* **20**: 7654–61.

106. **Holyoak CD, Stratford M, McMullin Z, Cole MB,** et al. 1996. Activity of the plasma membrane H(+)-ATPase and optimal glycolytic flux are required for rapid adaptation and growth of Saccharomyces cerevisiae in the presence of the weak-acid preservative sorbic acid. *Appl. Environ. Microbiol.* **62**: 3158–64.

107. **Monod J**. 1949. The Growth of Bacterial Cultures. *Annu. Rev. Microbiol.* **3**: 371–94.

108. **New AM, Cerulus B, Govers SK, Perez-Samper G,** et al. 2014. Different Levels of Catabolite Repression Optimize Growth in Stable and Variable Environments. *PLoS Biol.* **12**: e1001764.

109. **Crozet P, Margalha L, Confraria A, Rodrigues A,** et al. 2014. Mechanisms of regulation of SNF1/AMPK/SnRK1 protein kinases. *Front. Plant Sci.* **5**: 190.

110. **Zhang Y, Primavesi LF, Jhurreea D, Andralojc PJ,** et al. 2009. Inhibition of SNF1-related protein kinase1 activity and regulation of metabolic pathways by trehalose-6-phosphate. *Plant Physiol.* **149**: 1860–71.

111. **Rossouw D, Heyns EH, Setati ME, Bosch S,** et al. 2013. Adjustment of trehalose metabolism in wine Saccharomyces cerevisiae strains to modify ethanol yields. *Appl. Environ. Microbiol.* **79**: 5197–207.

112. **Schuetz R, Zamboni N, Zampieri M, Heinemann M,** et al. 2012. Multidimensional optimality of microbial metabolism. *Science* **336**: 601–4.

113. **Ostergaard S, Olsson L, Nielsen J**. 2001. In Vivo Dynamics of Galactose Metabolism in Saccharomyces cerevisiae : Metabolic Fluxes and Metabolite Levels.

114. **Van den Brink J, Akeroyd M, van der Hoeven R, Pronk JT,** et al. 2009. Energetic limits to metabolic flexibility: responses of Saccharomyces cerevisiae to glucose-galactose transitions. *Microbiology* **155**: 1340–50.

115. **Okumoto S, Jones A, Frommer WB**. 2012. Quantitative imaging with fluorescent biosensors. *Annu. Rev. Plant Biol.* **63**: 663–706.

116. **Gu H, Lalonde S, Okumoto S, Looger LL,** et al. 2006. A novel analytical method for in vivo phosphate tracking. *FEBS Lett.* **580**: 5885–93.

117. **Bermejo C, Haerizadeh F, Takanaga H, Chermak D,** et al. 2010. Dynamic analysis of cytosolic glucose and ATP levels in yeast using optical sensors. *Biochem. J.* **432**: 399–406.

118. **Shaner NC, Steinbach PA, Tsien RY**. 2005. A guide to choosing fluorescent proteins. *Nat. Methods* **2**: 905–9.

119. **Imamura H, Huynh Nhat KP, Togawa H, Saito K,** et al. 2009. Visualization of ATP levels inside single living cells with fluorescence resonance energy transfer-based genetically encoded indicators. *Proc. Natl. Acad. Sci.* **106**: 15651–6.

120. **Veening JW, Smits WK, Kuipers OP**. 2008. Bistability, epigenetics, and bet-hedging in bacteria. *Annu. Rev. Microbiol.* **62**: 193–210.

121. **Grimbergen AJ, Siebring J, Solopova A, Kuipers OP**. 2015. Microbial bet-hedging: the power of being different. *Curr. Opin. Microbiol.* **25**: 67–72.

122. **Delvigne F, Zune Q, Lara AR, Al-Soud W,** et al. 2014. Metabolic variability in bioprocessing: implications of microbial phenotypic heterogeneity. *Trends Biotechnol.* **32**: 608–16.

Acknowledgements

Completing this thesis has been an adventure of sorts. In many respects it was like traversing an unknown mountainous terrain with no map at hand. At times I got a bit lost and only the towering peaks of uncertainty were visible. During these periods, when progress was slow, the road ahead appeared very intimidating, but thankfully this was not a solo journey. With the help, inspiration and motivation of many people along the way I managed to complete the adventure. I would like to take the next few lines to acknowledge them.

Bas, thank you for having given me this opportunity. Back in 2008, when I was searching for PhD positions, I did not know the first thing about yeast or metabolism, but knew immediately that I wanted to join your group after a brief meeting in Wageningen. The idea that one could use "simple" mathematical models to describe complex biological phenomena was intriguing and something completely new to me. I have to admit that I had no clue what I was signing up for, as words like subpopulations and bistabilities were not part of my vocabulary. I ended up spending most of my time in the lab, chasing a statistically elusive anomaly and was relieved that you gave me the freedom to obsessively pursue this. I look back on the last few years with great satisfaction, having gained a whole new perspective on biological systems. Needless to say, this experience has changed my view of life and the myriad of processes that underlie it – no population of anything will ever look the same again. Thank you for your guidance and patience, and your insistence on going "all in" with a single large paper that was published in Science!

Jan and Filipe, we certainly never had a dull moment in Room N229-A. Although it felt mostly like fun and games, I learnt a great deal from the many hours we spent discussing our various (scientific) problems. Filipe you were a treasure trove of useful tips and facts, and your help in getting me started in the lab was indispensable. Your ability to critically analyse experimental strategies and their outcomes helped me a great deal in navigating my way towards the appropriate experiments. Besides the academic guidance, you also ensured that a healthy amount of distraction was added to our daily routine, with a seemingly endless supply of anecdotes and (sometimes) funny jokes. Jan, you got stuck with me from the moment I arrived at the VU, designated by Bas as my "caretaker". I remember the somewhat worried look on your face when I first tried to speak Dutch with you, luckily you were prepared to endure the often awkward constructions and strange word choices...Ik zal dus mijn best doen om de taalkennis die ik van jou

heb opgedaan niet te “verloren”. Your methodical and focused approach to any challenge (from sport to research) is something I admire and something I’m still striving to achieve. Sharing a daily cycling route provided fertile ground for exchanging cooking tips and recipes…dinners have become decidedly less diverse since then. I also owe you many thanks for the great job you did in translating the summary of this thesis into Dutch. Now that my thesis is completed, we can finally finish the amplification bias paper! Jan and Filipe, you have both become great friends and it is a privilege to have you as my paranymphs!

To all the other “original” Teusink group colleagues, Evert, Joost, Koen, Anisha, Pinar, Meike, Herwig and Domenico, thanks for the fun times at group retreats and the many stimulating conversations over the years. Meike, it was great working with you and our collaborative efforts turned out to be pretty fruitful! I really appreciated your willingness to always indulge my “can-you-quickly-implement-this-in-mathematica” requests. Koen, as the only other dedicated yeast experimentalist we were often stuck in the lab by ourselves. Luckily you always listened patiently when I explained yet another failed tps1Δ experiment. Thanks for all your advice and many useful suggestions. Your laidback manner was refreshing and I quickly learnt that lab work does not always have to be stressful.

Frank, thank you for the many interesting and insightful conversations and for your direct contributions to this thesis. While I could not always follow your more mathematical musings, I really enjoyed the occasional philosophical exchange (the existential debate along with Jan, at 1am in the morning on the staircase in the Grauer Bär, was a particular highlight) and your infectious enthusiasm. Douwe, thank you for your eagerness in always answering any statistical questions I had; the discriminant analysis performed in Chapter 5 is a direct result of discussions with you!

Marijke, Martin, José and Vera, you always made sure that everything in the lab ran smoothly and were always ready to assist and help wherever needed; this made my life a lot easier. Thank you for this.

I was fortunate enough to collaborate with the Cell Systems Engineering group in Delft. Sef, Aljoscha, and the rest of the group, thank you for your hospitality. Aljoscha, Luisa, Amit and Zheng: a key part of my thesis was generated with your help, thank you!

I also owe thanks to Yves and Tom for help in performing experiments that were crucial to my PhD research. Gertien, thank you for many useful suggestions during the yeast meetings and for sharing your pHluorin plasmid with us; it turned out to be an important weapon in my experimental arsenal.

To all the other members of the Systems Bioinformatics and Molecular Cell Physiology groups, past and present, thanks for patiently listening to me obsessively talk about subpopulations and tps1 mutants and for often providing me with useful suggestions or insights during group meetings. Jeannet, thank you for your assistance and willingness to help whenever I needed to figure out something administrative (which was often). Rick, it's great to have an "artist" to call on for creative advice - thanks for helping me with the cover of this thesis.

Then there are of course the students, Bahar, Sandra, Valentijn and Wen, who during their internships played an important part in helping me piece together the puzzle that would become this thesis.

Liewe Ma en Pa, julle het my altyd gemotiveer om my drome te volg. Dit was daarom 'n maklike beslissing toe ek in 2003 besluit het om tog maar Universiteit toe te gaan om 'n BSc in Molecular Biology te gaan doen. Self het ek nie gedink dat ek na 12 jaar nog steeds besig sou wees met studies nie, maar met ouers wat besluit het om weer studente te word in hulle middel dertigs, is dit miskien ook nie 'n verrassing nie. Baie dankie vir al die ondersteuning deur die jare en vir julle onvoorwaardelike liefde.

And finally, Dani, thank you for having shared this adventure with me! Looking back now, I certainly didn't know what we were getting into when we decided to come to Amsterdam. Thank you for your patience and caring support throughout. When at times I felt uncertain or intimidated by the task ahead of me, your own perseverance and entrepreneurial spirit always inspired me. I am so happy to have had you by my side. In between all the work, we also had lots of fun and even managed to get married! With this chapter concluded, I can't wait to turn the page…